Spring 2017

Surgical treatment for cervical myelopathy: the effect on spinal cord strain using magnetic resonance imaging and finite element modeling

Kirsten Elizabeth Stoner
University of Iowa

Recommended Citation

Stoner, Kirsten Elizabeth. "Surgical treatment for cervical myelopathy: the effect on spinal cord strain using magnetic resonance imaging and finite element modeling." PhD (Doctor of Philosophy) thesis, University of Iowa, 2017.
https://doi.org/10.17077/etd.clayx0e1

Follow this and additional works at: https://ir.uiowa.edu/etd
Part of the Biomedical Engineering and Bioengineering Commons

SURGICAL TREATMENT FOR CERVICAL MYELOPATHY: THE EFFECT ON SPINAL CORD STRAIN USING MAGNETIC RESONANCE IMAGING AND FINITE ELEMENT MODELING

by

Kirsten Elizabeth Stoner

A thesis submitted in partial fulfillment
of the requirements for the Doctor of Philosophy
degree in Biomedical Engineering in the
Graduate College of
The University of Iowa

May 2017

Thesis Supervisor: Professor Nicole M. Grosland

Graduate College
The University of Iowa
Iowa City, Iowa

CERTIFICATE OF APPROVAL

PH.D. THESIS

This is to certify that the Ph.D. thesis of

Kirsten Elizabeth Stoner

has been approved by the Examining Committee for
the thesis requirement for the Doctor of Philosophy degree
in Biomedical Engineering at the May 2017 graduation.

Thesis Committee:

Nicole M. Grosland, Thesis Supervisor

Matthew A. Howard

Nicole A. Kallemeyn

David G. Wilder

Vincent Magnotta

To Grammy, Pop-Pop, and Mom who always stressed the importance of education, hard work, and helping others.

And to Brigitta, the best sister there is.

Genius is one percent inspiration, ninety-nine percent perspiration.
-Thomas Edison

I just try to help my people.
-Rocco Santarelli III, age 4

ACKNOWLEDGEMENTS

I could not have completed my graduate studies without the people mentioned here. Thank you all for supporting me through the journey.

I first and foremost need to thank my adviser, Dr. Nicole Grosland. She has been the best adviser I could have hoped for. She has always been available and happy to give guidance I needed. Most importantly she’s taught me not to be afraid to ask questions and realize when my FE models are good enough; perfection is not the goal, answering the research question is!

I also need to thank my committee member, Dr. Vincent Magnotta, who was always willing to teach and help me understand the intricacies of MR imaging, and help me with all of my coding errors!

I would also like to thank Dr. Matthew Howard and Dr. Kingsley Abode-Iyamah for all of their clinical input in this project. Being able to interact directly with you, the surgeons, and patients in the neurosurgery clinic has been invaluable to my education.

Thank you to Dr. Nicole Kallemeyn and Dr. David Wilder for being on my committee and always asking interesting and thought provoking questions.

Dr. Nicole Watson also deserves a big thank you for all of her patience and help with my finite element models. You’re the best office-mate I could ask for!

Thanks to Lisa and Jenny at CCAD for always making things run smoothly!

Thank you to all of the good friends I’ve made over the last four years. Relaxing and having fun together has made this time wonderful.

Finally I need to thank my family, especially my mother and sister, for always supporting and loving me unconditionally.

ABSTRACT

Cervical myelopathy is the most common form of spinal cord injury in North America with roughly 19,000 new cases in the US every year. It results from chronic compression of the spinal cord by osteophytes, intervertebral disc herniation, and ossified ligaments. It commonly affects adults over the age of 50 years and causes upper extremity numbness, loss of hand dexterity, gait disturbances, and decreased proprioception. Recent studies imaging studies have shown this injury is highly dependent on the dynamic motion of the spine, often worsening in extreme flexion and extension. Surgical intervention is the accepted mode of treatment with the aim of decompressing the spinal canal and stabilizing the spine. However, 25% of patients have reoccurrence of symptoms indicating that surgical treatments may not be adequately addressing the injury. A main reason for this is little data has been reported on the spinal cord mechanics during cervical spinal motion in either healthy or cervical myelopathy subjects. To address this, we utilized MR imaging and finite element modeling to investigate spinal cord mechanics. As far as we know, we are the first group to obtain *in vivo* 3 dimensional spinal cord displacement and strain data from human subjects and the first to develop a C2 to T1 FE model of the healthy and cervical myelopathic spine and spinal cord.

Utilizing high resolution 3T MR imaging in neutral, flexion, and extension positions we were able to obtain spinal cord displacement and strain fields from both healthy subjects and cervical myelopathy subjects before and after surgical intervention. In healthy subjects, flexion motion of the spine causes the spinal cord to move superiorly and in extension the spinal cord moves inferiorly. During extension, localizations of high

principal strain can be seen in healthy subjects at areas of bony impingement and dural buckling. In both flexion and extension, cervical myelopathy subjects exhibited very little spinal cord displacement due to spinal cord compression. Principal strains during flexion and extension were greater in cervical myelopathy patients than healthy patients, specifically at the C4-6 vertebral levels. Surgical treatments for cervical myelopathy did restore spinal cord motion however, not in the same pattern or direction as healthy subjects. Additionally principal strains of the spinal cord were not reduced after surgical intervention. This indicates that surgical interventions are not adequately addressing the altered mechanics of the spinal cord during cervical myelopathy.

To determine the how common surgical techniques for cervical myelopathy affect spinal cord mechanics, a FE model of the cervical spine and spinal cord was developed. The spinal cord motion was validated against MR imaging data obtained from normal subjects. Once validated, the model was used to develop a FE model of cervical myelopathy and surgical interventions. The native FE model predicted spinal cord motion well and replicated bony spinal cord impingement and dural buckling seen in healthy subjects. The FE model of cervical myelopathy also replicated spinal cord motion well as compared to MR imaging data of cervical myelopathy. Principal strains obtained from the healthy and cervical myelopathy FE models were similar in flexion however in extension, principal strains were higher at the C3, C6 and C7 levels. This is different than the patterns exhibited in the MR imaging and is most likely due to the percent of spinal cord compression induced in the FE model.

Three, C4 to C7 surgical interventions were introduced to the model: anterior discectomy and fusion, anterior discectomy and fusion with laminectomy, and double door laminoplasty. In flexion, all surgical treatments doubled spinal cord principal strains at the C3 level and minimally reduced tensile strain at C4. The majority of strain reduction occurred at C5-7. In extension, all surgical techniques increased principal strains at the C3 and C4 levels. Little or no reduction in principal strains was seen at the C5 and C7 levels. All surgical techniques reduced principal strains at the C6 level. Of the surgical techniques, ACDF tended to reduce spinal cord principal strains the least in both flexion and extension and tended to induce the highest von Mises stresses.

Combining the data obtained from MR imaging and FE modeling we can see that cervical myelopathy alters spinal cord mechanics by limiting spinal cord motion and increasing spinal cord strain. Additionally, current surgical techniques are not addressing the change in spinal cord mechanics effectively. Specifically after surgery, and especially with ACDF, spinal cord displacements and strains are being increased and transferred to different sections of the spinal cord. This indicates not only the need and importance of further research in spinal cord mechanics but also the need to improve treatments for cervical myelopathy which adequately restore the spinal cord mechanics.

PUBLIC ABSTRACT

Cervical myelopathy is the most common form of spinal cord injury in North America with roughly 19,000 new cases in the US annually. It is caused by bony or soft tissue compression of the spinal cord which can get worse as a patient moves his or her head. Cervical myelopathy is very debilitating; these patients first loose feeling in their hands and as the injury worsens they can lose their ability to walk. The only way to stop this injury from progressing is to have a surgery that decompresses the cord. However, there are many different methods of doing this and no one knows exactly how each affects spinal cord compression. This means that sometimes, the first surgery doesn’t relieve the compression and secondary operations are needed.

What if we could know how each surgical method affects a patient’s spinal cord? This study focuses on using magnetic resonance imaging and computer models to answer this. Magnetic resonance imaging allows us to noninvasively “see” the spinal cord motion of cervical myelopathy patients. We can use this information to make computer models of cervical myelopathy, replicating the spinal cord compression during daily motion. Then we can try out different surgeries on this computer model and see which is best at decompressing the spinal cord. This information will enable surgeons to make more educated decisions when choosing surgical treatment methods for cervical myelopathy.

TABLE OF CONTENTS

LIST OF TABLES

LIST OF FIGURES

LIST OF ABBREVIATIONS

CM	Cervical Myelopathy
MR	Magnetic Resonance
3D	Three Dimensional
2D	Two Dimensional
FE	Finite Element
CSF	Cerebral Spinal Fluid
Pre-op	Pre-operative
Post-op	Post-operative
ACDF	Anterior Cervical Discectomy and Fusion
DDLami	Double Door Laminoplasty
JOA	Japanese Orthopaedic Association
DFT	Deformation Field Transform

CHAPTER 1: SIGNIFICANCE AND SPECIFIC AIMS

1.1 Significance

Cervical myelopathy (CM) is a devastating spinal cord injury resulting from chronic compression of the spinal cord. While it obtains less publicity than traumatic spinal cord injury, it is, in fact, the most common form of spinal cord injury and poses a significant burden to society. In North America it is estimated that the incidence and prevalence of cervical myelopathy is 41 and 605 per million, respectively.[1] The average age of diagnosis is 64 years and it is more common in males with a ratio of 2.7:1.[2] The number of patients presenting with cervical myelopathy is not decreasing. In the 1990s the number of hospital admissions for surgical treatment in the USA almost doubled rising from 9,623 patients in 1993 to 19,212 in 2002.[1] These surgeries are costly; a Canadian study reported direct costs for surgical treatment alone is roughly $17,000 USD not including post-operative rehabilitation, medications, and time off from work.[3] Without surgical intervention, symptoms can progress quickly as 75% of patients without surgical intervention have moderate to rapid increase in symptoms.[4]

There are several surgical techniques for treating cervical myelopathy, however, a consensus has not been reached as to which is most effective at reducing spinal cord compression.[5,6] One reason for this is a lack of knowledge of *in vivo* spinal cord mechanics. Many groups have investigated spinal cord mechanics in human cadavers and animal models.[7–11] Neither of these options is ideal, as the spinal cord degrades quickly postmortem and animal models are not always scalable. As an alternative, magnetic resonance (MR) imaging has been used to investigate *in vivo* human spinal cord motion, but these studies have focused on displacements in only one direction, negating the complex three dimensional movement of the spine and spinal cord.[12–15]

The goal of this study was to evaluate the effectiveness of surgical interventions for the treatment of cervical myelopathy. Using a multifaceted approach, we investigated spinal cord motion and strains in both healthy subjects and those afflicted with cervical myelopathy. Using this data we developed computational models to determine the most effective surgical treatment for cervical myelopathy.

1.2 Study Aims

1.2.1 Characterize In Vivo Spinal Cord Strain

The first aim of this study was to characterize spinal cord displacement and strain distributions during neck flexion and extension of healthy and cervical myelopathy subjects. We utilized high resolution MR imaging to obtain cervical spine images of human subjects during physiological motion. To characterize the displacement and strain distributions occurring during this motion, we developed registration techniques to map the MR images of the flexed and extended spine to the neutral spine. This mapping provided us with 3-dimensional (3D) displacement fields from which we calculated Eulerian strain.

1.2.2 Develop a Finite Element Model of the Healthy Cervical Spine and Cord

The second aim of this study was to develop a finite element (FE) model of the healthy cervical spine and spinal cord to model cord strain changes during physiologic motion. We created 3D FE models of the cord, pia, and dura and incorporated them into our previously validated cervical spine model. Physiologically accurate material properties were given to neurologic tissues. The model was validated from displacement and strain data collected in aim 1.

1.2.3 Alter Finite Element Model to Replicate Cervical Myelopathy and Incorporate Surgical Intervention

The third aim was to determine how the spinal cord strains change due to cervical myelopathy by expanding the cervical spine FE model to include abnormal anatomy of cervical myelopathy patients. To determine if surgical intervention reduces cord compression we incorporated surgical treatments into the cervical myelopathy FE model. We also investigated if a specific technique was better at reducing compression.

CHAPTER 2: INTRODUCTION

The cervical spine, or neck, is one of the most important parts of the body as it responsible for a multitude of functions. It supports and rotates the head allowing for an increased visual field over what normal eye movement allows. Most importantly it houses and protects the spinal cord which carries all vital signals for life from the brain to the rest of the body.

2.1 Anatomy of the Cervical Spine

The cervical spine consists of two anatomic groups: the musculoskeletal anatomy and the neural anatomy.

2.1.1 Musculoskeletal Anatomy

The cervical spine includes seven vertebrae which are comprised of cancellous and cortical bone providing rigid support of the neck (Figure 1). While the third to seventh vertebral bodies have similar anatomic features i.e. vertebral body, lamina, posterior process and facet joints, the first two cervical vertebrae, C1 and C2, differ (Figure 2). This difference is due to function. The C1 vertebra interfaces with the occipital section of the skull and allows the head to nod up and down as one does when saying “yes”. The C2 vertebra allows the head to rotate from side to side, as one does when he shakes his head “no”. This is possible because the C1 vertebra surrounds a process of the C2 vertebra, called the dens. The remaining vertebrae, C3 – C7 allow for additional flexion (bending forward), extension (bending backward), lateral bending (bending to the right and left), and axial rotation (twisting).[16]

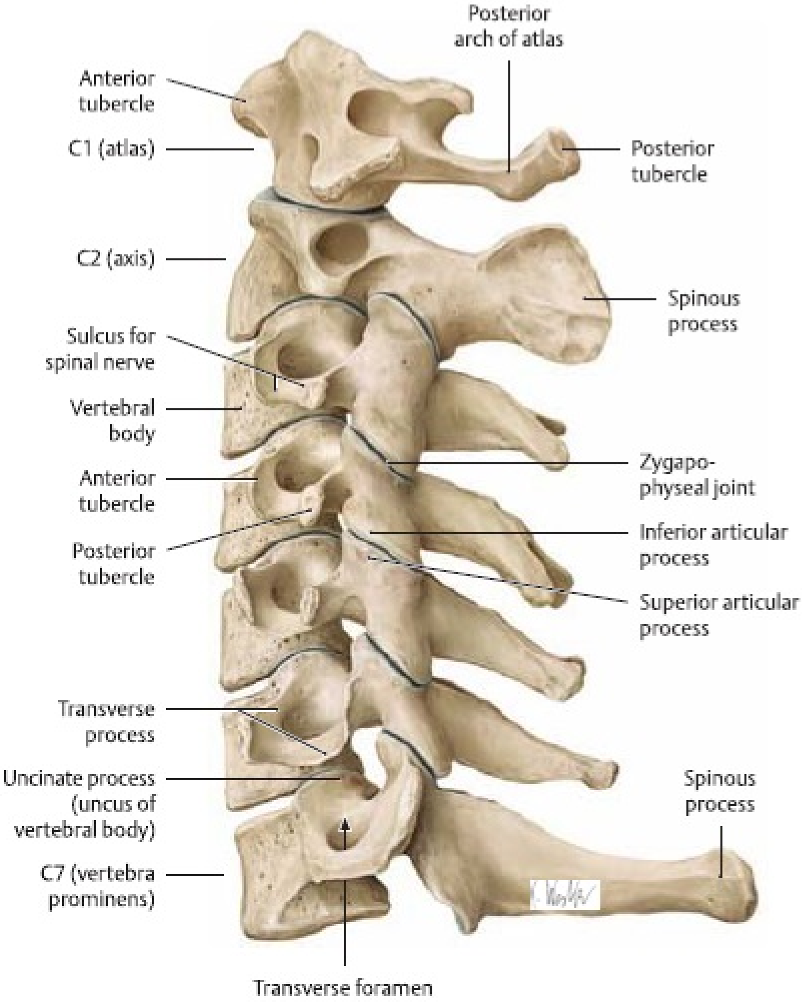

Figure 1: Anatomy of cervical vertebrae.[17]

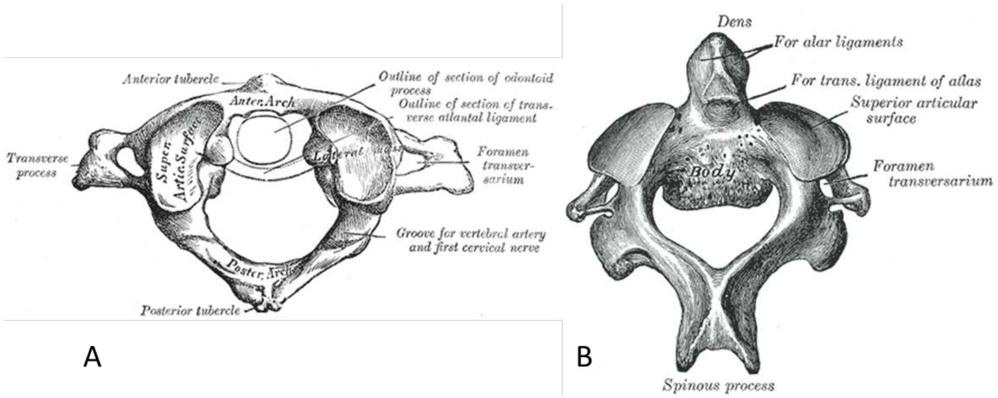

Figure 2: Anatomy of C1 (A) and C2 (B) vertebrae.[18,19]

Intervertebral discs are located between each of the vertebrae starting at the C2-C3 level (Figure 3). The intervertebral disc consists of the central nucleus pulposus surrounded by the ring like annulus fibrosis. The nucleus pulposus consists of an unorganized network of collagen II fibers within proteoglycan aggrecan. The annulus fibrosis contains the nucleus pulposis and is made of alternating layers of collagen I fibers.[20,21] The facet joints are synovial in nature and are located on the lateral sides of each vertebrae between the superior and inferior articulating surfaces (Figure 3). Connecting all of the cervical vertebrae are a series of six ligaments: anterior longitudinal ligament, posterior longitudinal ligament, capsular ligament, ligamentum flavum, inter-spinal ligament, and supraspinal ligament (Figure 4). The ligaments are responsible for limiting spine motion, protecting the spinal cord, and transferring tensile loads.[16]

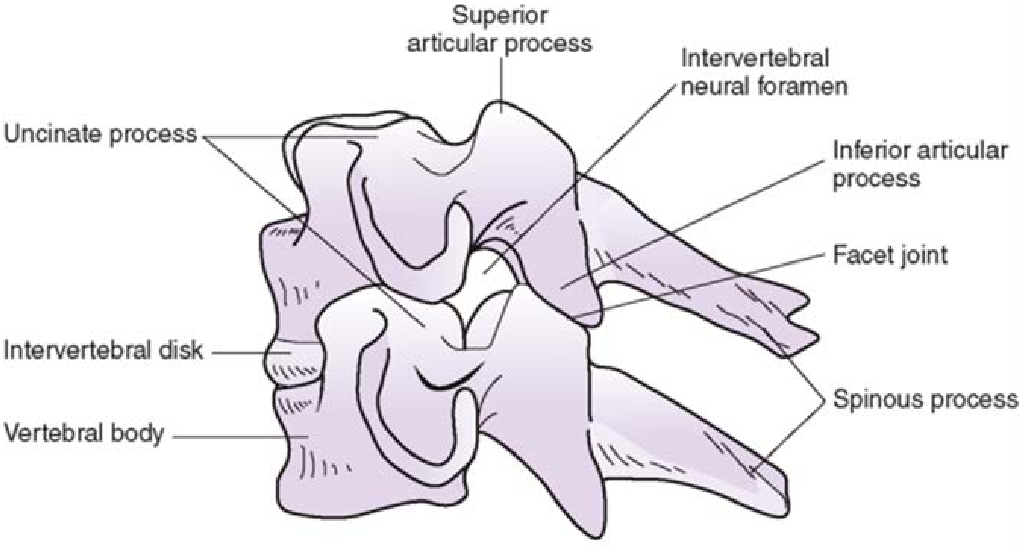

Figure 3: Anatomy of functional spinal unit. © The McGraw-Hill Companies, Inc. All rights reserved.[22]

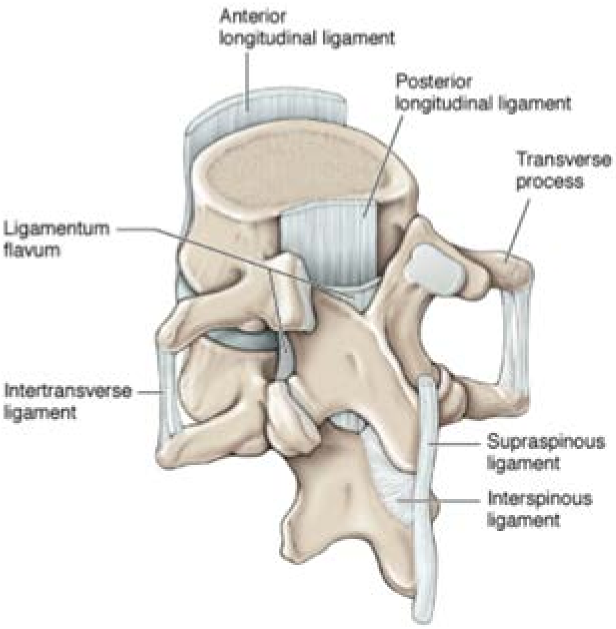

Figure 4: Ligaments of the spine.[23]

2.1.2 Neural Anatomy

The vertebral foramen of the C1 to C7 vertebral bodies comprise the spinal canal which houses and protects the neural components of the spine. These include the spinal cord, pia, dura, cerebral spinal fluid, and neural ligaments.

2.1.2.1 Spinal Cord

The cervical spinal cord is oval in cross-section and consists primarily of neurons and blood vessels which are supported in collagen connective tissue.[24] In the center of the spinal cord is the butterfly shaped grey matter which contains axons responsible for muscle contraction and tone. Surrounding the grey matter is the white matter which contains myelinated axons responsible for coordination, reflexes, and sensory function.[25] In order to innervate the muscles, skin and other tissues, nerve roots protrude laterally from the spinal cord at every vertebral level passing through the intervertebral foramen (Figure 5).

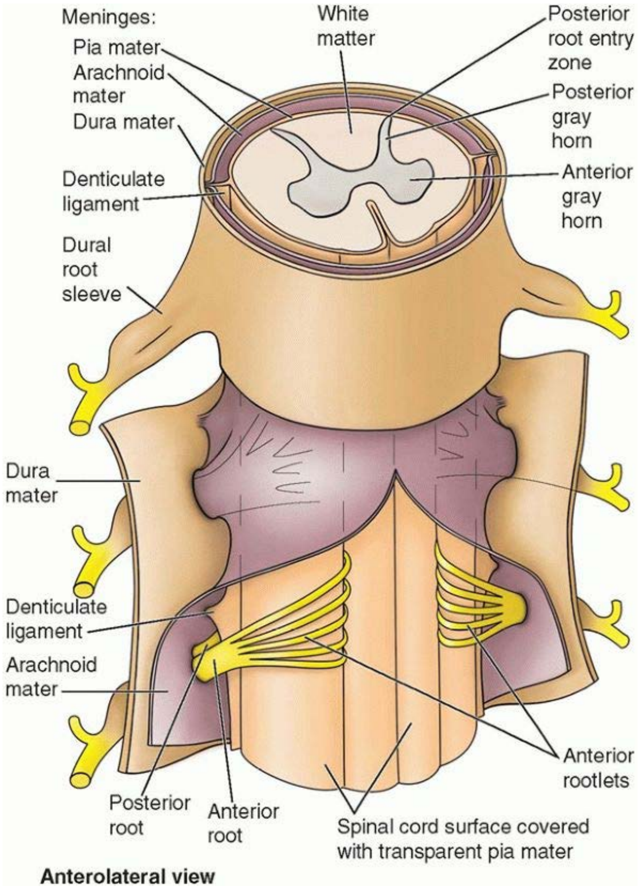

Figure 5: Anatomy of spinal cord.[26]

2.1.2.2 Pia

The spinal cord is surrounded by a membrane called the pia which is adherent to the cord (Figure 5). This membrane is thin but remarkably strong as it is comprised of an elastic fiber network. It also contains a network of blood vessels supplying some of the blood to the cord.[27] The pia is responsible for contributing to the majority of the mechanical integrity of the spinal cord providing tensile strength in both circumferential and longitudinal directions.[10]

2.1.2.3 Dura

The dura is the most external of the membranes surrounding the spinal cord. It abuts the spinal canal and encapsulates the cerebral spinal fluid around the spinal cord and pia (Figure 5). The dura consists of collagen fibers which are aligned in the superior/inferior direction. When the dura is lax these collagen fibers have a wavy appearance and under tension they straighten. Connecting the collagen fibers are elastin fibers which have no orientation. The collagen fibers allow the dura to resist tensile loads along the superior inferior axis and the elastin fibers resist circumferential forces.[28]

2.1.2.4 Cerebral Spinal Fluid

The cerebral spinal fluid (CSF) is comprised mostly of water and surrounds the brain and spinal cord, encapsulated by the dura. It is secreted by the choroid plexus in the brain and circulates around the brain and spinal cord in a pulsatile manner.[29] It consists of a variety of ions, vitamins, protiens, and growth factors essential for neural health.[30] The CSF is under positive pressure of approximately 20 mmHg providing a cushioning affect to the spinal cord and brain, protecting it from sudden mechanical stimulus.[31]

2.1.2.5 Neural Ligaments

Just as the musculoskeletal system has ligaments which attach adjacent bones together, the neural system also has ligaments. These are the dentate and meningovertebral ligaments.

2.1.2.5.1 Dentate Ligaments

Dentate ligaments, also called denticulate ligaments, connect the pia to the dura. They are fibrous in nature, located on the midline of the spinal cord and extend laterally from it (Figure 5). They are formed from a thickening of the pia and have a slightly triangular shape as they insert into the dura. The dentate ligaments connect the pia to the dura starting at the level of the foramen magnum and end at the filum terminale. At the cervical and thoracic levels the dentate ligaments are located between each root level, however it is common for a level or two to be absent.[32,33] Their purpose is to stabilize the spinal cord within the dura.

2.1.3.5.1 Meningovertebral Ligaments

The meningovertebral ligaments are fibrous tissues which connect the dura to the adjacent vertebrae. Their function is to stabilize the neural tissues within the spinal canal. They are most commonly located along the sagittal midline of the dura extending from its posterior surface. The meningovertebral ligaments generally follow a superior-anterior to inferior-posterior direction. The spacing typically follows that of the vertebrae along the spinal cord however number and location of these ligaments can vary.[34]

2.3 Cervical Myelopathy

Cervical myelopathy is the most common form of spinal cord injury. It is caused by chronic spinal cord compression, which in the most severe cases leads to quadriplegia.

2.3.1 Clinical Symptoms and Etiology

Patients often first present to the clinic when numbness and loss of function in the upper extremities becomes pronounced. Gait disturbances may also be present at this time. In order to ensure the presenting symptoms are caused by cervical myelopathy, magnetic resonance (MR) imaging is obtained to confirm cord compression.

Cervical myelopathy was first reported by Stookey in 1928, who observed patients with herniated discs had compression and displacement the spinal cord. These patients exhibited both sensory and motor losses in upper and lower extremities.[35] Since

Stookey's report, there have been many studies presenting patients with similar symptoms.[36–40] The cause of cervical myelopathy is chronic compression of the cervical spinal cord. This compression has been shown to be a result of many different factors including herniated discs, osteophytes, or ossified posterior longitudinal ligament.[4,35,41] While the direct compression of the spinal cord axons causes decreased signaling, secondary responses such as demyelination, ischemia, and axon cell death cause further damage.[42,43] This damage to the spinal cord can cause a variety of symptoms varying in severity. In the least severe, tingling, numbness, and mild dexterity losses are present in the upper extremities. As the cord compression progresses, more serious and debilitating symptoms arise, such as gait disturbances, loss of proprioception, loss of sphincter control, and quadriplegia.[35,44,45]

Until recently only spinal cord compression in the neutral position, with the patient looking straight ahead, was considered. While cord compression is often present in this position, studies have shown more severe cord compression can occur during flexion and extension (Figure 6).[4,46–48] Indeed, patients have reported shooting pain with motion of the neck.[4] Interestingly, a patient had reoccurrence of myelopathy after laminectomy surgery due to intermittent cord compression in extension caused by soft tissue collapsing into the canal.[49] This increased cord compression during physiologic movement indicates that the progression of cervical myelopathy is not simply due to static compression of the cord. It is a function of intermittent compression due to motion.

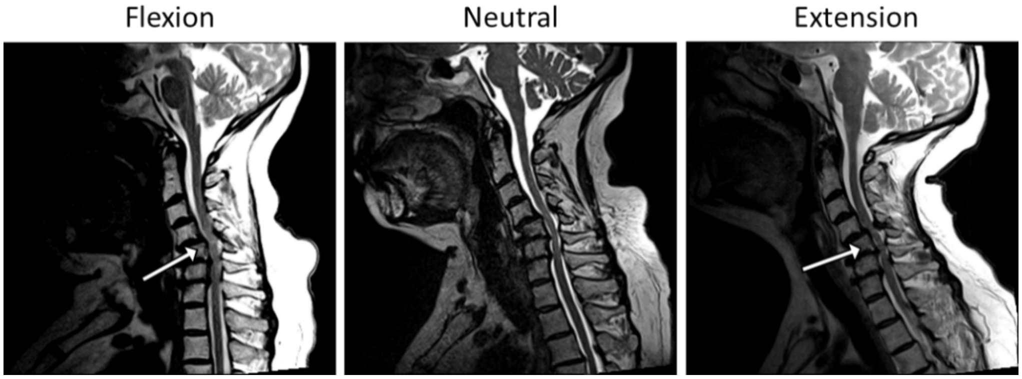

Figure 6: Flexion, neutral, and extension T2 weighted MRI of same patient from UIHC Department of Neurosurgery. Arrows indicate regions of increased spinal cord compression during movement.

2.3.2 Bone Changes

As previously stated, the spinal canal narrowing is the main cause of cervical myelopathy. This narrowing is often due to bony changes in the vertebral bodies as a result of osteophyte formation. Osteophytes are overgrowths of bone which occur due to mechanical overuse and/or advanced age. In cervical myelopathy, these typically form on the posterior sides of the vertebral bodies specifically at the superior and inferior edges (Figure 7). In severe degenerative cases, where there is little intervertebral disc, the superior and inferior osteophytes surrounding a disc level can fuse. Osteophytes can form at any level of the spine but are most common at the C4-C6 levels.[44]

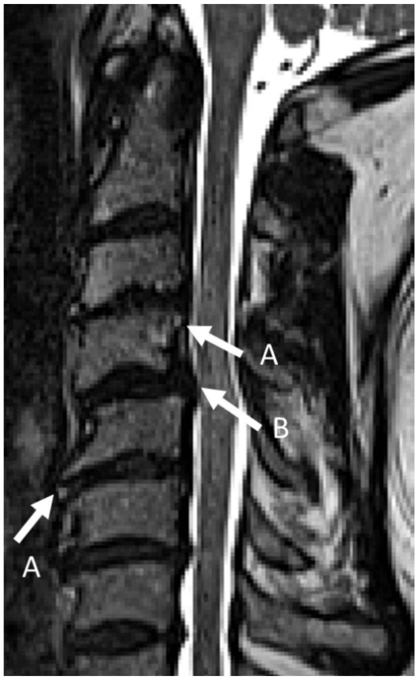

Figure 7: T2 weighted MR image of cervical spine of patient with vertebral osteophytes (A) and herniated disc (B).

2.3.3 Soft Tissue Changes

Soft tissue changes often precede, and present with, bony changes. Intervertebral disc bulging and herniation occurs as the gel-like nucleus of the intervertebral disc protrudes through the fibrous rings of the annulus pulposus. This occurs because during aging the mechanical integrity of the intervertebral disc declines as collaged fibril organization decreases and fissures develop. This disc bulging and herniation occupies spinal canal space, often pressing directly on the spinal cord.[50]

Ossification of spinal ligaments such as the posterior longitudinal ligament and ligamentum flavum also occurs. Ossification of both of these ligaments decreases spinal canal diameter, increasing the propensity of spinal cord compression. The etiology of ligamentous ossification is less understood than that of degenerative disc disease and osteophyte formation but is believed to be a multifactorial combination of genetics and mechanics.

2.4 Surgical Treatment for Cervical Myelopathy

If a patient presents with symptoms of cervical myelopathy and on MR evaluation compression is present, surgical intervention including cord decompression and stabilization is the common mode of treatment. Surgical approaches typically fall into either an anterior, posterior, or a combined approach. The selection criteria for the approach is a combination of factors based on compression presentation, surgeon preference, age, and comorbidities. However, a consensus for the best treatment for cervical myelopathy has not been made.[5,6,51–55]

2.4.1 Anterior Approach

The anterior approach addresses the anterior spinal canal and is often used when the intervertebral disc is involved. The intervertebral disc is removed in a procedure called a discectomy and is replaced by a cage or fusion material. At this time osteophytes on the posterior side of the vertebral body are also removed. The vertebral bodies adjacent to the affected disc level are fused together with a plate on the anterior surface of the vertebral bodies (Figure 8). This procedure, called an anterior discectomy and fusion (ACDF), both decompresses the spinal canal and fuses spinal column decreasing the chance of reoccurring spinal stenosis and myelopathy at that level. This approach is typically used when patients present with three or fewer levels of spinal canal stenosis. If more are present a posterior approach is used to ensure spinal canal stability.

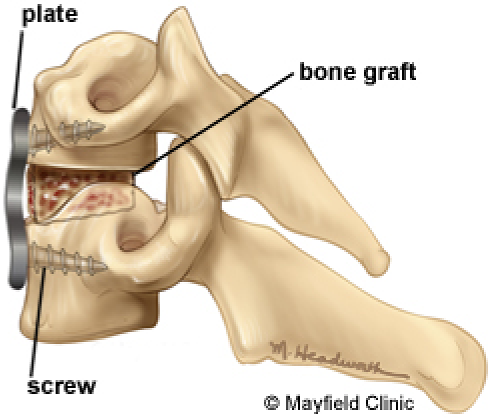

Figure 8: Anterior cervical discectomy and fusion of two vertebrae.[56]

2.4.2 Posterior Approach

The posterior approach also attempts to decrease the spinal cord compression via widening the spinal canal through removal of the lamina.

2.4.2.1 Laminectomy

A laminectomy consists of the complete removal of the lamina at the levels of stenosis (Figure 9). When this technique was first used for treatment of myelopathy, the spine was not fused after laminectomy. However, patients often experienced recurring myelopathic symptoms. Upon investigation, surgeons discovered the posterior soft tissue of the neck, which had been supported by the lamina, was buckling into the spinal canal and compressing the spinal cord.[49] To address this, surgeons now fuse the spine at the levels of the laminectomy to limit spine motion and stop soft tissue encroachment on the spinal cord.

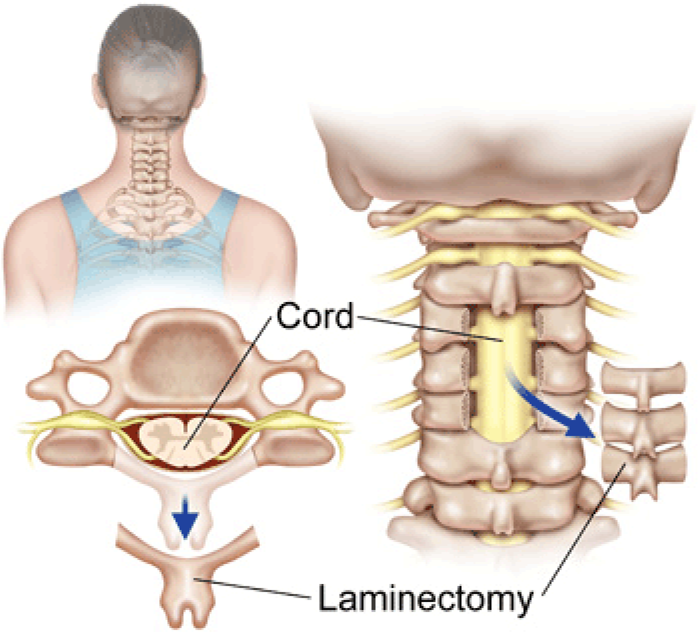

Figure 9: Laminectomy procedure.[57]

2.4.2.2 Laminoplasty

Laminoplasty consists of the partial removal of the lamina and the expansion of the spinal canal through mechanical opening of the lamina. There are two methods of laminoplasty: the open door and the double door. The open door method consists of the removal of only one side of the lamina which is then displaced and a small set of screws and plate are implanted to keep the lamina in an open position (Figure 10). The double door (DDLami) method includes removal of the posterior process of the vertebrae. The lamina is then spread laterally and a bone graft is placed between the cut surfaces to keep the lamina in an open position (Figure 10). As the facets are not disrupted in either laminoplasty method and the neural tissues are still protected by the lamina, fusion is not needed.

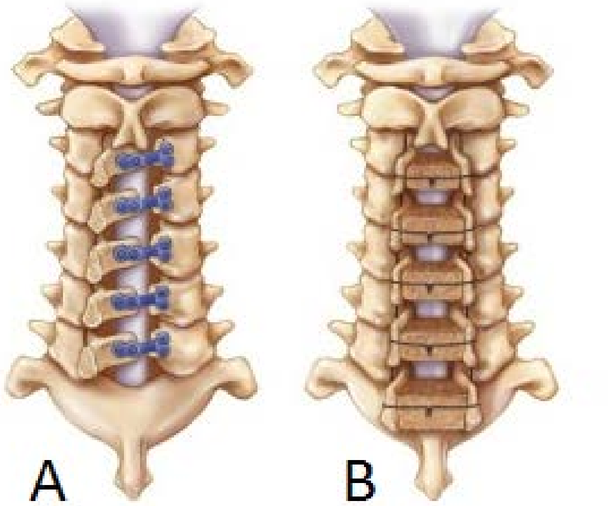

Figure 10: Open door (A) and double door (B) laminoplasty techniques.[58]

CHAPTER 3: IN VIVO SPINAL CORD STRAINS

3.1 Introduction

3.1.1 Spinal Cord Mechanics

In order to effectively understand, prevent, and treat cervical myelopathy it is necessary to better understand spinal cord mechanics. Al Breig was the pioneer of spinal cord mechanics, first describing the motion of the cord during physiologic movement in human cadavers.[46,59] He reported during extension the spinal cord is put into compression and in flexion the cord is put into tension. He also described the tensioning and bucking of the dura, motion of the nerve roots, and tensioning of the dentate ligaments in flexion, extension, lateral bending, and axial rotation.[7]

Others have used animal models to assess spinal cord mechanics during flexion, extension, and neck dislocation.[60,61] C. G. Smith investigated the change in spinal cord length and motion in rhesus monkeys during postural positions. In flexion, he found the spinal cord moves towards the fourth cervical vertebrae and increases in length at the cervical levels roughly 20%.[60] Kroeker and Ching investigated spinal cord strains in macaques during axial tensioning and found strain ranging from 5 to 28%.[61] While these data do help to give insight into spinal cord mechanics, animal models are not directly translatable to humans as there are differences in anatomy, spinal range of motion, and size which may directly affect spinal cord mechanics.

Unfortunately, many investigators, including those previously mentioned, used cadaveric specimen for human and animal ethical reasons. As the mechanics of the spinal cord degrades rapidly postmortem, *in vivo* methods for measuring spinal cord mechanics is necessary.[62]

3.1.2 3D Imaging of Spinal Cord Using MRI

The development of magnetic resonance (MR) imaging and its application in the medical fields has given researchers a non-invasive tool which allows them to investigate tissues *in vivo*.

3.1.2.1 Human Imaging

A few groups have used MR imaging to measure cord displacement of humans *in vivo*. Yuan *et al.* measured both stress and strain of subjects' spinal cord in flexion. They determined that the strains of the spinal cord correlated with head flexion angle where the posterior side of the cord stretched more than the anterior surface. The C2-C7 posterior strains varied from 6.8 to 13.6% and the anterior surface varied from 3.7 to 8.7%. At the C2-C5 level the cord displaced caudally with respect to the vertebral bodies and the C6-C7 displaced cephalad.[15] Others show patients with spondylosis have greater cord displacement due to pulsatile CSF flow than controls.[63] Our neurosurgery collaborators have assessed the displacement of the thoracic cord during flexion using MR imaging. By using root-cord junctions as landmarks, they found the average thoracic spinal cord displacement within the canal to be 8.5 ± 6.0 mm and the average axial stretch of the cord to be 3.5 ± 2.6 mm.[12]

3.1.2.2 Animal Imaging

The previously mentioned measurements of the cord displacement and strain are unfortunately measured primarily in the cranial to caudal direction. However during cervical myelopathy, compression of the spinal cord is mostly in the anterior to posterior direction. Currently only the Oxland group has assessed spinal cord strains in three dimensions. Their work is tailored to injury mechanisms of dislocation and contusion injuries, specifically in rats. Through high resolution MR images of rat spine pre- and post-injury they are able to register the post-injury images to the pre-injury images resulting in displacement and strain fields. During contusion and dislocation they measured the rat cord displaces a maximum of 1.8 mm and 2.5 mm in the dorsal-ventral direction, respectively. The corresponding strains were roughly 200% in contusion and 180% in dislocation. While this technique of 3D strain measurement has only been utilized in injury mechanics its application to both physiologic motion and myelopathy is a natural one.[64,65]

3.1.3 Study Aims

The aim of this study is to utilize MR imaging to obtain three-dimensional displacement and strain fields of the cervical spinal cord during physiologic motion among healthy subjects and subjects diagnosed with cervical myelopathy before and after surgical intervention. We hypothesize that normal subjects will have lower strain magnitudes than those of cervical myelopathic patients. We also hypothesize that surgery will alter the strain and displacement fields of the cervical myelopathic patients.

3.2 Methods

3.2.1 Subject Selection

Nine healthy subjects, four females and five males with and average age of 48 ± 28 years, were enrolled in the study. Subjects were volunteers from the community and had no neurologic defects and no history of injury, surgery, or disease to the spinal cord and/or spine. Ten subjects with cervical myelopathy, four females and six males, with average age of 64 ± 10 years, were enrolled into the study prior to their surgical treatment. All cervical myelopathy subjects presented at the University of Iowa Hospitals and Clinics Department of Neurosurgery and were diagnosed with cervical myelopathy. Patients with prior surgical spine interventions or spinal cord tumors were excluded from this study. Additionally, no subjects had contraindications for MR imaging, such as embedded metallic bodies or pacemakers. The study was approved by the University of Iowa Institutional Review Board office, IRB# 201411728. Demographic data including age, BMI, canal grade, JOA Score, Nurick Score, and level of most stenosis was collected for all subjects (Table 1).

3.2.2 MR Image Acquisition

Using a 3T MR scanner T2 weighted images were acquired of each subjects' cervical spine in neutral, flexed, and extended positions. Images were collected in the sagittal plane using a 3D SPACE sequence with the following parameters: TE = 132 ms, TR = 1500 ms, NEX = 2, FOV = 250 x 250 x 48 mm, Matrix = 320 x 320 x 60, and Bandwidth = 625 Hz/pixel. The resulting images had a 0.8mm isotropic resolution. The range of flexion and extension for each subject was based on the individual's level of comfort and space available in the MR receiver coil. To minimize motion and increase subject comfort, the head and neck were supported with cushions. Normal subjects had only one set of MR images taken. Cervical myelopathy subjects had two sets of MR images taken. The first set was taken during their pre-operative screening examination, roughly two weeks prior to surgery. Each patient then underwent a decompression and fusion surgery as chosen by their neurosurgeon. The second set of MR images was taken at post-operative follow-up examination, roughly six weeks after surgery. Five of the ten cervical myelopathy subjects did not partake in post-operative imaging. This was due to being lost to follow-up, post-operative discomfort, or travel distance to hospital.

Table 1: Demographic data of subjects. Asterisk indicates subjects who returned for post-operative follow-up.

Subject	Age (Years)	Gender	BMI	Flexion Angle (Deg)	Extension Angle (Deg)	Level of Most Stenosis	Neutral Canal Grade	Flexion Canal Grade	Extension Canal Grade	JOA Score	Nurick Score	Surgical Intervention
Healthy Controls												
1	35	F	36.9	8.8	17.3	C5/6	0	0	0	18	0	N/A, Healthy
2	26	M	22.0	32.7	5.3	C5/6	0	0	0	18	0	N/A, Healthy
3	30	M	45.3	34.8	37.5	C4/5	0	0	0	18	0	N/A, Healthy
4	28	F	20.2	20.1	34.4	C4/5	0	0	0	18	0	N/A, Healthy
5	32	M	22.2	26.4	22.8	C4/5	1	1	1	18	0	N/A, Healthy
6	28	M	24.5	25.2	26.9	C5/6	0	0	0	18	0	N/A, Healthy
7	89	F	30.4	17.9	14.7	C6/7	1	1	1	18	0	N/A, Healthy
8	96	M	32.4	2.2	1.9	C3/4	1	0	1	18	0	N/A, Healthy
9	64	F	36.3	10.7	17.7	C5/6	1	1	2	18	0	N/A, Healthy
CM PreOp												
10	42	M	30.7	34.0	9.3	C4/5	3	3	3	15	2	C4-7 ACDF*
11	60	M	37.3	18.1	22.2	C4/5	3	3	3	14	1	C4/5 ACDF*
12	68	F	25.3	18.0	8.4	C4/5	2	2	2	14	3	C4-6 ACDF
13	63	M	17.5	10.8	15.1	C4/5	3	3	3	8	4	C3-7 laminectomy, C2-T2 posterior fusion
14	62	M	34.1	2.2	11.4	C5/6	3	3	3	10	2	C3-6 ACDF, C3-7 laminectomy, C2-T2 posterior fusion
15	67	F	33.6	25.0	11.5	C5/6	3	3	3	15	2	patient refused opertation
16	58	F	30.2	31.1	14.7	C4/5	2	2	2	15	2	C4-6 ACDF*
17	71	M	31.8	11.5	8.9	C3/4	2	1	2	12	3	C3/4 ACDF
18	82	F	28.8	12.6	19.4	C6/7	2	2	2	12	2	C6/7 ACDF*
19	70	M	30.1	15.5	7.6	C4/5	1	1	2	15	2	C4-6 ACDF*
CM PostOp												
10	42	M	30.7	1.0	17.0	C4/5	3	3	3	15	1	see above
11	60	M	37.3	10.9	7.8	C4/5	3	3	3	14	2	see above
16	58	F	30.2	18.4	17.3	C4/5	1	1	2	17	0	see above
18	82	F	28.8	7.7	29.4	C6/7	2	2	2	12	2	see above
19	70	M	30.1	1.6	12.1	C4/5	1	1	2	14	2	see above

3.2.3 MR Image Registration

The resulting flexion and extension images were registered to the neutral image utilizing a landmark based deformation field transform (Insight Tool Kit, Kitware, Clifton Park, NY). This registration technique first uses landmarks to drive the registration then a kernel based three-dimensional B-Spline to obtain displacements at each voxel. Landmarks were manually selected using Seg3D (SCI Institute, Salt Lake City, UT). Thirty-five neural landmarks were located at the following positions: neural root exit from cord, anterior and posterior spinal canal superior level of T1, ponds, cerebellar tonsil, and basilar artery. Thirty-two bony tissue landmarks were located at the following locations: center of C2-T1 vertebral bodies, center of the posterior arch of C1, most superior aspect of the C2-T1 spinous processes, facets of C2-T1, and the anterior and posterior foramen magnum. First, the registration was optimized to register the neural tissues, then was optimized to register the bony tissues. The displacement field resulting from this registration is not uniform across the image. Instead the displacement field has unique displacements at each voxel of the image. This displacement field represents the displacement the spinal cord undergoes during motion (Figure 11).

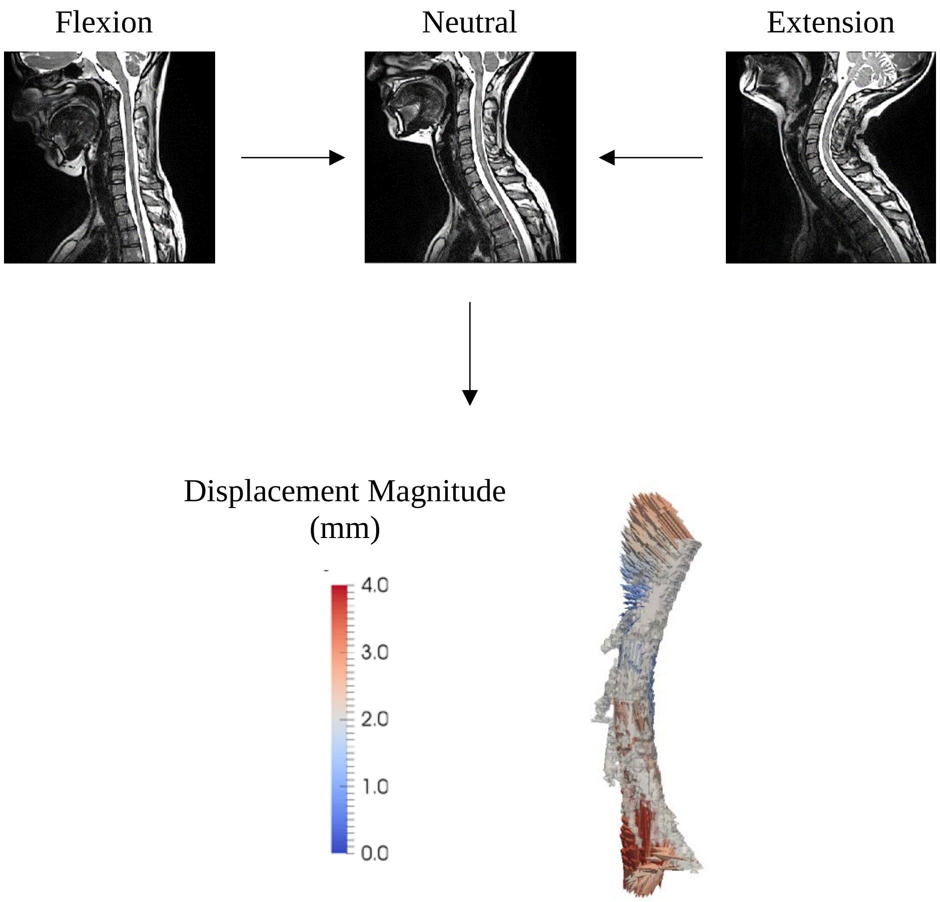

Figure 11: Schematic picturing registration of flexion and extension MR images registered to the neutral MR image, resulting in a displacement field.

3.2.4 Spinal Cord Segmentation

The spinal cord and nerve roots of each subject were manually segmented using Seg3D (SCI Institute, Salt Lake City, UT). Each binary segmentation was exported as an image for use in strain calculations.

3.2.5 Eulerian Strains

The displacement field of the bony tissue represents the “rigid body” motion of the spine and was subtracted from the neural displacement field utilizing the Subtract Image Filter in ITK (Insight Tool Kit Kitware, Clifton Park, NY). The resulting image displacement field (**d**) represents only the motion of the spinal cord within the canal. This image displacement field, **d**(**x**,t), is described in terms of current coordinates (coordinates of the flexed or extended spinal cord), **x**. As our images are static, the displacement field is constant with respect to time, t (Figure 12).

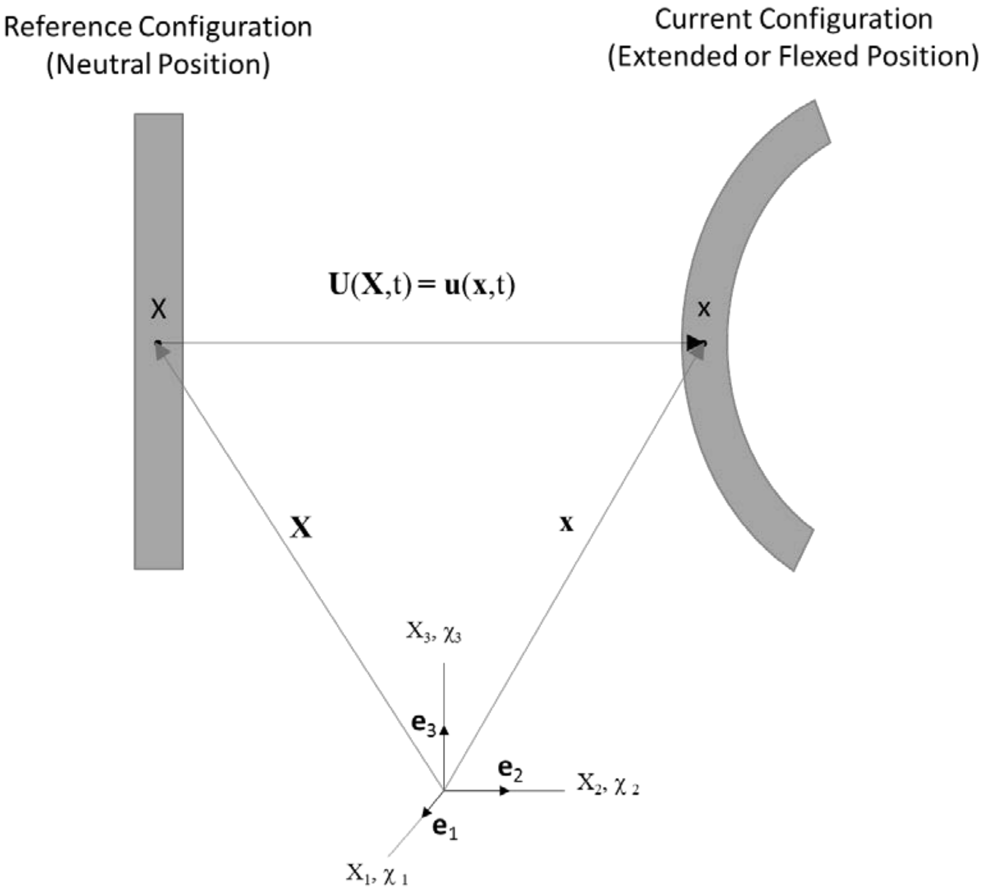

Figure 12: Schematic of displacement field of neutral and flexed/extended spinal cord.

From this displacement field the Eulerian strain of the spinal cord (**e**) can be calculated as follows:

$$\boldsymbol{X}(\boldsymbol{x},t) = \boldsymbol{d}(\boldsymbol{x},t) + \boldsymbol{x} \qquad (1)$$

Where **X**(**x**,t) is the reference coordinate (neutral spinal cord) in terms of current coordinates. Therefore:

$$\boldsymbol{d}(\boldsymbol{x},t) = \boldsymbol{X}(\boldsymbol{x},t) - \boldsymbol{x} \qquad (2)$$

And the displacement field (**u**) as defined in classical continuum mechanics of a material moving from the reference position to the current position is [66]:

$$\boldsymbol{u}(\boldsymbol{x},t) = \boldsymbol{x} - \boldsymbol{X}(\boldsymbol{x},t) \qquad (3)$$

Therefore displacement field required for the neutral spinal cord to reach the location of the flexed or extended spinal cord position is the negative of the displacement field obtained by image registration or:

$$\boldsymbol{u}(\boldsymbol{x},t) = -\boldsymbol{d}(\boldsymbol{x},t) \qquad (4)$$

Taking the gradient of the displacement field yields:

$$\frac{d\boldsymbol{u}(\boldsymbol{x},t)}{d\boldsymbol{x}} = \frac{d\boldsymbol{x}}{d\boldsymbol{x}} - \frac{d\boldsymbol{X}(\boldsymbol{x},t)}{d\boldsymbol{x}} \qquad (5)$$

Where,

$$\boldsymbol{F}^{-1} = \frac{d\boldsymbol{X}(\boldsymbol{x},t)}{d\boldsymbol{x}}, \ \boldsymbol{I} = \frac{d\boldsymbol{x}}{d\boldsymbol{x}} \qquad (6,7)$$

Eulerian strain is defined as:

$$\boldsymbol{e} = \frac{1}{2}(\boldsymbol{I} - \boldsymbol{F}^{-\boldsymbol{T}}\boldsymbol{F}^{-\boldsymbol{1}}) \qquad (8)$$

Or

$$\boldsymbol{e} = \frac{1}{2}(grad^{T}\boldsymbol{u} + grad\boldsymbol{u}) - \frac{1}{2}(grad^{T}\boldsymbol{u}grad\boldsymbol{u}) \qquad (9)$$

where *grad* indicates the gradient. Knowing $\boldsymbol{u}(\boldsymbol{x},t) = -\boldsymbol{d}(\boldsymbol{x},t)$, equation 4, we get the final form of Eulerian strain in terms of our image displacement field (**d**):

$$\boldsymbol{e} = -\frac{1}{2}(grad^T\boldsymbol{d} + grad\boldsymbol{d}) - \frac{1}{2}(grad^T\boldsymbol{d}grad\boldsymbol{d}) \qquad (10)$$

In addition, maximum and minimum principal Eulerian strains of the spinal cord were calculated by obtaining the maximum and minimum eigenvalues of the Eulerian strain tensor (**e**), respectively. This was performed on our discrete data using Paraview (Kitware, Clifton Park, NY). To only obtain data from the spinal cord, the strain field was filtered to only include data occupying the same space as the corresponding flexion and extension spinal cord segmentations. Spinal cord strains were analyzed from the superior surface of the C3 body to the inferior surface of the C7 body to minimize boundary errors.

3.2.6 Image Registration and Strain Validation

There are several areas where error can be generated in this analysis. These include, but are not limited to, landmark selection error, bony landmark registration error, neural landmark registration error, and numerical calculation error. To evaluate the error stemming from each of these processes, several virtual and physical phantoms were created with known shape changes so theoretical values could be compared against the computed outcomes.

A virtual phantom was created using SimpleITK (Kitware, Clifton Park, NY) to assess strain error due to a single image transform and numerical calculation in Paraview. This virtual phantom was a three-dimensional image of a white rectangular box, 16mm x 78mm x 78mm, on a black background with image resolution of 0.8mm x 0.8mm x

0.8mm. Both rigid body rotation and deformation were artificially applied to this phantom by creating secondary images where the white rectangular box was increased in length, height, and/or width by 10 percent and rigidly rotated and/or translated (Table 2). The deformed/translated image was registered to the original image using the same landmark based deformation field transform method as mentioned in section 3.2.3 however registration landmarks were located at the eight corners of the rectangular box and not chosen manually but chosen based on the known locations of the original and "strained" phantoms. To remove additional error generated from obtaining the rigid body displacement field using the deformation field transform, the rigid body displacement field was obtained from the rigid body rotation used to move the image. Strains were then calculated as previously described using Paraview (Kitware, Clifton Park, NY).

Table 2: Dimensions, translation, and rotation of virtual phantoms.

Virtual Phantom	**Length X (mm)**	**Length Y (mm)**	**Length Z (mm)**	**Translation (mm)** *(X,Y,Z)*	**Rotation (deg)** *(X,Y,Z)*
1	16.00	78.13	78.13	--	--
2	16.00	78.13	85.94	(0,0,0)	(0,0,0)
3	16.00	85.94	85.94	(0,0,0)	(0,0,0)
4	17.60	78.13	70.31	(0,0,0)	(0,0,0)
5	17.60	70.31	78.13	(0,0,0)	(0,0,0)
6	14.40	85.94	85.94	(0,0,0)	(0,0,0)
2b	16.00	78.13	85.94	(-50,10,-25)	(0,0,0)
2c	16.00	78.13	85.94	(-50,10,-25)	(-5.16,1.72,9.74)
6b	14.40	85.94	85.94	(-50,10,-25)	(0,0,0)
6c	14.40	85.94	85.94	(-50,10,-25)	(-5.16,1.72,9.74)

To determine the amount of combined error present due to neural anatomy registration, bony registration, and numerical strain calculations, physical phantoms were manufactured. These represented spinal cords, with similar sizes and neural roots. Just as with the virtual phantoms an “undeformed” phantom was created and then various “deformed” phantoms with rigid and non-rigid bends and twists were created (Table 3). Holes were placed at the same length locations along the length of the physical phantom for use in rigid body registration as bony anatomy was not present (Figure 13). T1 weighted MR images were obtained of these phantom. Phantoms without cord rotation had 0.8 mm isotropic image resolution and phantoms with cord rotation had 0.4 mm isotropic image resolution. The undeformed cord phantom was scanned at both resolutions to keep resolution consistent during image registration. Landmarks were manually chosen for both the neural and rigid body registrations. Strains were obtained as previously described.

Table 3: Dimensions of physical phantoms.

Phantom	Diameter (mm)	Length (mm)	Root Diameter (mm)	Distance Between Roots (mm)	Bend (deg)
P1	10	120	2.5	12	0
P2	10	132	2.5	13.2	0
P3	9	120	2.5	12	0
P4	10	120	2.5	12	20 anterior
P5	9	132	2.5	13.2	20 anterior
P6	10	120	2.5	12	20 lateral

To determine how sensitive strain calculations are to errors in landmark selection, the landmarks of phantom P5 were artificially moved. This was done by altering the landmark coordinates of one side of the phantom by adding the distance equal to one voxel to the x and y components and subtracting the distance of one voxel from the z components. This was then repeated for the distance of two voxels. Images were registered using the artificially moved landmarks and strains were calculated.

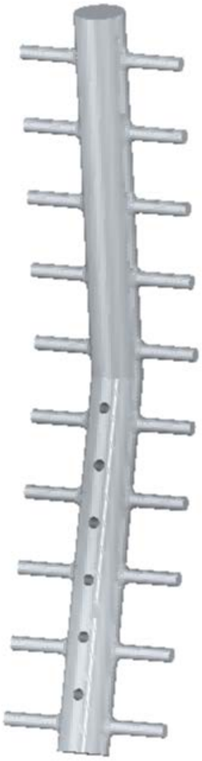

Figure 13: Rendering of physical phantom.

To determine the amount of error due to image registration, Python code was developed based on the SimpleITK Registration Utilities Code (Kitware, Clifton Park, NY). This reports the average, standard deviation and max error in distance from the moving landmarks to the fixed landmarks. If a perfect registration is obtained the average error should be zero with zero standard deviation.

3.2.7 Radiologic Measurements

Change of neck angle in flexion and extension from the neutral position was measured for each subject on a mid-sagittal MR slice using ImageJ (NIH, Bethesda, MD). Neck angle was defined as the angle between the intersection of lines drawn parallel to the posterior surfaces of the C2 and T1 vertebral bodies.[67] Spinal canal and spinal cord anterior/posterior diameter was also measured on a mid-sagittal MR slice at, above, and below the level of most stenosis for all subjects. To quantify how much of the spinal canal is occupied by the spinal cord, a cord-canal ratio was established as follows:

$$ccRatio = \frac{d_{cord}}{d_{canal}} * 100 \qquad (11)$$

Where ccRatio is the cord-canal ratio, d_{cord} is the diameter of the spinal cord at level of most stenosis and d_{canal} is the diameter of the spinal canal at the level of most stenosis.

3.2.8 Statistics

To determine differences in continuous data, a Student's T-test with a significance level of 0.05 was used. For nonparametric data, a Wilcoxon Rank Sum Test with a significance level of 0.05 was used. A Pearson correlation, significance level of 0.05, was used to evaluate the relationships between demographic factors and strain.

3.3 Results

3.3.1 Displacement, Strain, and Demographic Outcomes of Healthy Subjects

When comparing average displacements along the entire cord, there was no difference between flexion and extension in healthy subjects. However, when displacement was sectioned into 5 axial sections aligning with the adjacent vertebral body, two different trends could be seen. In flexion, the C3 level of the cord moves inferiorly and the C7 level of the cord moves superiorly, with location of inflection at the C45 disc (Figure 14A). In extension the opposite occurs, the C3 level of the cord moves superiorly and the C7 level moves inferiorly, with the location of inflection at the C34 disc level (Figure 14B). The cord canal ratio is significantly reduced from 0.69 ± 0.15 in both neutral and extension to 0.61 ± 0.16 in flexion, $p \leq 0.05$. Strain is distributed evenly along the length of the control spinal cords (Figure 15), with high strains most commonly occurring at the C5-C7 levels in flexion and C3, C6 and C7 levels in extension. Spinal canal grades were 0.44 ± 0.53, 0.33 ± 0.50, 0.56 ± 0.73 in neutral, flexion, and extension, respectively. Nurick score was 0 ± 0, 0 indicating no deficit and 5 being bedridden. JOA score was 18 ± 0, 18 indicating no deficit and 0 complete paralysis.[68] In control subjects, greater age was correlated with greater anterior cord displacement in flexion, greater ccRatio in extension, and lower flexion angles, $p \leq 0.05$.

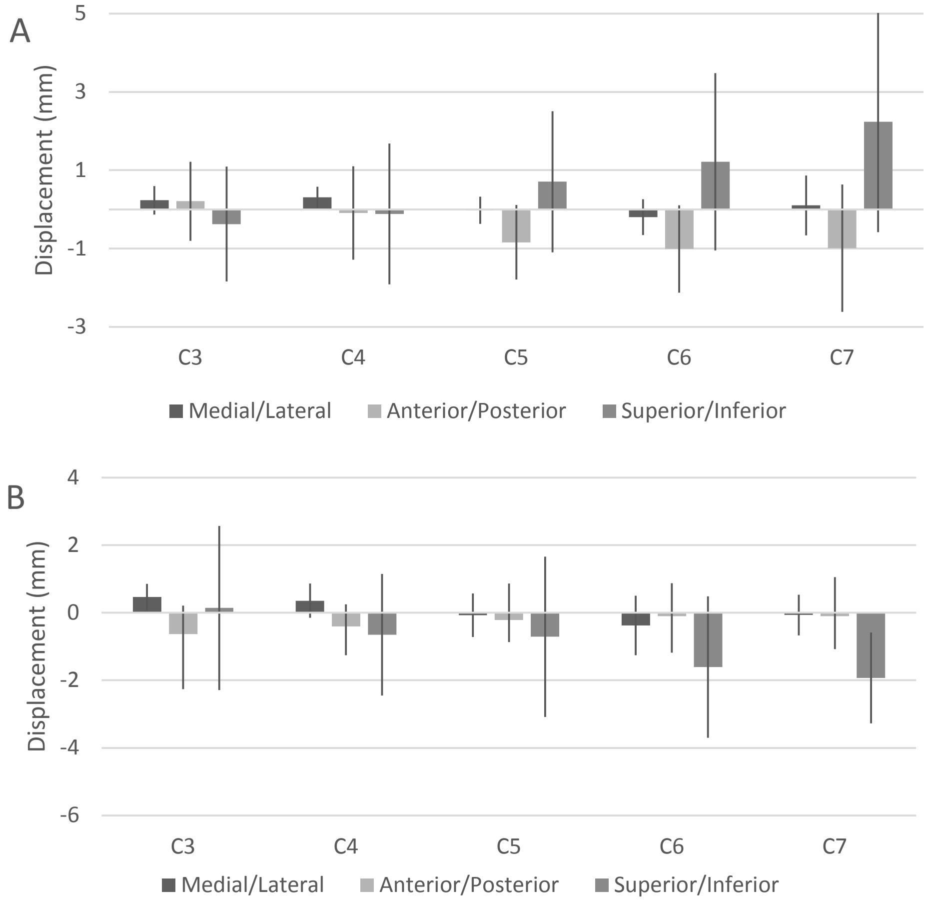

Figure 14: Cervical spinal cord displacement of healthy subjects during flexion (A) and extension (B). Data presented as mean ± one standard deviation.

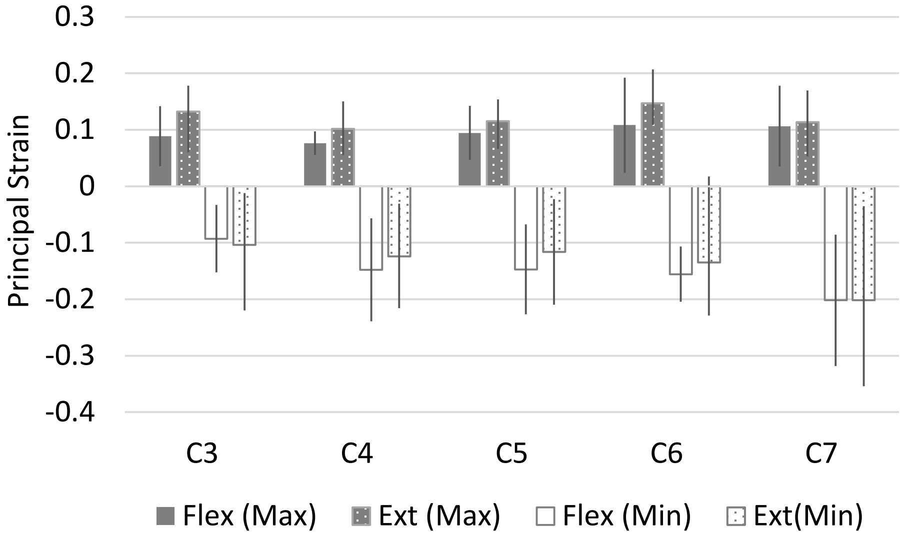

Figure 15: Maximum and minimum principal strain of healthy subjects in flexion and extension. Data presented as mean ± one standard deviation.

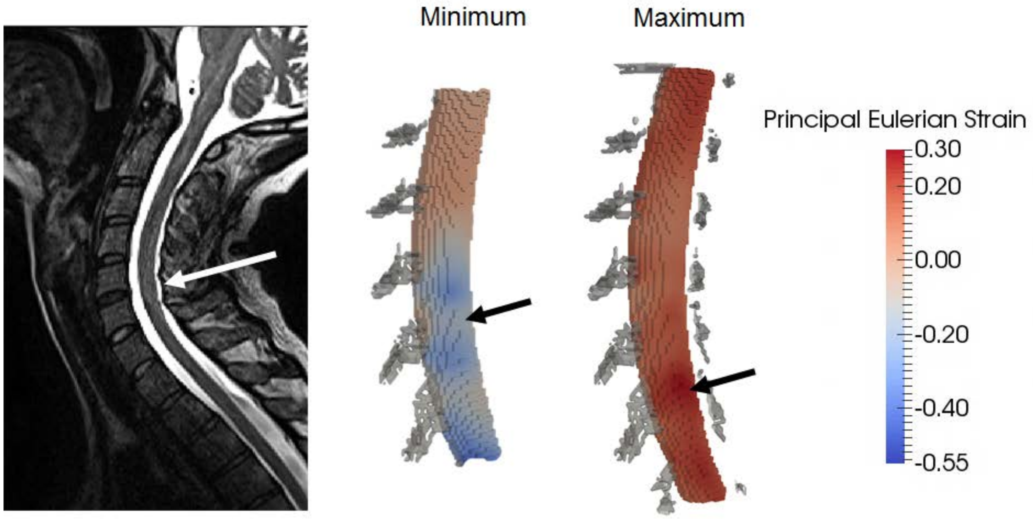

Figure 16: MR image of healthy subject in extension (left). White arrow indicates mild compression at C56 and C67. 3D figure of minimum and maximum principal Eulerian strain of same subject's spinal cord. Black arrows indicate areas of high compressive (middle) and tensile (right) strains as result of compression. Spinal cord roots are shown in grey.

3.3.2 Displacement, Strain, and Demographic Outcomes of Cervical Myelopathy Subjects Pre-Operatively

In cervical myelopathy pre-operative subjects there was no difference in average cord displacement between flexion and extension. Additionally, the cord displacement at specific levels in flexion and extension was very little compared to the normal subjects, but this was not statistically significant (Figure 17). Strain was less evenly distributed along the spinal cord. The highest tensile strain occurred at C5 and highest compressive strain at C3 in both flexion and extension (Figure 18). High strains were also common at C7 in flexion and extension. Cervical myelopathy pre-operative subjects had less superior/inferior displacement of the spinal cord in extension at the C7 level than healthy subjects, $p \leq 0.05$. There is less motion in the anterior/posterior direction at the C5 level during flexion in cervical myelopathy pre-operative subjects than healthy subjects, $p \leq 0.05$. In flexion and extension, principal strain along the entire cord tends to be higher in cervical myelopathy pre-operative subjects than healthy controls although not statistically significant (Figure 19). The ccRatio is not different in neutral, flexion, or extension for cervical myelopathy pre-operative subjects. In cervical myelopathy, pre-ccRatio is 0.91 ± 0.16 in neutral, 0.87 ± 0.13 in flexion, and 0.92 ± 0.11 in extension. Pre-operative ccRatios were significantly greater in all positions than those of healthy controls, $p \leq 0.05$. In cervical myelopathy pre-operative subjects increased age correlated with a lower ccRatio, $p \leq 0.05$. Additionally, cervical myelopathy pre-operative subjects had higher neutral, flexion and extension ccRatios than healthy subjects, $p \leq 0.05$. Pre-operative spinal canal grades were 2.4 ± 0.70, 2.3 ± 0.82, 2.5 ± 0.53 in neutral, flexion, and extension, respectively. Nurick score was 2.3 ± 0.82 and JOA score as 13 ± 2.4. All spinal canal grades of cervical myelopathy pre-operative subjects were worse than healthy subjects, as were JOA and Nurick scores, p ≤ 0.05.

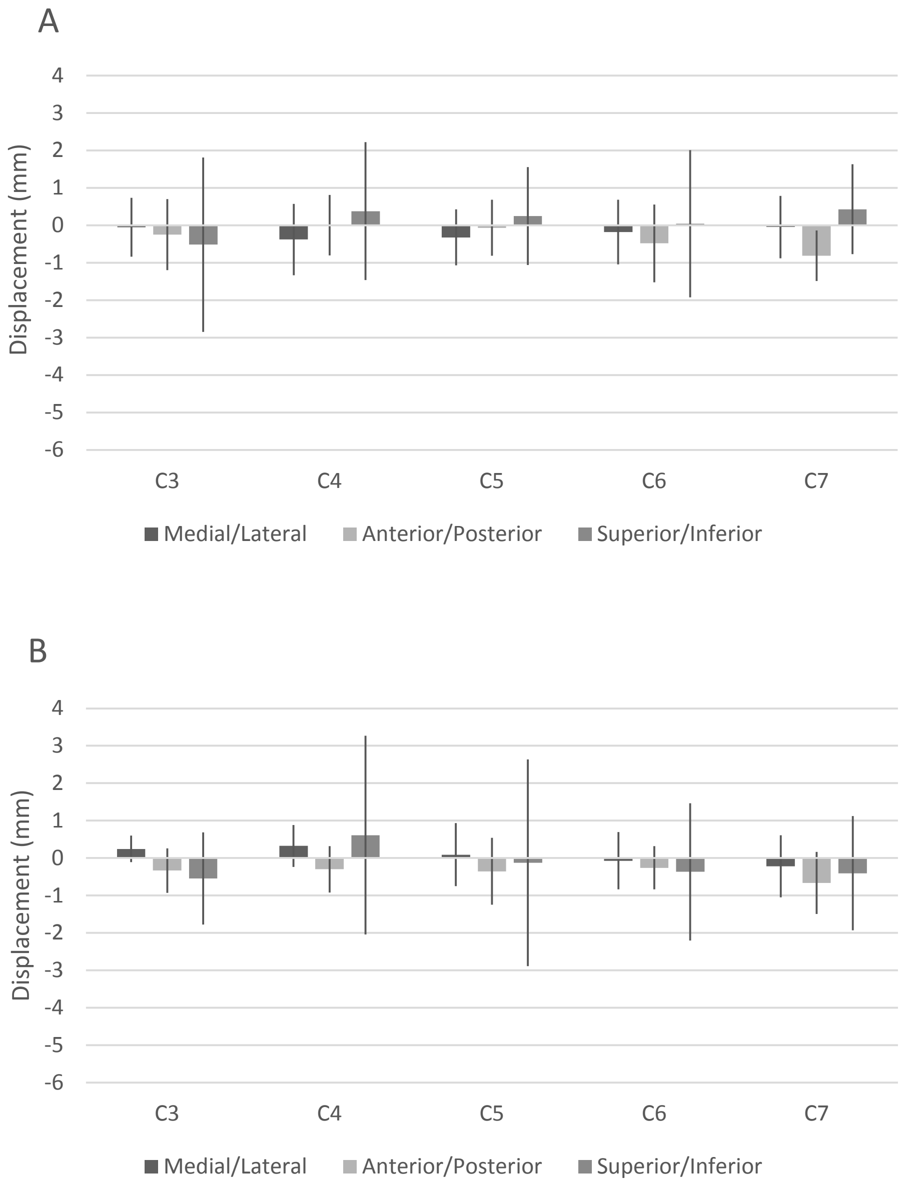

Figure 17: Cord displacement of pre-operative CM subjects during flexion (A) and extension (B). Data is presented as mean ± one standard deviation.

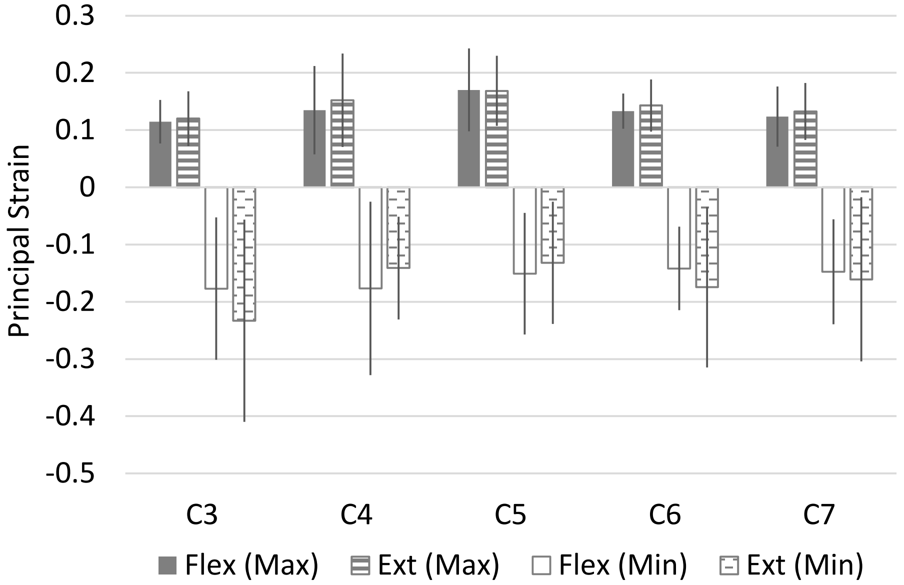

Figure 18: Principal minimum and maximum spinal cord strain in pre-operative CM subjects during flexion and extension. Data is presented as mean ± one standard deviation.

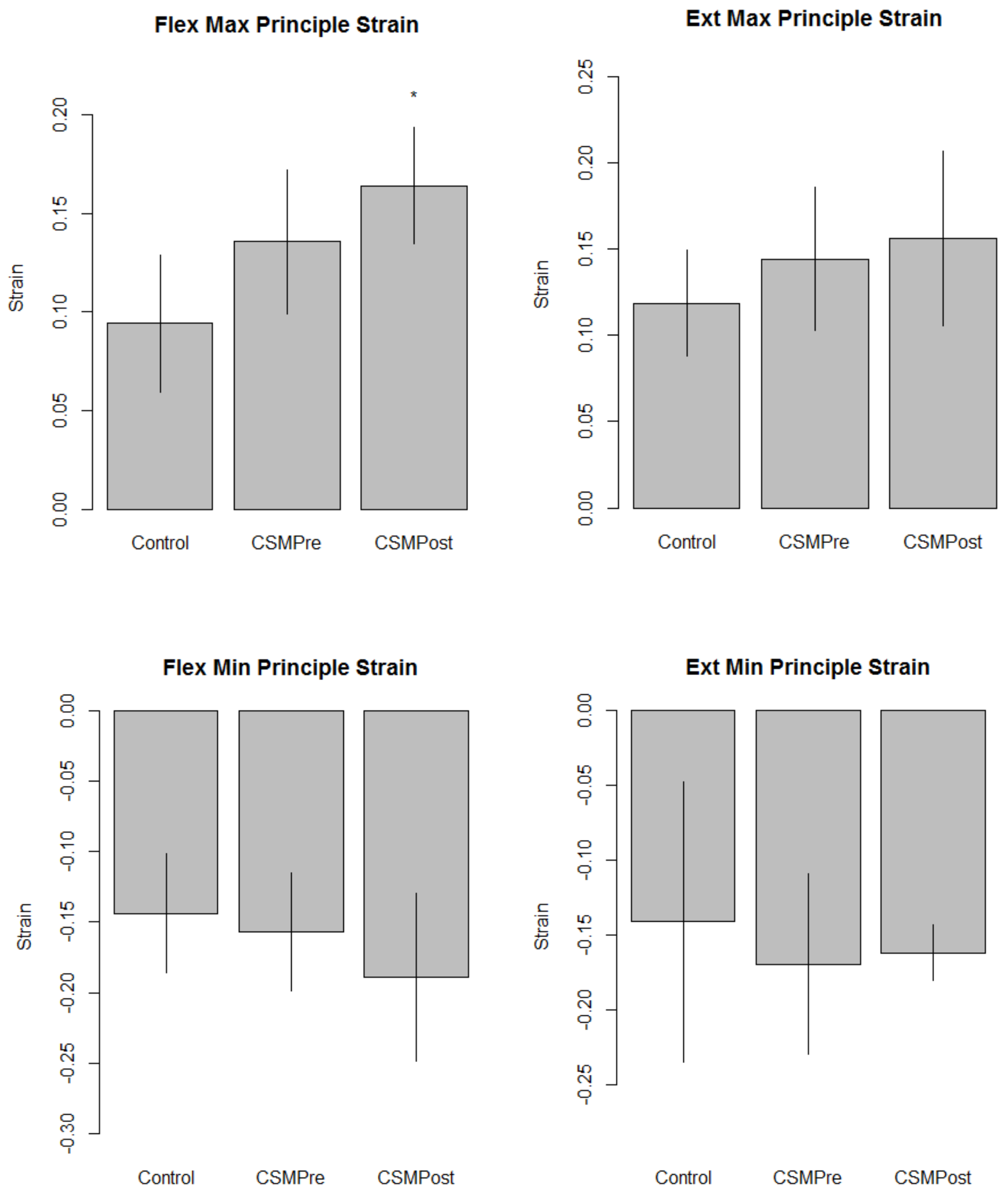

Figure 19: Average principal strain along spinal cord. Asterisk indicates statistical difference from healthy control subjects, p ≤ 0.05. Data is presented as mean ± one standard deviation.

3.3.3 Displacement, Strain, and Demographic Outcomes of Cervical Myelopathy Subjects Post-Operatively

Cervical myelopathy post-operative subjects had no difference in average cord displacement between flexion and extension. Displacement as recorded at the specific levels of the spine increased in both flexion and extension compared to pre-operative displacement but this was not statistically significant (Figure 20). Cervical myelopathy post-operative principal strain was more evenly distributed than pre-operative strain however the strain was still higher than control subjects (Figure 18 and 21). Most common locations of high strain occurred at the C3, C4 and C5 levels. There was no difference in strain or displacements along the cord between cervical myelopathy pre-operative and cervical myelopathy post-operative subjects. In flexion, cervical myelopathy post-operative subjects had higher strain at the C4 level than healthy subjects, $p \leq 0.05$. There was no difference in cord canal ratio between neutral, flexion, and extension positions. In cord canal ratio was 0.70 ± 0.06 in neutral, 0.77 ± 0.11 in flexion, and 0.85 ± 0.13 in extension. The flexion ccRatio was significantly higher than that of healthy subjects, $p \leq 0.05$. There was no difference in ccRatios pre- and post-operatively. Age was negatively correlated with higher principal max strains in flexion and lower principal min strain is extension, $p \leq 0.05$. Post-operative subjects also had greater flexion cord canal ratios and greater flexion max principal strains than control subjects, $p \leq 0.05$. Spinal canal grades were 2.0 ± 1.0, 2.0 ± 1.0, and 2.4 ± 0.6 in neutral, flexion, and extension, respectively. Nurick score was 1.4 ± 0.9 and JOA score was 14.4 ± 1.8. Spinal grades in all positions, Nurick score and JOA score were worse for cervical myelopathy post-operative subjects than healthy controls, $p \leq 0.05$, and there was no difference between cervical myelopathy pre- and post-operative subjects.

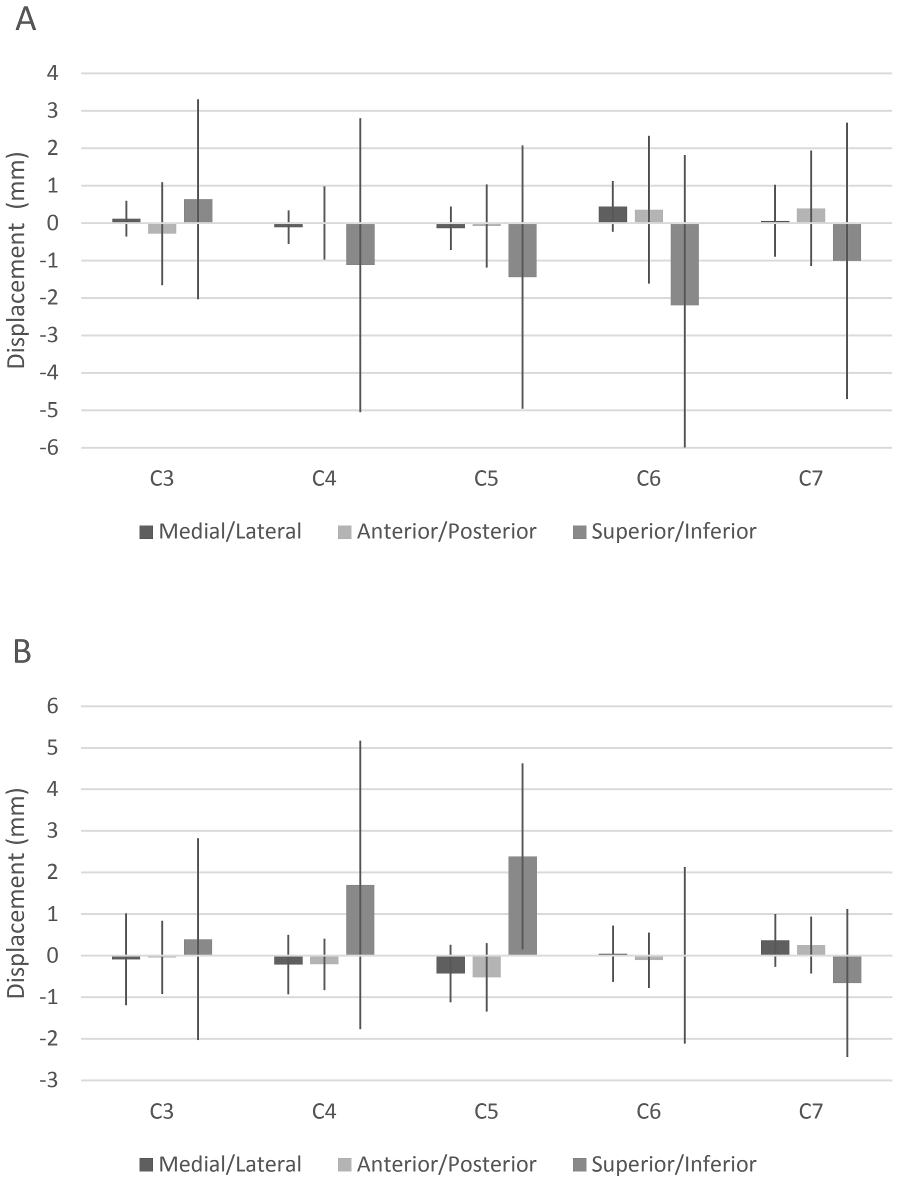

Figure 20: Cord displacement of post-operative CM subjects during flexion (A) and extension (B). Data is presented as mean ± one standard deviation.

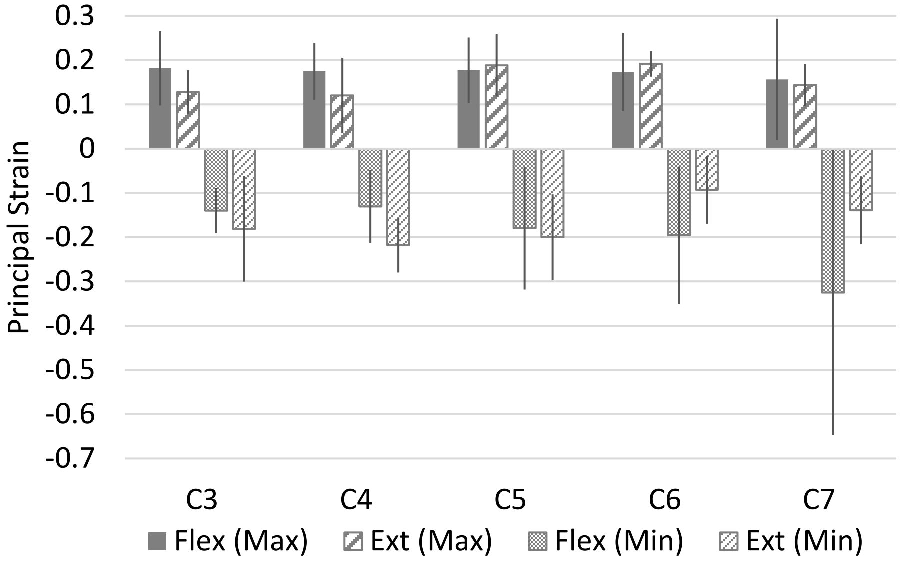

Figure 21: Principal minimum and maximum spinal cord strain in post-operative CM subjects during flexion and extension. Data is presented as mean ± one standard deviation.

3.3.4 Error Evaluation

3.3.4.1 Virtual Phantoms

Average error in strains calculated from DFT registration was 18.41 ± 8.32% in the medial/lateral direction, 16.73 ± 6.64% in the anterior/posterior direction, and 15.07 ± 5.16% in the superior/inferior direction (Table 4). Average error in the maximum and minimum principal strains, which varied in direction, were 12.93 ± 3.94% and 22.80 ± 3.96%, respectively.

3.3.4.2 Physical Phantoms

Average error in strains calculated from DFT registration were 72.72 ± 61.77% in the medial/lateral direction, 57.89 ± 54.79% in the anterior/posterior direction, and 26.37 ± 21.08% in the superior/inferior direction (Table 5). Average error in the maximum and minimum principal strains, which varied in direction, were 15.37 ± 15.58% and 55.03 ± 44.47%, respectively.

Table 4: Strains of virtual phantoms.

	Theoretical Strain					Eulerian Strain From DFT					DFT %Error				
Virtual Phantom	*X*	*Y*	*Z*	*Max Principal*	*Min Principal*	*X*	*Y*	*Z*	*Max Principal*	*Min Principal*	*X*	*Y*	*Z*	*Max Principal*	*Min Principal*
1	--	--	--	--	--	--	--	--	--	--	--	--	--	--	--
2	0	0	0.1	0.1	0	0.00	0.00	0.09	0.09	0.00	--	--	12.47	12.47	--
3	0	0.1	0.1	0.1	0	0.00	0.09	0.09	0.09	0.00	--	12.47	12.47	12.47	--
4	0.1	0	-0.1	0.1	-0.1	0.09	0.00	-0.12	0.09	-0.12	9.30	--	18.67	9.30	18.67
5	0.1	-0.1	0	0.1	-0.1	0.09	-0.12	0.00	0.09	-0.12	9.30	18.67	--	9.30	18.67
6	-0.1	0.1	0.1	0.1	-0.1	-0.12	0.09	0.09	0.09	-0.12	24.57	12.47	12.47	12.47	24.57
2b	0	0	0.1	0.1	0	0.00	0.00	0.09	0.09	0.00	--	--	12.47	12.47	--
2c	0	0	0.1	0.1	0	0.00	0.00	0.09	0.09	0.00	--	--	12.87	12.66	--
6b	-0.1	0.1	0.1	0.1	-0.1	-0.12	0.09	0.09	0.09	-0.12	24.57	12.47	12.47	12.47	24.57
6c	-0.1	0.1	0.1	0.1	-0.1	-0.12	0.07	0.07	0.08	-0.13	24.34	27.59	26.67	22.76	27.54

Table 5: Strains of physical phantoms.

Phantom	Theoretical Strain					Eulerian Strain From DFT					DFT %Error				
	X	*Y*	*Z*	*Max Principal*	*Min Principal*	*X*	*Y*	*Z*	*Max Principal*	*Min Principal*	*X*	*Y*	*Z*	*Max Principal*	*Min Principal*
P1	--	--	--	--	--	--	--	--	--	--	--	--	--	--	--
P2	0	0	0.1	0.1	-0.1	-0.01	-0.04	0.09	0.10	-0.06	--	--	11.47	4.35	35.86
P3	-0.1	-0.1	0	0	-0.1	-0.13	-0.12	-0.01	0.02	-0.21	29.04	19.15	--	--	105.87
P4	0	0	0	0	0	0.03	0.06	0.02	0.12	-0.06	--	--	--	--	--
P5	-0.1	-0.1	0.1	0.1	-0.1	0.02	0.00	0.06	0.13	-0.08	116.40	96.63	41.28	26.38	23.37
P6	0	0	0	0	0	0.04	0.08	-0.06	0.15	-0.13	--	--	--	--	--

Moving landmarks on one side of P5 in the anterior direction by 0.4mm altered strain error by 27.06% in the medial/lateral direction, 11.91% in the anterior/posterior direction, and 1.67% in the superior/inferior direction. Moving the same landmarks by 0.8mm in the anterior altered error by 27.42% in the medial/lateral direction, 42.22% in the anterior/posterior direction, and 1.61% in the superior/inferior direction.

Moving landmarks on one side of P5 0.4 mm laterally, 0.4 mm anteriorly, and 0.4 mm inferiorly altered strain error by 43.28% in the medial/lateral direction, 11.44% in the anterior/posterior direction, and 1.18% in the superior/inferior direction. Moving landmarks on one side of P5 0.8 mm laterally, 0.8 mm anteriorly, and 0.8 mm inferiorly altered strain error by 87.08% in the medial/lateral direction, 86.39% in the anterior/posterior direction, and 39.00% in the superior/inferior direction.

3.3.4.3 Image Registration Error

Registration errors for all physical phantom registrations were less than the size of one voxel. Phantoms scanned at an isotropic resolution of 0.8 mm had average registration error of 0.04 ± 0.03 mm. Phantoms scanned at an isotropic resolution of 0.4 mm had an average registration error of 0.02 ± 0.01 mm. Only phantoms 4 and 5 required rigid body registration (isotropic resolution of 0.4 mm) which had a registration error of 0.02 ± 0.02 mm.

Registration errors for all subjects were within acceptable limits. All registration errors were less than two voxels (1.6mm) with the majority being less than a voxel and an half. Normal subject neural tissue and bony tissue registration error were 0.13 ± 0.04mm and 0.06 ± 0.01mm, respectively. Pre-operative cervical myelopathy subject neural tissue and bony tissue registration error were 0.09 ± 0.03mm and 0.06 ± 0.02, respectively. Post-operative cervical myelopathy subject neural tissue and bony tissue registration error were 0.10 ± 0.07mm and 0.06 ± 0.01mm, respectively.

3.4 Discussion

Cervical myelopathy is an extremely debilitating and common spinal cord injury. Current medical treatment is surgically based with the aim of altering the mechanics of the spinal cord. However, little is known regarding *in vivo* spinal cord mechanics of the human. It was the aim of this study to quantify the *in vivo* spinal cord displacement and strain during physiologic motion utilizing MR imaging in both healthy subjects and those with cervical myelopathy who were undergoing surgical treatment.

Movement of the spinal cord is driven by the motion of the surrounding bony anatomy as shown by several groups.[7,15,60,61,69,70] There is consensus that in flexion the overall length of the spinal cord increases and in extension it decreases. However, there is some discrepancy as to how the spinal cord translates within the spinal canal. Breig believed spinal cord motion was due only to spinal cord deformation, where Smith and Reid believed it was a combination of deformation and sliding within the canal.[7,60,69] +Smith reported during flexion of the head and neck of the rhesus monkey, the cervical spinal cord moves towards the C4/5 intervertebral disc.[60] Reid also showed that the lower cervical spinal cord moves 1.4-4.5mm cephalad during flexion and 0-5mm caudally during extension.[69] Bilston and Yuan *et al.* both used MRI imaging to obtain spinal cord motion within the canal.[15,70] Bilston found at 20 degrees of flexion the C3 cervical cord displaced 1 mm caudally and the C7 cervical cord displaced 2 mm cranially. In extension of 40 degrees the C3 level displaced 1 mm caudally and the C7 only displaced 0.5 mm caudally, however the C6 cord displaced 4 mm caudally.[70] Yuan *et al.* investigated only flexion and found the C2 cord displaces 1.1-2.6 mm caudally and the C7 cord displaces 2.1-2.7mm cranially.[15]

Spinal cord displacements found in the current study agree in both direction and magnitude as previously reported literature. For healthy controls, where little impingement is present, most motion occurs in the superior/inferior direction. During flexion, the C3 level of the spinal cord moves cephalad and the C7 level moves caudal. The opposite occurs during extension where the C3 level moves caudally and the C7 level moves cephalad. Additionally, during extension and flexion, there seems to be a shift in displacement directionality around the C4 level. Both Smith and Yuan *et al.* report similar finding in their flexion data however, the location of directionality shift is located at the C5 level.[15,60] This difference in location is reasonable as Smith performed his study on rhesus monkeys and Yuan *et al.* had a sample size of five which smaller than our cohort. Due to the variability in spinal cord motion between subjects, a sample size of 5 may not be large enough to capture extremes.

Average principal strains ranging in magnitude from 5-20% in both flexion and extension agree with human axial strain magnitudes during flexion of 4-15% as reported by Yuan et al, Smith, Bilston, and Reid.[15,60,69,70] Bilston also reported extension strain magnitudes of up to 20%.[70] Additionally Kroeker et al reported axial cord strains ranging from 8 to 23% in a primate extension injury model [61]. Where our study differs is whether the strain is compressive or tensile. For all of these listed studies, strains were obtained along one plane of the spinal cord, usually at a mid-sagittal section. In this mid-sagittal section the average strain of the spinal cord across all studies agrees with the traditional hypothesis, “elongation in flexion, shortening in extension”. However if we consider how strains in all three directions contribute to the total strain of the spinal cord, as shown by maximum and minimum principal strains, a slightly different pattern of strain emerges.

Rather than having *only* compressive or tensile strain along the cord, as is often reported, each level of the cord experiences *both* compressive and tensile strains of roughly the same magnitude (Figure 15). This follows classical solid mechanics of a cylindrical bar under pure bending and was proposed by Breig.[7,71] However, if one looks at the 3D strain distribution it is not as straight forward as pure bending. There are locations of compression and tensile strains on both anterior and superior surfaces of the cord. This is because the various neural attachments of the spinal cord, such as dentate ligaments and neural roots cause local strains. In fact, Bilston reported that even in their 2D measurements, specific levels of the spinal cord experienced compressive strains while the adjacent levels experienced tensile strains.[70]

Mild impingement of the cord also produces both compressive and tensile strain. We can see in the healthy subject shown in Figure 16, the dura buckles close to the spinal cord at the C56 and C67 posterior canal. This causes mild compressive strains on the spinal cord but also causes tensile strains just below the level of compression. Bhatnagar reported similar findings in 3D strains of the contusion injuries in rats.[11]

In addition to characterizing the cord motion of healthy subjects we also characterized cord motion of the cervical myelopathy subjects before and after surgical intervention. As far as we are aware, we are the first group to report spinal cord movement during flexion and extension of subjects with cervical myelopathy. While these data were not statistically different, trends are apparent. First, cervical myelopathy subjects had less cord motion in general than healthy subjects. We believe this is due to the decrease in spinal canal space in patients with cervical myelopathy. This was measured two ways in this study. First by qualitative clinical grading and then by quantitative cord canal ratio measurements. Both methods showed the cervical myelopathy cohort had significantly narrower spinal canals in neutral, flexion and extension than the healthy cohort. This leaves very little room for the cord to slide along and in the canal. Instead it is often pinned between the anterior and posterior sides of the canal, resulting in limited motion of the cord during flexion and extension.

As shown in healthy subjects, even the slightest amount of impingement can induce spinal cord strain. Specifically at the C5 level, cervical myelopathy subjects have higher maximum principal strain than healthy subjects in both flexion and extension. This is interesting as the most common location for cervical myelopathy is at the C4-C6 levels, and was the most common location of stenosis in our patients. Additionally as we hypothesized, compressive strain was slightly higher than controls across all spinal levels in both flexion and extension. This increase in strain along the cord in cervical myelopathy subjects is most likely a contributing factor to functional deficits. Studies have shown that compression and strain on the spinal cord negatively affect the neural signaling.[72,73] In fact, when our subjects self-reported their ability to perform daily tasks via the JOA Score and Nurick Score, cervical myelopathy subjects perform significantly lower than healthy controls.

As hypothesized, surgical intervention did affect spinal cord motion and strain. It tended to improve cord displacement, allowing it to move within the canal. However, the cord did not have the same displacement distribution as normal subjects. There was an increase in motion both in flexion and extension at the C4-C5 levels but minimal motion at C7. This is opposite of the normal patient and may explain why the post-operative strains, while more evenly distributed along the cord, are slightly higher than both pre-operative and normal subjects. This increase in strain may also indicate why JOA and Nurick scores did not improve after surgery.

To assess the fact that we had a 50% follow-up, we looked at how each cervical myelopathy subject's strain changed after surgery. The sole subject who had tensile and compressive strain reduction in both flexion and extension was the only subject who had a single level ACDF operation. All other subjects in the post-operative group had multi-level ACDF operations. This indicates two things. First, having fewer affected levels is better for post-operative strain outcomes as the cord is less compressed at multiple levels. Second, single level operations allow for more spine motion which could affect, and possibly reduce, adjacent level cord strain if the affected level is free to move. The trend that surgical intervention alters cord displacement and strain but does not restore the levels to that of normal subjects also indicates why some patients do not get relief from a primary surgery. As all of our post-operative subjects had an anterior surgical approach it would be efficacious to assess how spinal cord displacements and strains change with posterior intervention using patient data and/or finite element modeling.

All studies have limitations and ours is no exception. First our sample size was low and had a larger sample size been used statistical significance may have been met on a larger number of data. A power analysis had been performed based on previous cord strain studies indicating a sample size of 10 to be sufficient, however, 3D data variation was larger than expected. This variation is most likely a result of patient variability and error in strain acquisition. Extensive assessment of the image registration and strain calculation was performed as described in the methods. The largest source of error is from variations in manually choosing landmarks for image registration. Ideally this could be eliminated if an automated method was used. Additionally, having a 50% follow-up is not ideal. Finally, our MR imaging is not a true “dynamic image” and only gives a single frame snapshot of how the spinal cord moves at the extremes of motion during flexion and extension. Even with these limitations, clear trends and differences could be seen between all three groups giving us a successful and important first look into *in vivo* 3D motion and strains of the spinal cord.

In conclusion we have characterized the three dimensional movement and strains of the normal, pre- and post-operative myelopathic cervical spinal cord during flexion and extension. This information is extremely beneficial for understanding the etiology of cervical myelopathy and can be used to help improve current treatment of cervical myelopathy. We aim to utilize this data for building normal and cervical myelopathic finite element models of the spinal cord to evaluate the effectiveness of various surgical techniques for cervical myelopathy.

CHAPTER 4: DEVELOPMENT OF NATIVE FE MODEL

4.1 Introduction

Ethical reasons prevent invasive *in vivo* testing on humans, pushing researchers to develop both animal and finite element (FE) models of cervical myelopathy. Much of the animal modeling has focused on the electrophysiology and histological changes after spinal cord compression with only a subset investigating *in vivo* spinal cord mechanics.[61,64,74–78] Even fewer researchers, including the study in Chapter 3, have investigated *in vivo* human spinal cord mechanics.[12,14,15] Due to lack of animal models and human *in vivo* data, FE modeling of the spinal cord has been used to investigate stress and strain distributions.[78–83]

4.1.1 Previous FE Models of the Spinal Cord

Most cervical spinal cord FE models to date have focused on modeling the injured spinal cord. There are only three studies we are aware of which use FE modeling to investigate healthy spinal cord mechanics.[84–87] Scifert et al. was the first to do this, in 2002, by creating a 3D model of the C5-C6 spinal unit incorporating the spinal cord, dura, dentate ligaments, and “connecting fibers”. Scifert et al. then put the FE model into flexion and extension to determine the axial strain in the cord during normal motion.[87] Sparrey et al. utilized a 2D FE model of the spinal cord cross-section to determine how stress and strain distributions are different in white and grey matter when the spinal cord is exposed to compressive loading.[85] Similar to Scifert et al., Bahramshahi et al. also investigated how flexion and extension motions affect spinal cord stresses using a 3D FE model, but over a larger spinal segment spanning levels C3-C5.[86]

There is one other study which is worth noting for its completeness, but does not fall into the category of investigating healthy spinal cord mechanics. Henao et al. have developed a 3D T1-S1 spinal column model which incorporates the thoracic and lumbar spinal cord, pia, dura, and dentate ligaments. This model was then modified to simulate scoliotic anatomy on which surgical interventions are performed to determine the amount of stress and strain occurring on the spinal roots during the procedures.[88]

Each of these models have provided an important incremental step into both understanding spinal cord mechanics and developing better, more comprehensive FE models of the spinal cord. However, none of these studies incorporated a full spinal segment, i.e. cervical, thoracic, or lumbar, in physiologic motion to model the mechanics of the healthy spinal cord.

4.1.2 Study Aims

The aim of this study is to develop a complete FE model of the C2-T1 cervical spine. This model will incorporate both musculoskeletal and neurological anatomy including the vertebrae, discs, ligaments, spinal cord, pia, dura, dentate and meningovertebral ligaments. This will enable us to predict the spinal cord stresses and strains present during physiological movement in healthy individuals.

4.2 Methods

4.2.1 Spine Finite Element Model

The FE model initiated with a FE model of the C2 to T1 spine which was developed and validated previously in our lab (Figure 22).[89,90] Briefly, this model consists of roughly 116,000 elements. The vertebral bodies were modeled as rigid bodies and meshed with four-noded rigid elements. The posterior processes were meshed with eight-noded brick elements and modeled as cortical bone. Intervertebral discs were also meshed with eight-noded brick elements and fibrous lamellae were included in the disc material properties. Facet regions were modeled with contact surfaces which simulated the contact and thickness of articular cartilage. All ligaments were modeled as tension only truss elements.

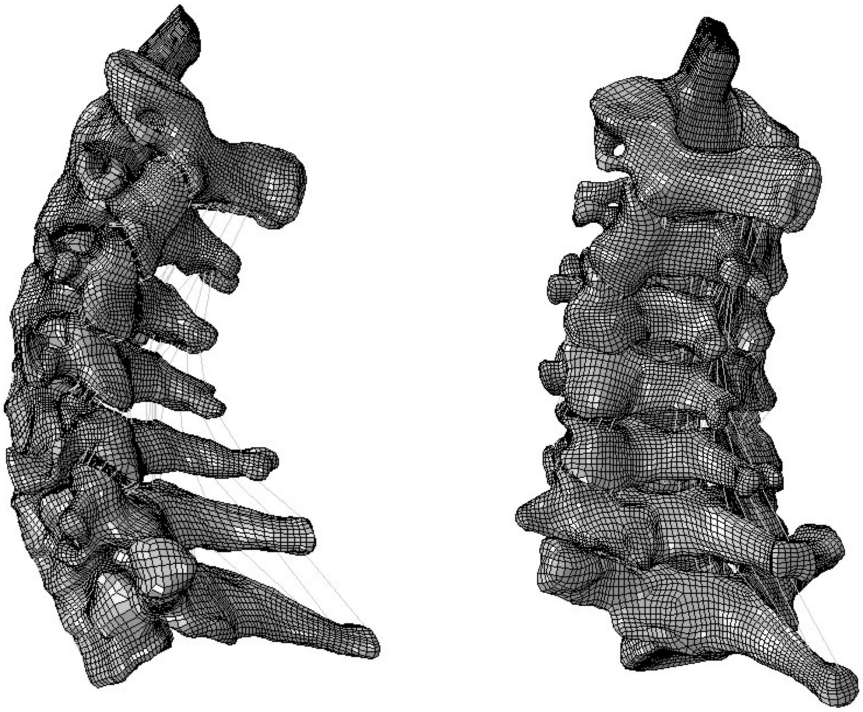

Figure 22:Previously created and validated C2-T1 spine model.[89]

4.2.2 Neural Anatomy Model

4.2.2.1 Spinal Cord

The spinal cord anatomy was based on histologic cross-sections of the C3, C5, and C7 spinal cord. Images of the histologic cross-sections were imported into PTC Creo (PTC Needham, MA).[91] These cross-sections were then traced and a sweep tool was used to connect the cross-sections. The spinal cord was then scaled to fit the anatomy of the previously mentioned C2-T1 FE spine model. Additionally, spinal cord roots were added at locations which matched the size and anatomy of this FE model. A stereolithography surface file of the spinal cord was exported from PTC Creo and imported into custom written software for meshing the spinal cord with eight-noded brick elements. A multi-block method was used to mesh the spinal cord and mesh seeding was set to obtain a total of 22,551 elements (Figure 23).[92]

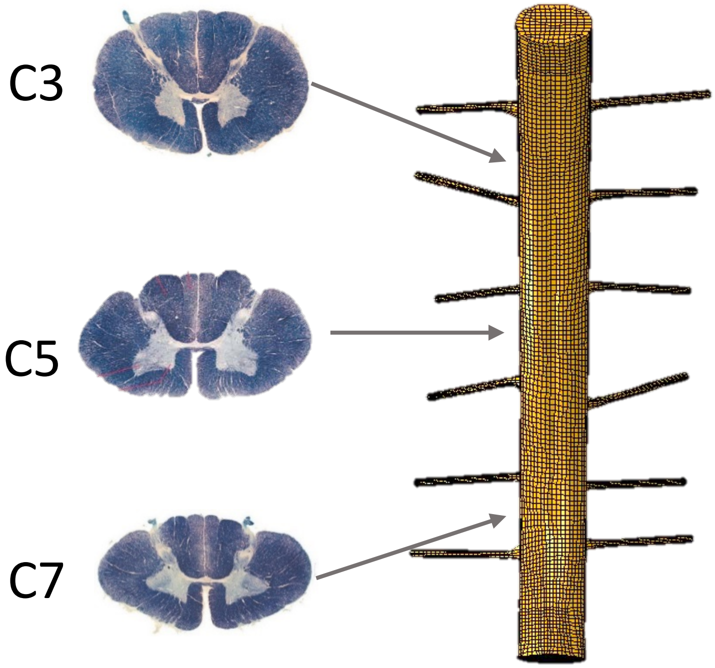

Figure 23: Histologic cross-sections (left) used for cord anatomy and meshed cord (right).

4.2.2.2 Pia

As the pia is a thin membrane, it was meshed using four-noded large strain shell elements. The pia lies directly on and is attached to the spinal cord, therefore the pia mesh was created by extracting a surface mesh from the mesh of the spinal cord. This allowed the nodes of the spinal cord and pia to be shared, bonding the pia to the spinal cord (Figure 24). The pia mesh consisted of 9,592 elements with thickness of 0.1 mm.

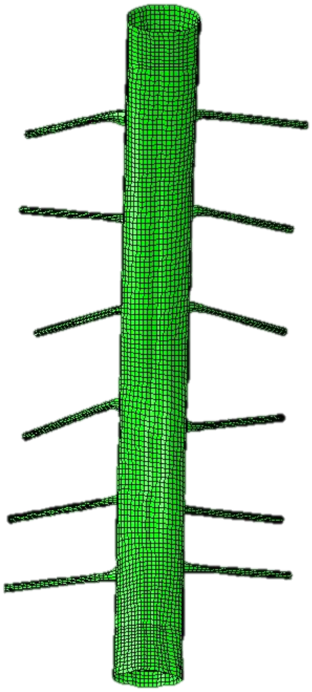

Figure 24: Finite element mesh of pia.

4.2.2.3 Dura

As the dura abuts the spinal canal, the interior bounds of the canal were used to guide the definition of the dura using techniques similar to those outlined for the cord definition. Tubular dura regions surrounding the roots were added to this surface to match the neural root placement of the previously described spinal cord. As the dura is also membranous it was meshed with four-noded large strain shell elements using in house multi-block software.[92,93] The dural surface was connected to the end of the cord at the superior (C2) and inferior (T1) surfaces and at the end of every root (Figure 25). This allowed for enclosure of the CSF. The dura mesh consisted of 10,096 elements with thickness of 0.4 mm.

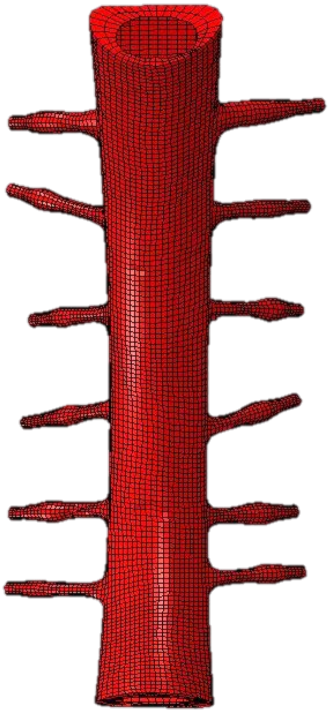

Figure 25: Finite element mesh of the dura.

4.2.2.4 Cerebral Spinal Fluid

The CSF was modeled as a pressurized fluid filled cavity with no fluid exchange. The initial pressure of the CSF was set to 20 mmHg or 2.6 kPa. This is equivalent to the CSF pressure of a lumbar puncture. While no data has been reported on cervical puncture, it is important to note that lumbar puncture pressure varies little with patient positioning making it a reasonable estimation.[31]

4.2.2.5 Neural Ligaments

Both the meningovertebral and dentate ligaments were modeled using non-compressive truss elements with cylindrical cross-sections (Table 6).[32,34] The location and number of meningovertebral ligaments included was based on cadaveric anatomic studies.[34] For a meningovertebral ligament to be included, it had to be present in at least 50% of the population. The dentate ligaments were located on the lateral sides of the spinal cord, halfway between each nerve root (Figure 26).

Table 6: Cross sectional area of neural ligaments.

Ligament	**Cross Section (mm^2)**
Meningovertebral C1-C2	7.107
Meningovertebral C3-C4	0.2436
Meningovertebral C4-C5	0.2574
Meningovertebral C5-C6	0.1744
All Dentate	0.00785

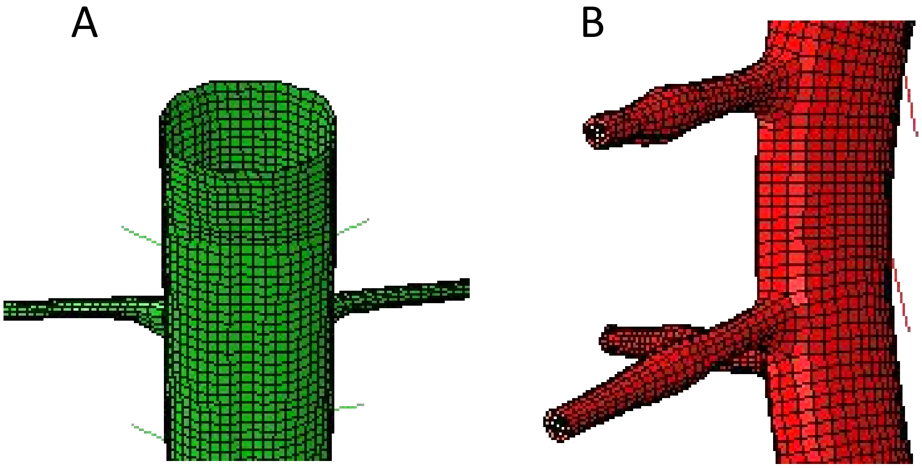

Figure 26: Zoomed in view of the pia to show dentate ligaments (A) and dura to show meningovertebral ligaments (B).

4.2.3 Convergence Study

A convergence study was performed to ensure solution stability and computational efficiency. The size of the pia and dura meshes are a direct result of the size of the cord mesh as they are either extruded from the cord, in the case of the pia, or use the same multi-blocks and seeding for mesh generation, in the case of the dura. Therefore, only a convergence study on the spinal cord mesh was needed. Seven spinal cord meshes of sizes ranging from 252 to 36,356 were created. To mimic general impingement, a rigid cylindrical impactor of 12.1 mm radius was displaced 2.5 mm into the posterior spinal cord at the C5/6 level. The spinal cord was fixed in all directions along the anterior surface and at the superior and inferior ends (Figure 27). Displacement and von Mises Stress values were taken at three nodes located under the impactor. These were located anterior, middle and posterior along a mid-sagittal cut at least one element from the surface of the spinal cord. Solution stability was reached with roughly 9,000 elements however as small impingements may occur, a higher mesh refinement of 22,551 elements was used (Figures 28 and 29).

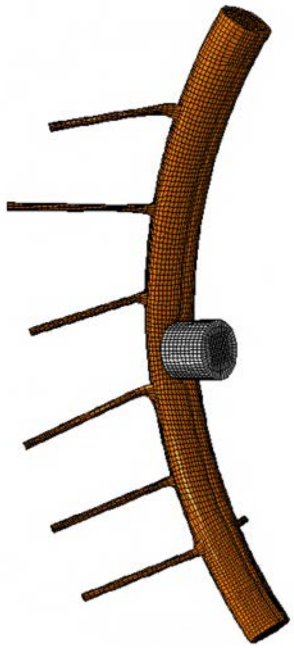

Figure 27: Convergence model showing indentation of impactor on spinal cord.

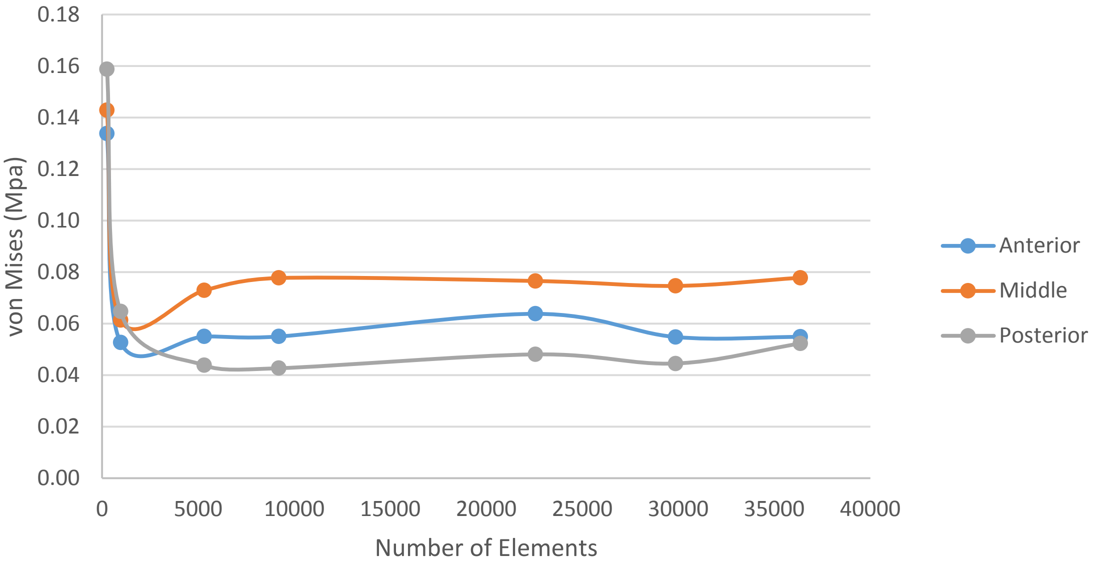

Figure 28: Convergence of von Mises stress at anterior, middle, and posterior node locations under impactor.

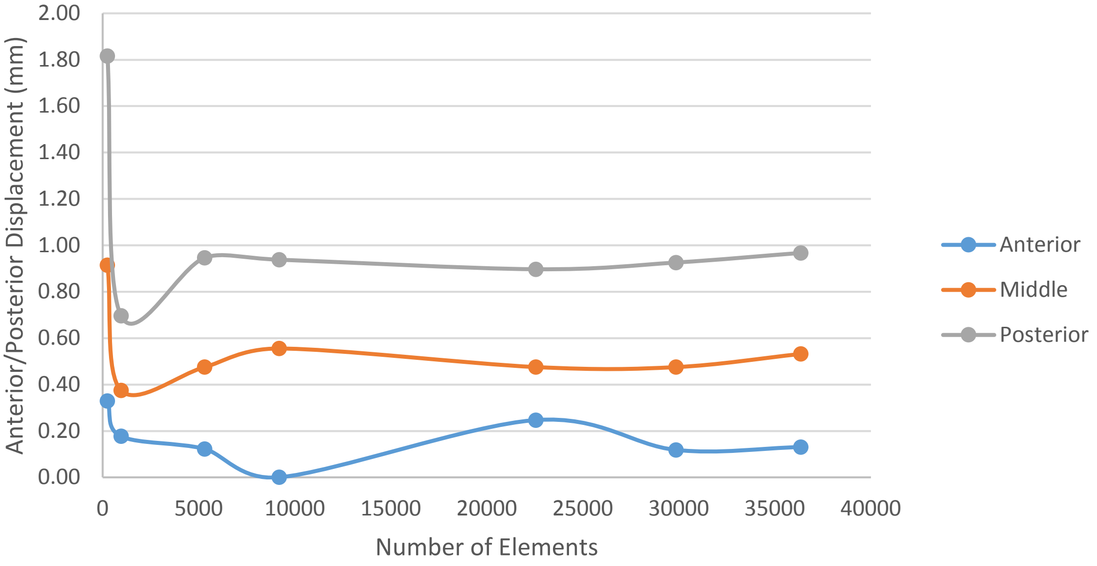

Figure 29: Convergence of anterior/posterior displacement at anterior, middle, and posterior node locations under impactor.

4.2.4 Material Properties

Material properties are summarized in Table 7 at the end of this section.

4.2.4.1 Spinal Cord

The spinal cord was modeled as a hyper-elastic Mooney-Rivlin material with the strain energy potential (U) of the following form, excluding effects of temperature:

$$U = C_{10}(\bar{I}_1 - 3) + C_{01}(\bar{I}_2 - 3) + \frac{1}{D_1}(J - 1)^2 \qquad (12)$$

Where C_{10}, C_{01}, and D_1 are material parameters, J is the total volume ratio, and $\bar{I}_1$ and $\bar{I}_2$ are the first and second deviatoric strain invariants.[94] No distinction was made between the grey and white matter as it is unclear how their material properties differ.[40,95] The material parameters, C_{10}, C_{01}, and D_1, were calculated using the following relationships, assuming incompressibility of materials.

$$\nu = \frac{\frac{3k_0}{\mu_0} - 2}{\frac{6k_0}{\mu_0} + 2} \qquad (13)$$

$$k_0 = \frac{2}{D_1} \qquad (14)$$

$$\mu_0 = 2\,(C_{10} + C_{01}) \qquad (15)$$

Where k_0 and μ_0 are, respectively, the initial bulk modulus and initial shear modulus of the material and ν is the Possion's ratio of the material. Using the following approximate equation, we can relate Young's Modulus (E) of the material to the material properties C_{10} and C_{01} and relate C_{10} to C_{01} as follows.[96]

$$E \approx 6(C_{10} + C_{01}) \qquad (16)$$

$$C_{01} = \tfrac{1}{4} C_{10} \qquad (17)$$

The spinal cord was assigned a Young's Modulus of 0.44 MPa and Poisson's ratio of 0.3. The Young's Modulus was based on published FE models[81] and unpublished mechanical testing of human spinal cord. The Poisson's ratio was based on bovine tensile testing.[40,97] The spinal cord was given a density of 1040 kg/m^3 based on previous FE modeling.[98]

4.2.4.2 Pia

The pia is also highly non-linear and was modeled as a Mooney-Rivlin hyperelastic material and material parameters C_{10}, C_{01}, and D_1 were calculated as previously mentioned. The Young's Modulus was assumed to be 2.3 MPa based on tissue testing of rabbit pia.[9] No data has been reported on the pia Poission's ratio so it was assumed to have the same value as the dura, 0.45.[99] The density of the pia was set at 1130 kg/m^3 based on previous FE modeling.[98]

4.2.4.3 Dura

The dura was also modeled as a hyper-elastic Mooney-Rivlin material with material parameters C_{10}, C_{01}, and D_1 calculated as mentioned. The Young's Modulus was obtained from literature of canine tissue level tests and was assumed to be 5 MPa.[28] The Poisson's ratio, 0.45, was also based on literature of bovine dural tensile testing.[99] The density of the dura was set at 1130 kg/m^3 based on previous FE modeling.[98]

4.2.4.4 Cerebral Spinal Fluid

As previously stated the CSF was modeled as a fluid filled cavity. As the CSF is comprised mostly of water the mechanical properties were assigned to be equal to those of water.[29] The fluid bulk modulus was assumed to be 2200 MPa and the density is assumed to be 1000 kg/m^3.[100]

4.2.4.5 Dentate Ligaments

The dentate ligaments were modeled as linear elastic. The Young's modulus was assumed to be 5.8 MPa and density 1130 kg/m^3 based on previous FE modeling.[81,98]

4.2.4.6 Meningovertebral Ligaments

The meningovertebral ligaments were also modeled as linear elastic. The meningovertebral ligaments have been reported to be stiffer than other neural tissues and more similar to that of the spinal ligaments.[34,81] With that knowledge, the Young's modulus was based on previous FE modeling and set to 35.7 MPa and the density was based on spinal ligament data and set to 670 kg/m^3.[34,81,101]

4.2.5 Boundary Conditions

The FE model was run with Abaqus/Standard 6.14 using the dynamic stress/displacement analysis option with quasi-static application. The model was aligned such that the axial plane of C4 and C5 vertebral bodies was perpendicular to the +y axis with +z pointing anteriorly and +x pointing to the left. The T1 vertebrae is fixed in all directions. In extension the C2 vertebrae was rotated 19.82° in the –x direction and in flexion 19.88° in the +x direction. These rotations correspond to the average healthy subject neck rotation presented in Chapter 3. Frictionless general contact was enforced for the entire model. The spinal cord, dura, and pia were not constrained and allowed to slide and stretch within the canal.

Table 7: Material properties of neural elements.

Feature	Material Type	Material Property	C_{10} (MPa)	C_{01} (MPa)	D_1 (1/MPa)
Cord	hyperelastic Mooney-Rivlin	E = 0.44 MPa, $\nu = 0.45$	0.06	0.01	6.3
Pia	hyperelastic Mooney-Rivlin	E = 2.3 MPa, $\nu = 0.45$	0.31	0.08	0.27
Dura	hyperelastic Mooney-Rivlin	E = 5.0 MPa, $\nu = 0.45$	0.67	0.17	0.12
CSF	fluid cavity	$\rho = 1.0\ (10^{-6})\ \text{kg/mm}^3$	--	--	--
Dentate Ligament	linear elastic	E = 5.3 MPa	--	--	--
Meningovertebral Ligament	linear elastic	E = 35.7 MPa	--	--	--

4.3 Results

4.3.1 Model Validation

While the musculoskeletal motion was previously validated, the motion of the neural anatomy model needed to be validated. Average displacement of the spinal cord within the canal at corresponding vertebral bodies was compared against spinal cord motion obtained in Chapter 3 of healthy subjects. The superior/inferior FE spinal cord displacement in both flexion and extension matched the imaging data extremely well (Figures 30 and 31). The medial/lateral and anterior/posterior displacements were sufficiently close to that of the imaging data, being within a standard deviation of the average for most levels (Fig 32 and 33).

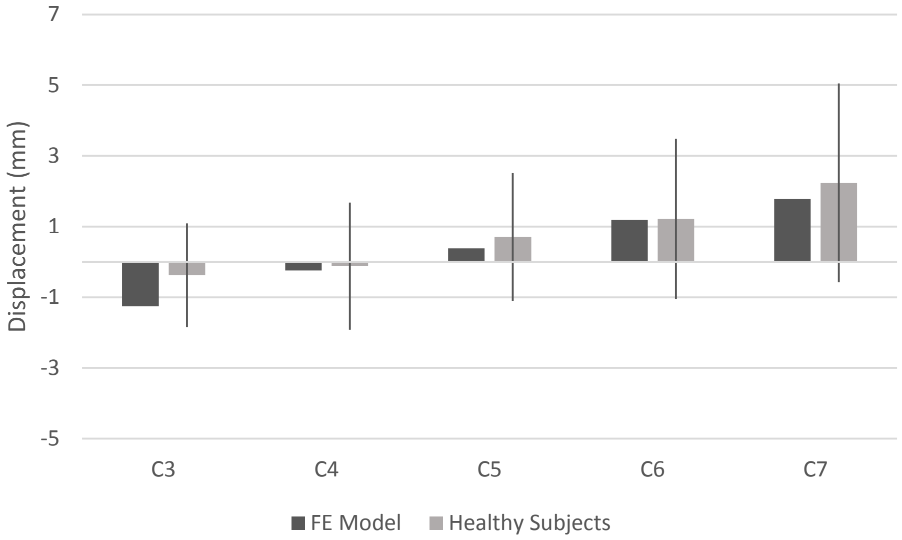

Figure 30: Superior/inferior spinal cord displacement during flexion. Patient Data is presented as mean ± one standard deviation.

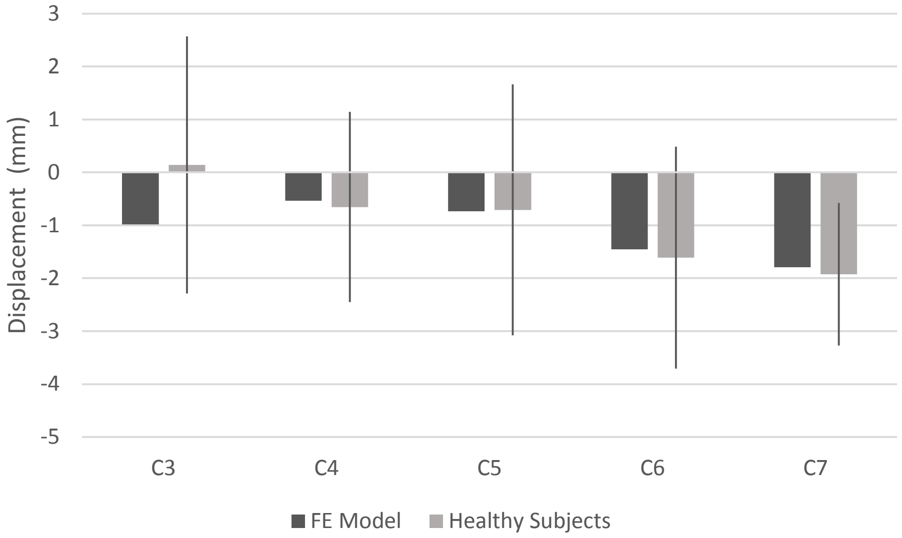

Figure 31: Superior/inferior spinal cord displacement in extension. Patient data is presented as mean ± one standard deviation.

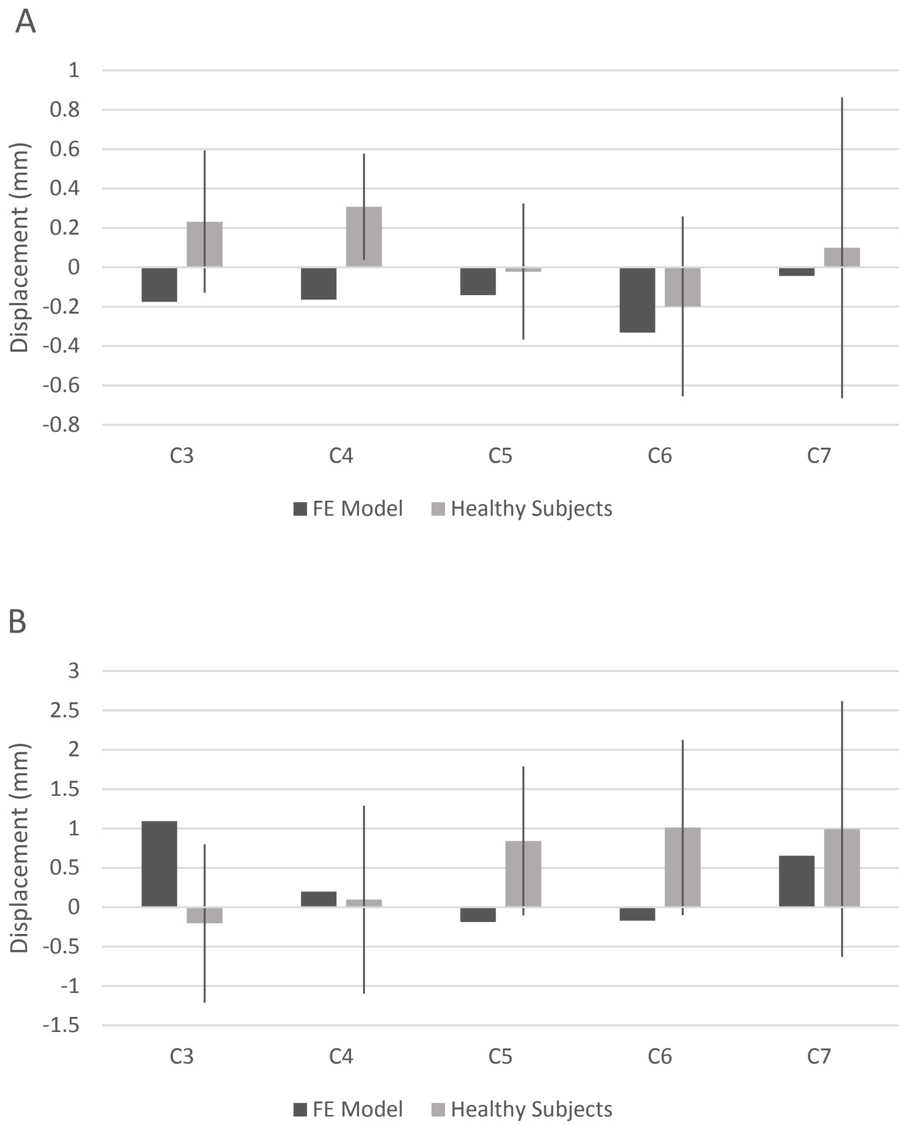

Figure 32: Medial/lateral (A) and anterior/posterior (B) displacement of the spinal cord in flexion. Patient data is presented as mean ± one standard deviation.

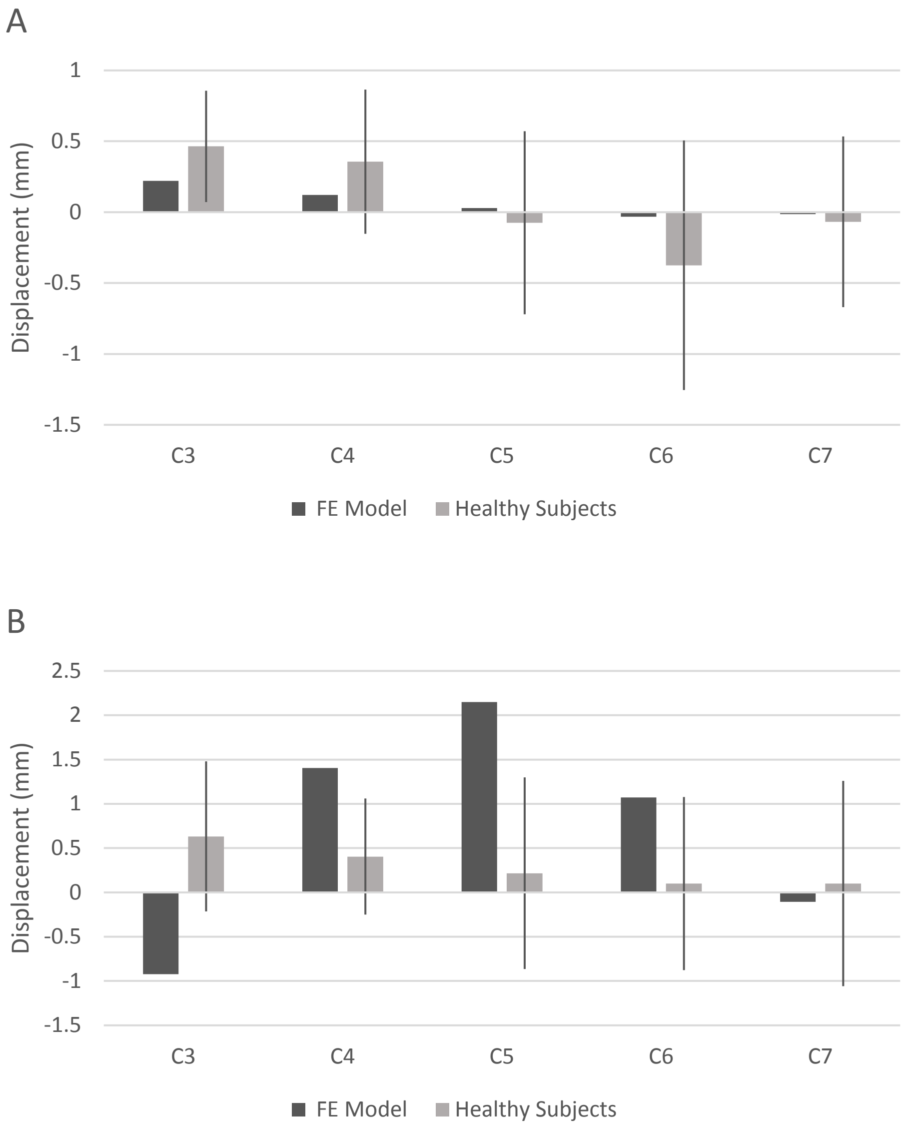

Figure 33: Medial/lateral (A) and anterior/posterior (B) displacement of the spinal cord in extension. Patient data is presented as mean ± one standard deviation.

4.3.2 Spinal Cord Strain

Spinal cord principal strains in both flexion and extension were highest at the C4, C5, and C6 levels. The distribution of strain follows that of a cylinder in pure bending, where maximum and minimum strain magnitudes are roughly equal (Figure 34). In flexion, the maximum tensile principal strain occurs on the posterior side of the cord where the maximum compressive principle strain occurs on the anterior side (Figure 35). The opposite occurs in extension; where maximum principal tensile strains occur on the anterior surface and maximum principal compressive strains on the posterior surface (Figure 36). While strain patterns are similar to those seen in healthy control image data, the average of the strains at each level are lower in the FE model than those reported in our imaging study (Table 8).

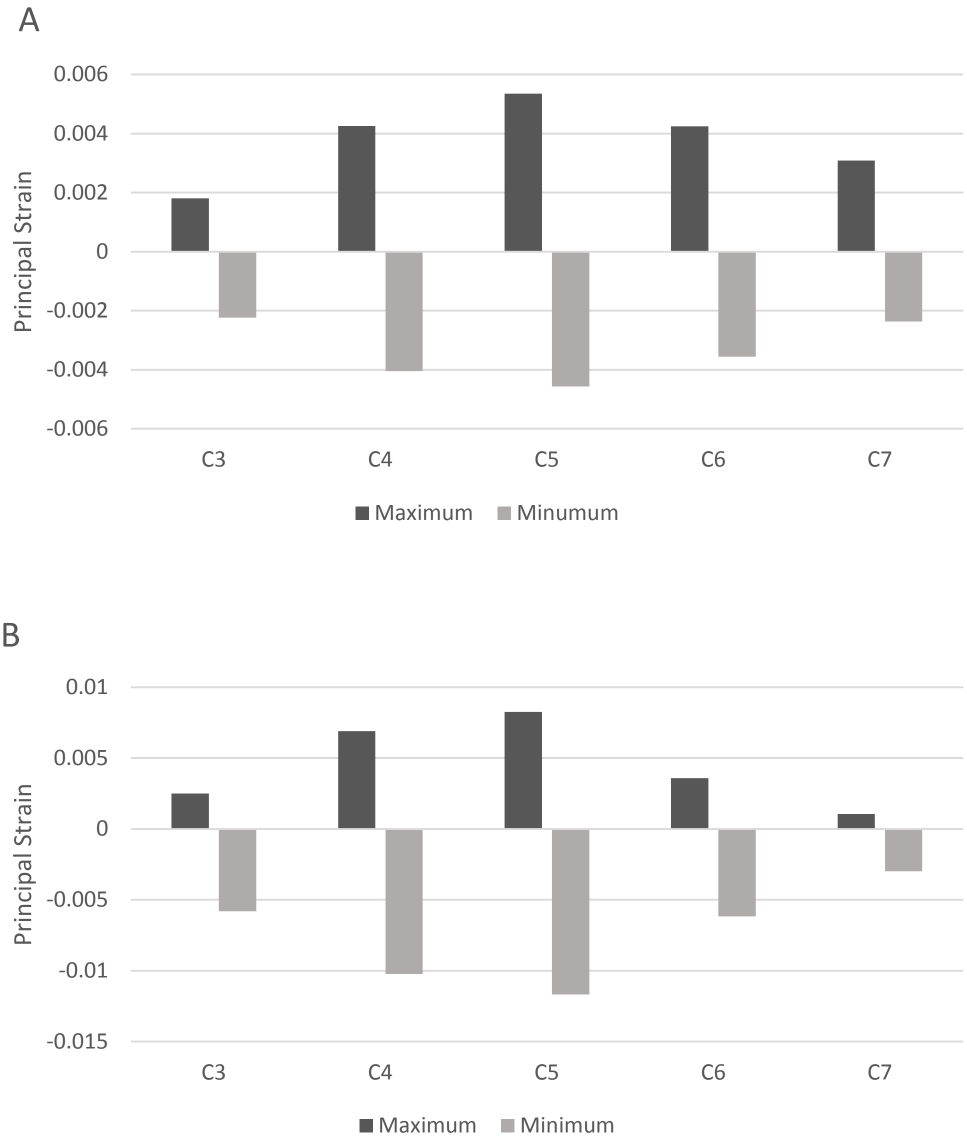

Figure 34: Maximum and minimum principal strain of spinal cord in flexion (A) and extension (B).

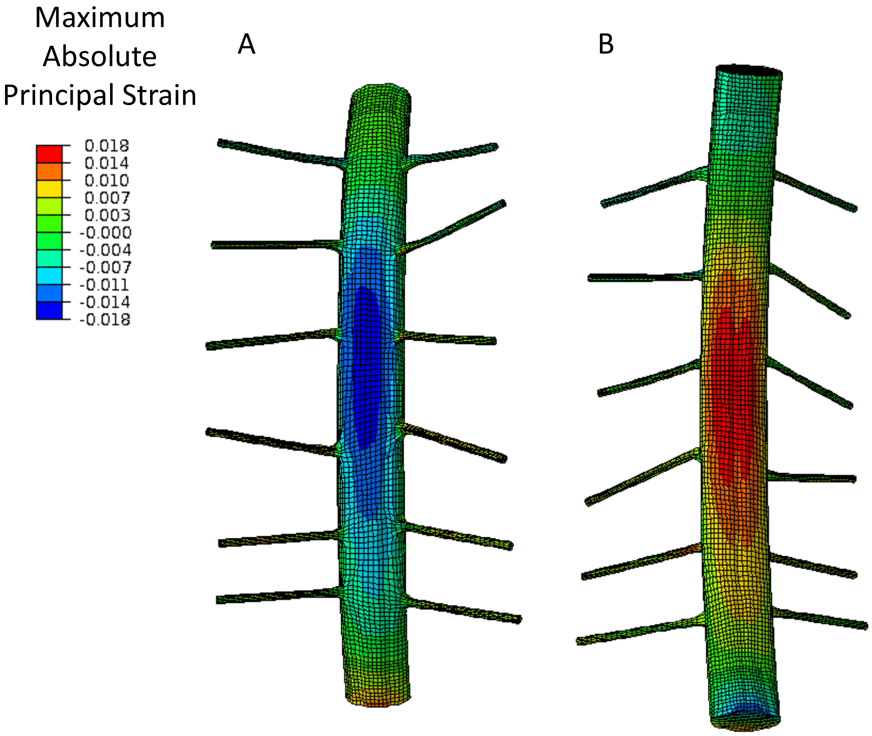

Figure 35: Maximum absolute principal strain of spinal cord in flexion on anterior (A) and posterior (B) spinal cord.

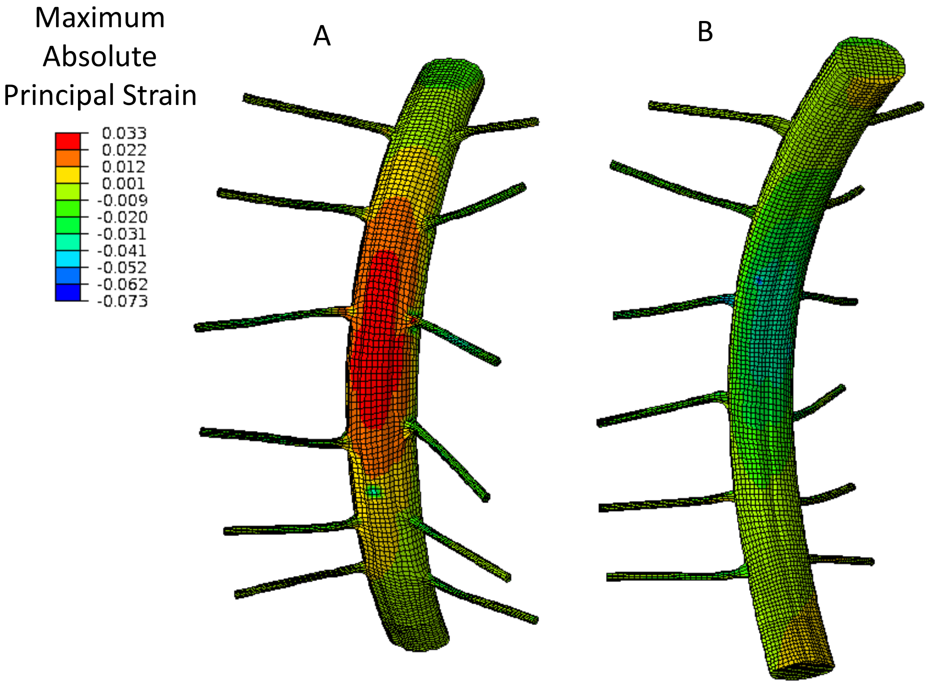

Figure 36: Maximum absolute principal strain of spinal cord in extension on anterior (A) and posterior (B) spinal cord.

Table 8: Average principal strains of FE model and MR imaging in flexion and extension.

Flexion

	FE Model Principal Strain		**MR Imaging Principal Strain**	
Level	*Min*	*Max*	*Min*	*Max*
C3	-0.0058	0.0025	-0.10 ± 0.091	0.13 ± 0.046
C4	-0.0102	0.0069	-0.12 ± 0.093	0.10 ± 0.049
C5	-0.012	0.0083	-0.12 ± 0.094	0.12 ± 0.039
C6	-0.0062	0.0036	-0.14 ± 0.15	0.13 ± 0.060
C7	-0.0030	0.0011	-0.20 ± 0.17	0.11 ± 0.056

Extension

	FE Model Principal Strain		**MR Imaging Principal Strain**	
Level	*Min*	*Max*	*Min*	*Max*
C3	-0.0022	0.0018	-0.093 ± 0.060	0.13 ± 0.053
C4	-0.0040	0.0043	-0.15 ± 0.091	0.076 ± 0.021
C5	-0.0046	0.0053	-0.15 ± 0.080	0.095 ± 0.048
C6	-0.0036	0.0042	-0.16 ± 0.049	0.14 ± 0.084
C7	-0.0024	0.0031	-0.20 ± 0.12	0.11 ± 0.072

During extension, there are two localized regions of high compressive strain. The first of these occurs on the anterior surface of the cord and is caused by bony impingement. The second is located on the posterior surface and is a result of dural buckling (Figure 37).

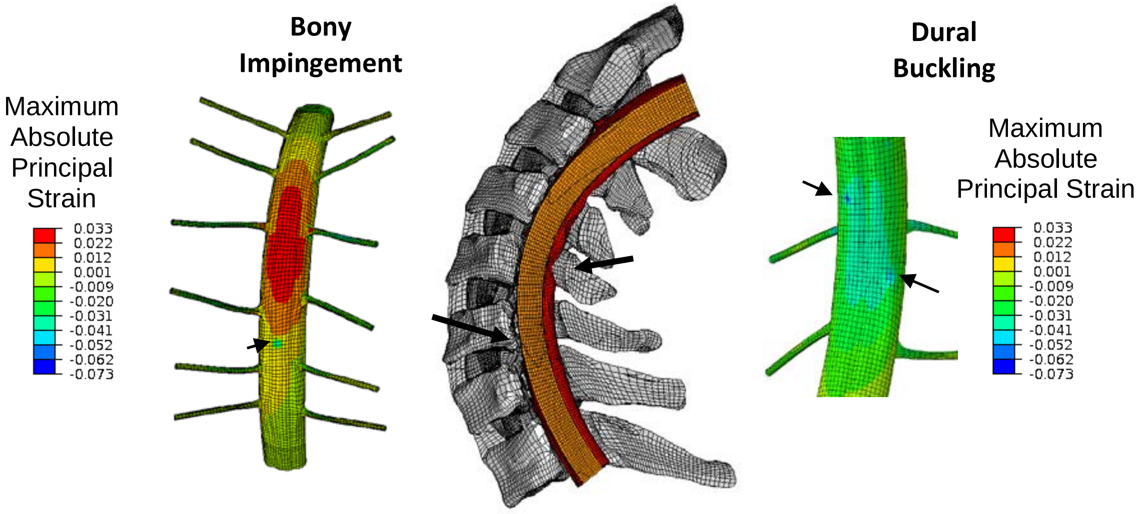

Figure 37: Local strain increases due to C6 bony and dural impingement.

4.3.3 Spinal Cord Stress

Stress distributions follow the strain distributions with the highest von Mises stress located at the C4-C6 levels in flexion and extension (Figure 38). In extension, compression of the posterior vertebral body at C6 and dura buckling also induces local increases in stress. Higher von Mises stress magnitudes are seen in extension than in compression.

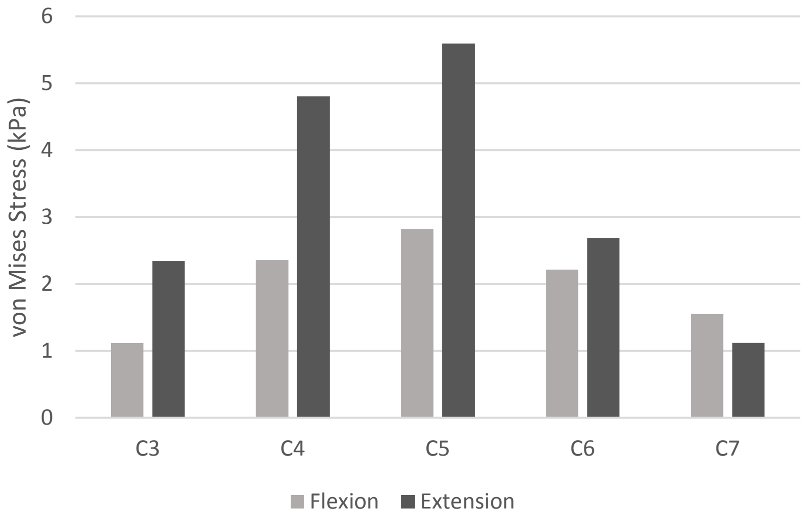

Figure 38: von Mises stress in spinal cord during flexion and extension.

4.4 Discussion

In this study we developed a comprehensive finite element model of the healthy cervical spine and spinal cord which replicates the mechanics of the healthy musculoskeletal and neurologic tissues during physiologic motion. While other groups have used FE modeling to investigate spinal cord injury mechanisms and strains across a functional unit of the spine, this is this first study we are aware of which has developed a FE model of a complete spinal section with the aim of investigating spinal cord mechanics during physiologic motion. Additionally, this is the first FE model of the spinal cord which has been validated with *in vivo* spinal cord displacements obtained from MR imaging.

This FE model predicts the superior/inferior spinal cord displacements in both flexion and extension well, when compared against spinal cord displacements obtained from *in vivo* MR imaging of healthy subjects. In both literature and in our MR imaging study, we found the spinal cord moves primarily in the superior/inferior direction.[7]

Therefore, it was imperative that our model match this motion over all other directions. Flexion and extension spinal cord displacement in the medial/lateral and anterior/posterior directions sufficiently matched that of the MR imaging data, being within a standard deviation at most levels. It is not surprising that the FE model did not match in these two directions as well as the superior/inferior direction for several reasons. First, the placement of the spinal cord within the canal was estimated. We expect changes in this placement both medial/laterally and anterior/posteriorly would slightly affect the displacement of the cord during motion. Placement of the nerve roots in the FE model, which drive the superior/inferior motion of the cord, are more likely to match the subject anatomy as nerve root location is based the foramen at each vertebral level. Additionally, the coupled motion which occurs in our model during flexion and extension may not be exactly the same for every person due to subject specific anatomy. One of the main reasons more anterior/posterior spinal cord displacement occurs in the FE model is due to patient positioning in the MR. Patients are lying on their backs during imaging, resulting in the spinal cord laying slightly more posterior in the canal due to gravity than if they were standing upright. The FE model does not include this gravitational force, allowing the cord to move more.

This FE model of the cervical spinal cord shows the same patterns of spinal cord strain seen in healthy subjects which was described in Chapter 3. First, in both flexion and extension the spinal cord emulates a bar in pure bending, just as the strains obtained from healthy controls did. This shows more complicated strain patterns are present than the traditionally accepted “tension in flexion, compression in extension” paradigm.[7] As the spinal canal goes into flexion the posterior side of the cord stretches and the anterior side is compressed as lordosis is lost. The opposite occurs in extension. It is also important to note that both the largest tensile and compressive principle strains and von Mises stresses occur at the C4-C6 levels in both flexion and extension. This is the location most often affected by cervical myelopathy, indicating that as spinal cord strain and stresses are already high here during normal motion, the cord may be predisposed to injury.

Along those lines, one of the most exciting and promising aspects of this model is that it accurately represents local spinal cord compression due to bony impingement and dural buckling which was seen in our MR imaging study. In extension, bony impingement of the C6 vertebrae causes local compressive strains in an area which is otherwise in tension. If we look at the posterior side of the FE model in extension, we see buckling of the C4-C6 dura which is also present in healthy subjects (Figure 39). This is important as it shows the ability of this model to replicate the complex loading of the spinal cord.

Figure 39: Sagittal slice of a T2 weighed MR image of healthy subject in extension. Arrow highlights dural buckling at the C4-C6 level.

When comparing the average principle strain magnitudes obtained from the FE model to those obtained from our MR imaging study, the strains obtained from MR imaging are ten to one hundred times larger than the FE model. While the model is correctly predicting the spinal cord displacement and strain patterns, it is underestimating strain magnitudes. However, our strains are comparable with those of previously published FE models investigating spinal cord mechanics during physiologic motion. Scifert et al. developed a C5-C6 FE model of the spine and spinal cord. Their motion segment was subjected to 3.5º of flexion which is equivalent to 23º across the C0-T1 levels and is similar to the current study's flexion. Rotational displacement was not given for extension. They reported anterior and posterior spinal cord strains in the range of -0.8 to 2.0% which is similar to the maximum absolute principal strains in our model.[87] Scifert et al. also reports increases in strains due to disc impingement during both flexion and extension. Bahramshahi et al. is the only other group to use FE modeling to investigate spinal cord mechanics during normal motion and created a C3-C5 model. They too report strains similar to our model, ranging from -1% to 0.9%.[86]

It is interesting that all these FE models report similar strain levels even though both Scifert et al. and Bahramshahi et al. used linear elastic material properties for their neural anatomy and we used hyper-elastic Mooney-Rivlin material properties. This sheds light on the fact that none of our material models fully capture the viscoelastic properties of the spinal cord.[102,103] Additionally, due to limited reported tissue properties for the spinal cord, each of these models incorporated Young’s modulus and Poisson’s ratio values based on the work of Bilston et al.[24] This may be an indication that further study is needed to fully characterize the tissue level mechanics of the spinal cord.

As with all studies, ours is not without limitations. First our model is based on one cadaveric subject anatomy and therefore cannot capture the diverse anatomical differences present across the general population. Additionally, the anatomy of the spinal cord and the associated neural tissues was approximated from literature. Therefore, the positioning of the spinal cord and dura within in the canal and chosen locations of spinal cord roots may differ from the true location for this subject. Secondly, a combination of human and animal tissue properties were used due to lack of published material properties for the human neural tissues. Finally, no muscle forces were incorporated in this model. However, both musculoskeletal and neural components of this model have been fully validated and predict physiologic motion.[89] Specifically this is the first FE model of the spinal cord which has been validated against *in vivo* human data.

In conclusion, to our knowledge, we are the first group to develop a complete, physiologically correct FE model of the cervical spine incorporating the spinal cord for use of predicting spinal cord displacement, stress, and strain during physiologic motion. This model accurately predicts the spinal cord displacement and strain patterns present in both flexion and extension of the healthy subject. We aim to further utilize this model to investigate spinal cord injury, such as cervical myelopathy and its surgical treatment. Additionally, this model can be adapted to study fluid dynamics of the cerebral spinal fluid and electrophysiology of the spinal cord during motion.

CHAPTER 5: DEVELOPMENT OF CERVICAL MYELOPATHY FE MODEL WITH SURGICAL INTERVENTION

5.1 Introduction

5.1.1 FE Models of Spinal Cord Injury

Measuring stress and strain of the injured spinal cord can be difficult due to anatomy, spinal cord degradation, and in humans *in vivo* studies are unethical. As a result, researchers have turned to finite element modeling to estimate the stresses exhibited on the spinal cord during injured states. Most of these models have been basic either in geometry, material property definition, or both. The simplest representation of the spinal cord is the plane or 2D model. Sparrey et al. used this modeling technique to investigate how changes in the material properties of the white and grey matter affect stress and strain presentation during spinal cord compression.[85]

In general, 3D models of the spinal cord have become more prevalent than 2D models. The majority of these 3D models only incorporate the spinal cord and meninges using simplified boundary conditions to model bony contact.[79,80,82,83,98,104,105] For example, Kim et al. modeled compression of the spinal cord by using a rigid plate as the lamina and compressing it anteriorly with a cylindrical rigid body.[83]

There are a few groups who have included the bony anatomy of the spine in their spinal cord injury models.[78,81,106,107] These models have focused mainly on traumatic injuries of the spinal cord, such as dislocation, rather than myelopathy. Both Maikos et al. and Russel et al. have created FE models of the rat spine and spinal cord to model impaction trauma to the spinal cord.[78,107] Russel et al. also extended his model to include dislocation injury. Graeves et al. created a FE model incorporating the C4-C6 human musculoskeletal anatomy and spinal cord, dura, and neural ligaments to simulate contusion, distraction, and dislocation injuries.[81]

There are FE models which address the effects of cervical myelopathy.[79,82,83,106,108] However, the majority of these, as previously mentioned, have simplified boundary conditions. Khuyagbaatar et al. is the first group to incorporate comprehensive spinal canal anatomy with the spinal cord to investigate cord compression caused by the ossified posterior longitudinal ligament. They also investigated how common surgical techniques release the stress on the cord.[106] While the model was anatomically correct, it was not rotated to mimic physiologic motion. This is a major drawback as it has been reported that cervical myelopathy is dynamic and often worsens during neck movement.[48]

5.1.2 Study Aims

The aim of this study is to create an anatomically correct 3D FE model of cervical myelopathy allowing us to model how stress and strain changes in this spinal cord injury. Surgical decompression techniques will then be implemented to determine if surgical interventions adequately restore the cord stress and strains to that of the normal state.

5.2 Methods

5.2.1 FE Model of Cervical Myelopathy

The previously described FE model of the C2-T1 cervical spine and neural anatomy was used to create an FE model of cervical myelopathy. As cervical myelopathy occurs most commonly at the C4-C6 levels, osteophytes and disc herniation were created at the C4/5, C5/6, and C6/7 disc levels.[44] To do this, a preprocessing finite element model was created consisting of only the C4 to C7 vertebrae and discs, spinal cord, pia, dura, CSF, and neural and skeletal ligaments corresponding to the C4-C7 levels. For each mentioned level, the posterior nodes of the intervertebral disc and adjacent bone were pulled until an osteophyte and disc herniation protruding roughly 2 mm was created (Figure 40 A and B). This amount was specified as the average size of disc herniation and osteophyte protrusion by our neurosurgeon collaborators. To ensure only the posterior vertebral body nodes moved, the nodes of the anterior half of the vertebral bodies were held fixed in all directions. The cord, pia, and dura were held fixed at the superior and inferior ends. General contact was used to allow the disc herniation and osteophytes to impinge and compress the neural tissues (Figure 40 C). The final node locations of the disc herniation, osteophytes, and compressed neural tissues were used as the new initial node locations for the cervical myelopathy model. Material properties of the model were not altered and are described in Chapter 4.

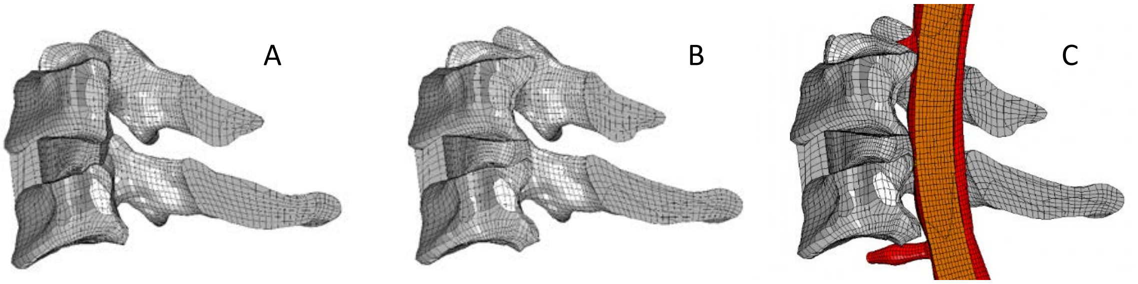

Figure 40: Creation of CM at C5/6 level. Healthy anatomy at C5/6 (A). Osteophytes and disc herniation (B) which compresses the neural tissues (C).

5.2.2 FE Model of Anterior Cervical Discectomy and Fusion

The ultimate goal of an anterior cervical discectomy and fusion (ACDF) is to have complete fusion of the operated vertebral bodies. To model this, the material properties of the C4/5, C5/6, and C6/7 intervertebral discs are increased to a level above that of bone to simulate a rigid body, as has been done in previous FE modeling.[109] The Young's Modulus was set to 5000 MPa and Poisson's ratio was 0.25. The density of the intervertebral discs were set to be that of cortical bone, 1990 kg/m^3.[110]

5.2.3 FE Model of Anterior Cervical Discectomy and Fusion with Laminectomy

In this surgical technique the ACDF is modeled as previously mentioned. To replicate the laminectomy, the posterior spinous processes and laminae are removed from the C4 to C7 vertebrae by deleting the corresponding elements (Figure 41 A).[90] The facets remain intact. The inter-spinal ligaments, ligamentum flavum, and meningovertebral ligaments which attached to the C4 to C7 posterior processes and laminae are also removed.

5.2.4 FE Model of Double Door Laminoplasty

To create the double door laminoplasty the technique of Kode et al. was used.[109] First the spinous processes of C4-C7 were split in the mid-sagittal plane and opened 10 mm. The tip of the spinous process was also removed as were the midline inter-spinal ligaments and ligamentum flavum. A trapezoidal spacer was put in the 10 mm gap and was tied to the adjacent sides of the spinous process cut using the TIED command in ABAQUS (Figure 41 B). The spacer was modeled with eight-noded brick elements and was given the material properties of hydroxyapatite: Young's modulus of 26 GPa and Poisson's ratio of 0.27.[109] As hydroxyapatite can be manufactured with a specified porosity and has similar chemical composition to bone, it was assumed to have a density of cancellous bone, 1920 kg/m^3.[110,111]

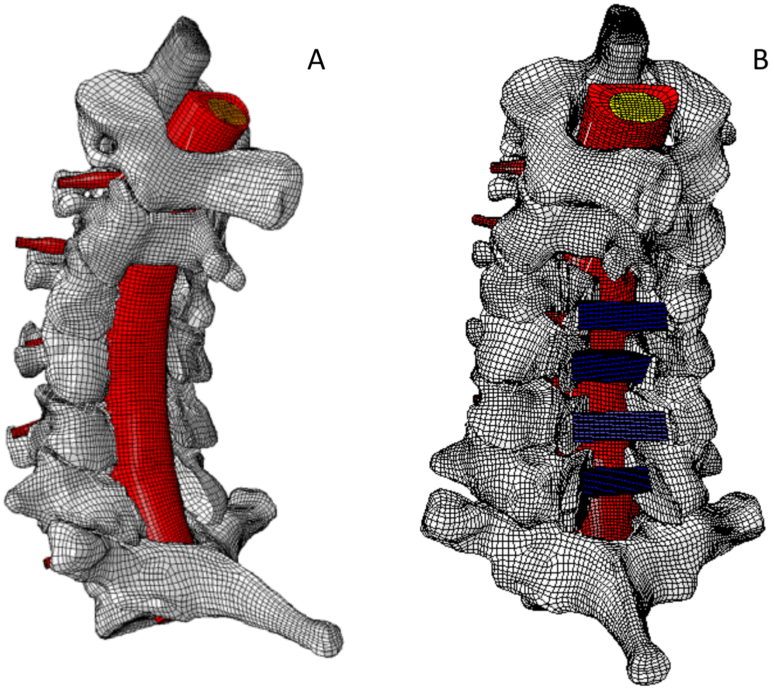

Figure 41: FE Model of ACDF with laminectomy (A) and double door laminoplasty (B).

5.2.5 Boundary Conditions

Just as with the normal C2-T1 model, the cervical myelopathy and surgical models were run with Abaqus/Standard 6.14 using the dynamic stress/displacement analysis option. The T1 vertebrae is fixed in all directions. Extension and flexion motions were rotated to the full amount achieved by healthy subjects as previously mentioned (19.82º in extension, 19.88º in flexion). This range of motion is greater than patients with cervical myelopathy were able to achieve both pre-operatively; 12.86º in extension 17.87º in flexion, and post-operatively; 16.74º in extension and 7.91º in flexion. However, the models can be analyzed at an earlier increment corresponding to these extension and flexion angles in order to directly compare results between FE and imaging. General contact is enforced for the entire model. The spinal cord, dura, and pia are not constrained and allowed to slide and stretch within the canal.

5.3 Results

5.3.1 Spine Flexion and Extension Rotation

Introduction of osteophytes and disc herniation had minimal effect on flexion and extension angles of the spine (Figure 42). However, surgical interventions incorporating ACDF altered flexion and extension angles. Specifically, there is little rotation at C4/5, C5/6, and C6/7 levels and an increase in rotation at the C2/3, C3/4 and C7/T1 levels. In comparison, double door laminoplasty retains spinal extension closer to the motion of healthy and cervical myelopathy models, with an increase only at the C3/4 level. However during flexion, there is an increase in motion at the C2/3 and C3/4 levels and a decrease in motion at the C6-T1 levels (Figure 42).

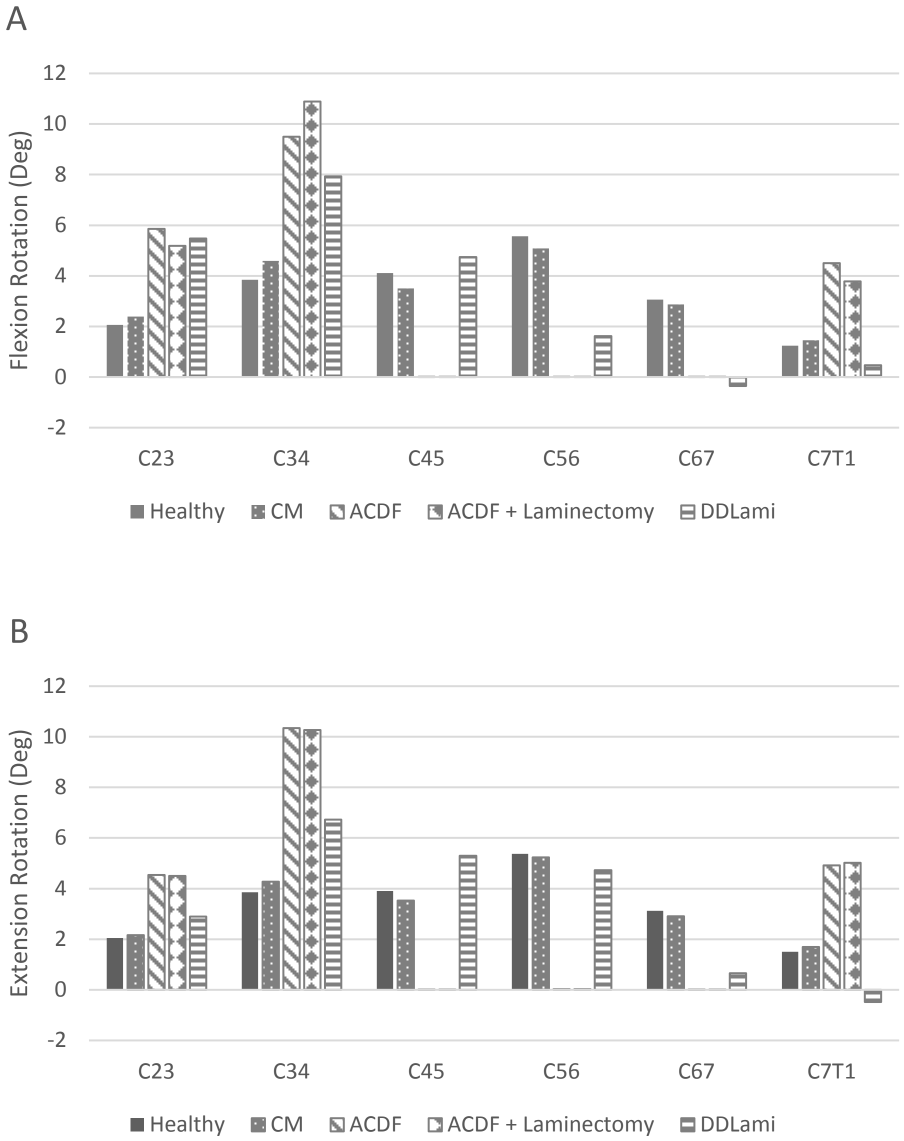

Figure 42: Flexion (A) and extension (B) intersegmental rotation of the FE models under 19.88º flexion and 19.82º extension.

5.3.2 Spinal Cord Displacement

The superior/inferior spinal cord displacements obtained from the cervical myelopathy FE model were compared to the superior inferior spinal cord displacements of cervical myelopathy subjects obtained from MR imaging in Chapter 3. The superior/inferior FE spinal cord followed that of MR imaging in both flexion and extension, being within a standard deviation of the average for all levels (Figures 43 and 44).

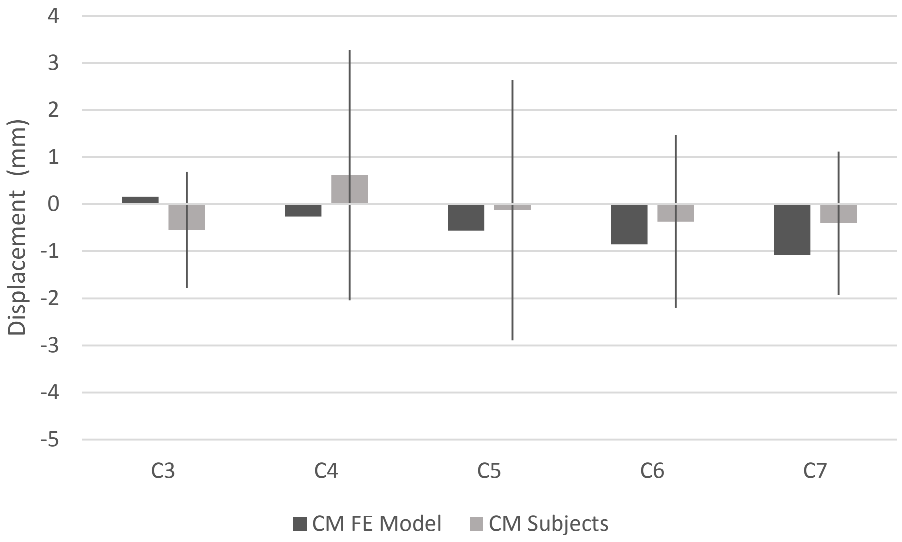

Figure 43: Superior/inferior spinal cord displacement of CM FE model in flexion. Patient data is presented as average ± one standard deviation.

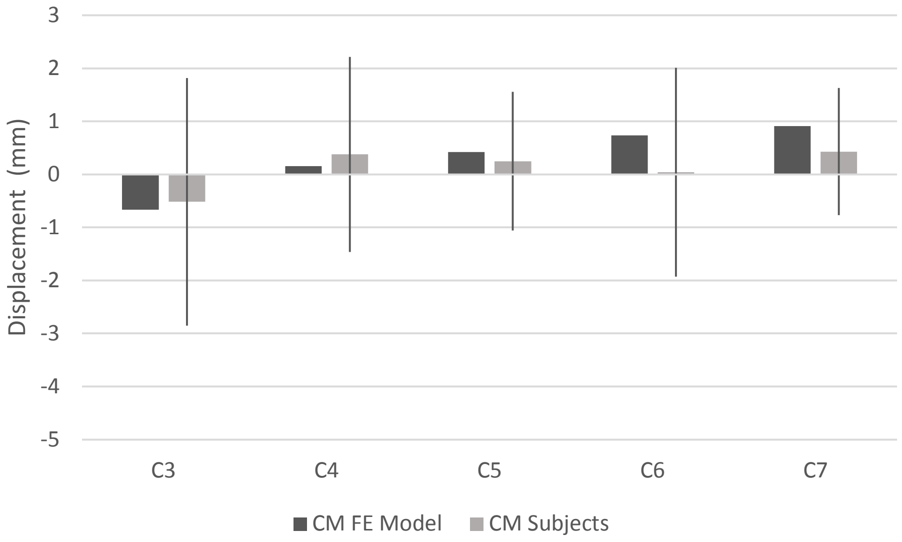

Figure 44: Superior/inferior spinal cord displacement of CM FE model in extension. Patient data is presented as average ± one standard deviation.

Superior/inferior displacements of the spinal cord obtained from ACDF, ACDF + laminectomy, and double door laminoplasty (DDLami) FE models were compared to superior/inferior cord displacements of cervical myelopathy post-operative cord displacements described in Chapter 3. FE models of surgical interventions all represented cord displacement well, being within one standard deviation at each level in both flexion and extension (Figures 45-50).

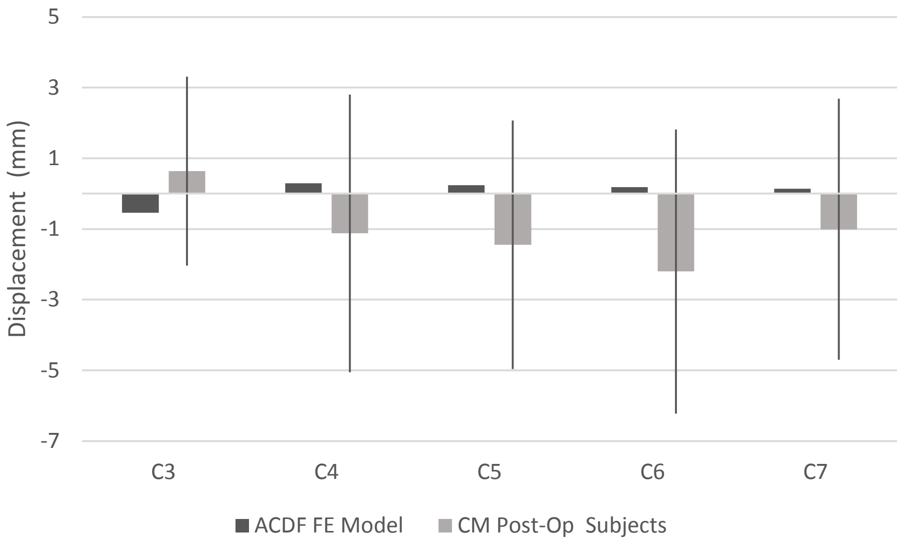

Figure 45: Superior/inferior spinal cord displacement of ACDF FE model in flexion. Patient data is presented as average ± one standard deviation.

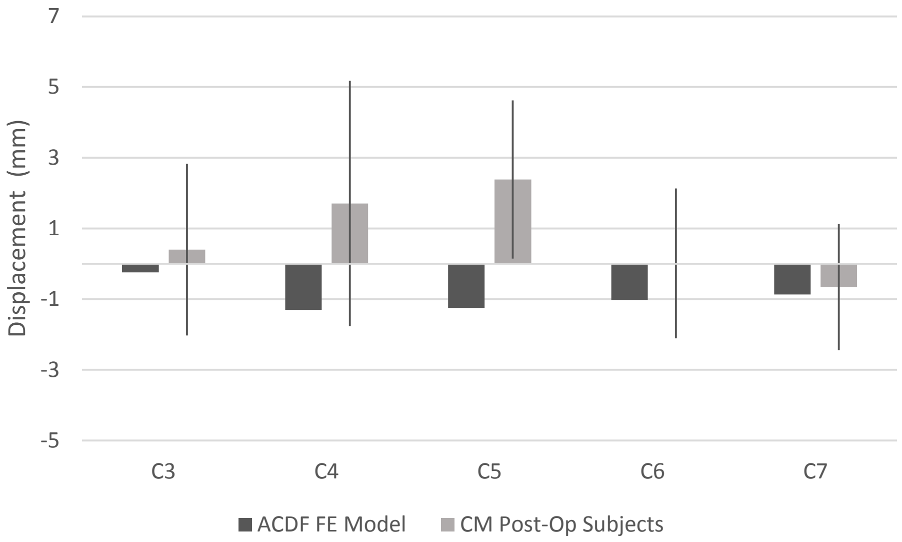

Figure 46: Superior/inferior spinal cord displacement of ACDF FE model in extension. Patient data is presented as average ± one standard deviation.

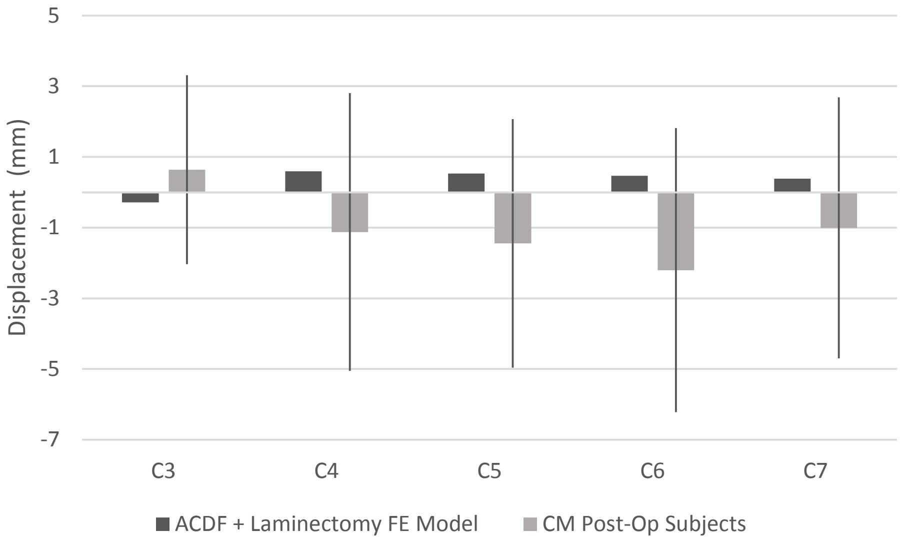

Figure 47: Superior/inferior spinal cord displacement of ACDF + Laminectomy FE model in flexion. Patient data is presented as average ± one standard deviation.

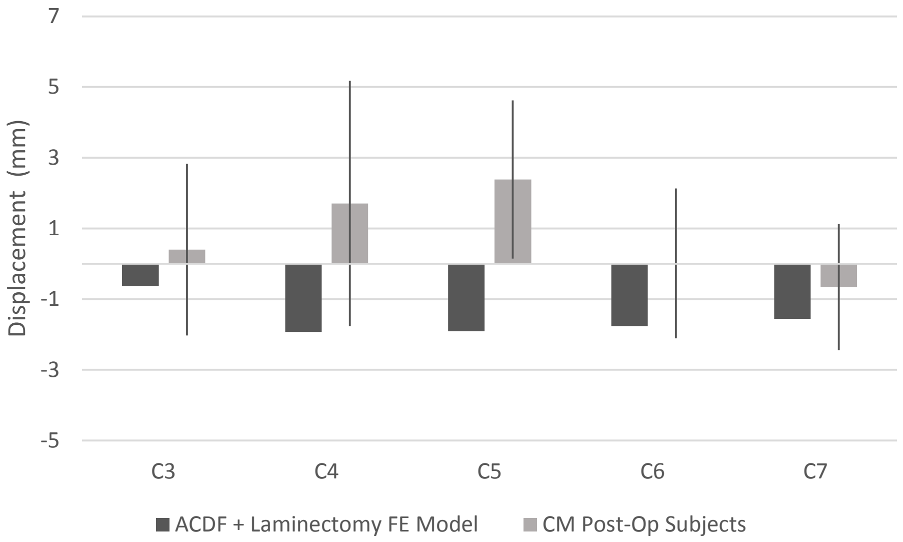

Figure 48: Superior/inferior spinal cord displacement of ACDF + Laminectomy FE model in extension. Patient data is presented as average ± one standard deviation.

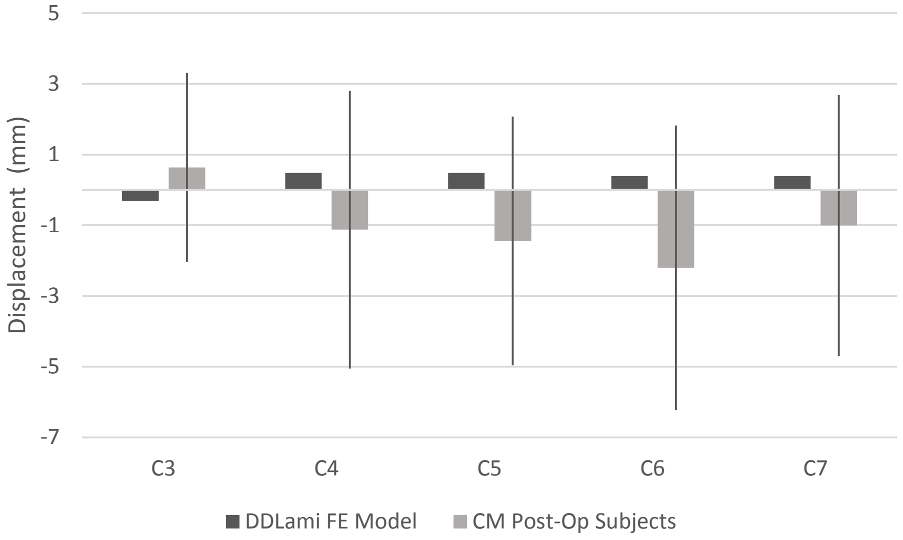

Figure 49: Superior/inferior spinal cord displacement of double door laminoplasty FE model in flexion. Patient data is presented as average ± one standard deviation.

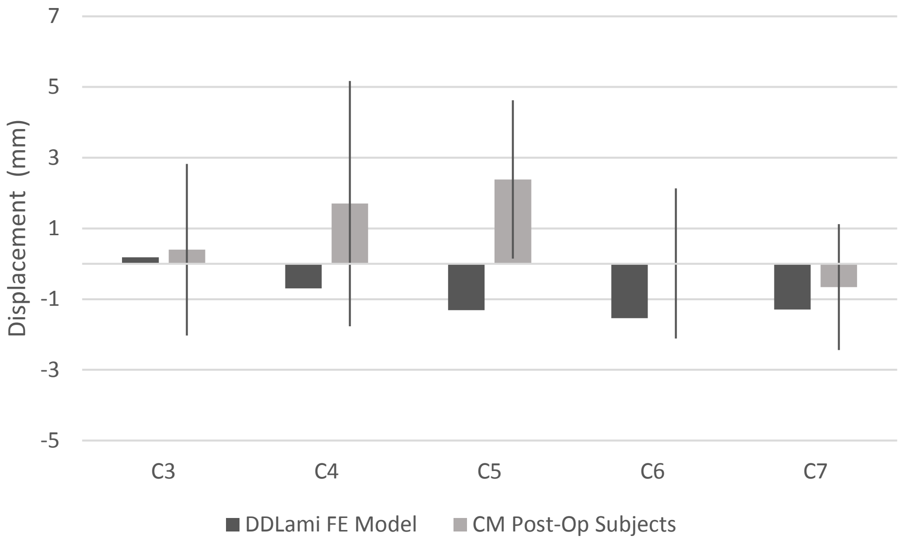

Figure 50: Superior/inferior spinal cord displacement of double door laminoplasty FE model in extension. Patient data is presented as average ± one standard deviation.

5.3.3 Spinal Cord Strain

Average principal spinal cord strain magnitudes and distribution in the CM FE model is similar to that of the healthy FE model in flexion (Figure 51). During extension, the CM model has higher principal tensile strains in the spinal cord at the C3 level and higher compressive principal strains at the C3, C6 and C7 levels (Figure 52).

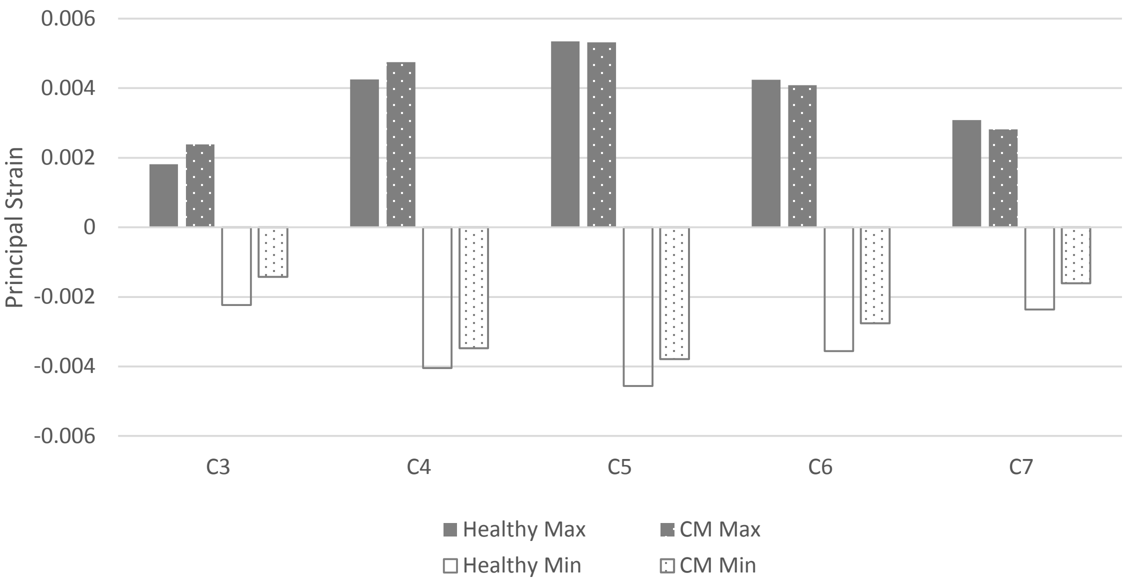

Figure 51: Principal strain in spinal cord in healthy and CM FE models in flexion. Data is reported at maximum range of motion obtained in each corresponding subject cohort. Healthy: 19.88º, CM Pre-Op: 17.87º.

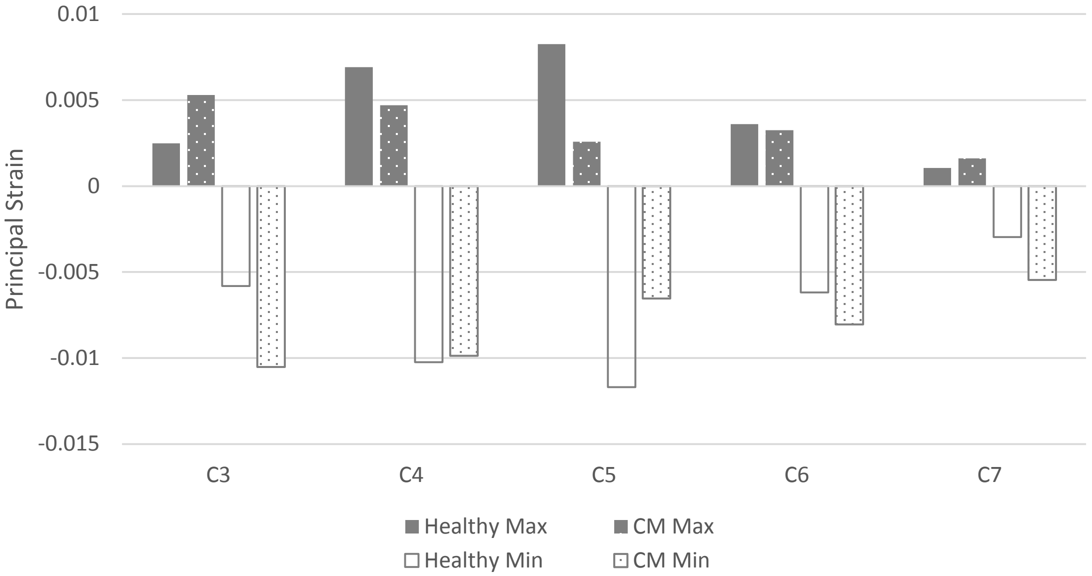

Figure 52: Principal strain in spinal cord in healthy and CM FE models in extension. Data is reported at maximum range of motion obtained in each corresponding subject cohort. Healthy: 19.82º.CM Pre-Op: 12.86º.

All surgical interventions for cervical myelopathy affected spinal cord strain. In flexion, all surgical methods increased principal tensile and compressive spinal cord strain at the C3 level and reduced principal tensile and compressive strain at the C4 to C7 levels (Figure 53). In extension, surgical methods increased tensile and compressive principal strains in the spinal cord at the C3 and C4 levels. At the C5 and C6 levels, surgical interventions decreased tensile and compressive principle strains but did not affect strains at the C7 level (Figure 54). Of these surgical techniques, the ACDF tends to increase strains the most at the C3 and C4 locations (Figure 55).

As was reported in the healthy FE model, principal strains from both cervical myelopathy FE models and cervical myelopathy surgical intervention FE models were roughly ten to one hundred times smaller than those reported from MR imaging (Table 9 and 10).

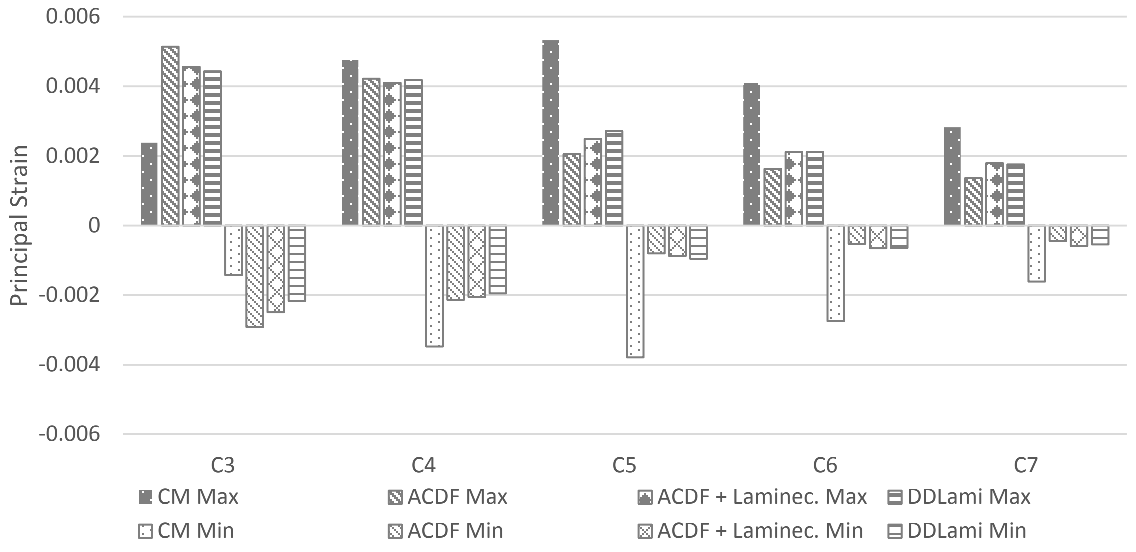

Figure 53: Comparison of principal strains in the spinal cord between CM and surgical intervention FE models in flexion. Data is reported at maximum range of motion obtained in each corresponding subject cohort. CM Pre-Op: 17.87º, CM Post-Op: 7.91º.

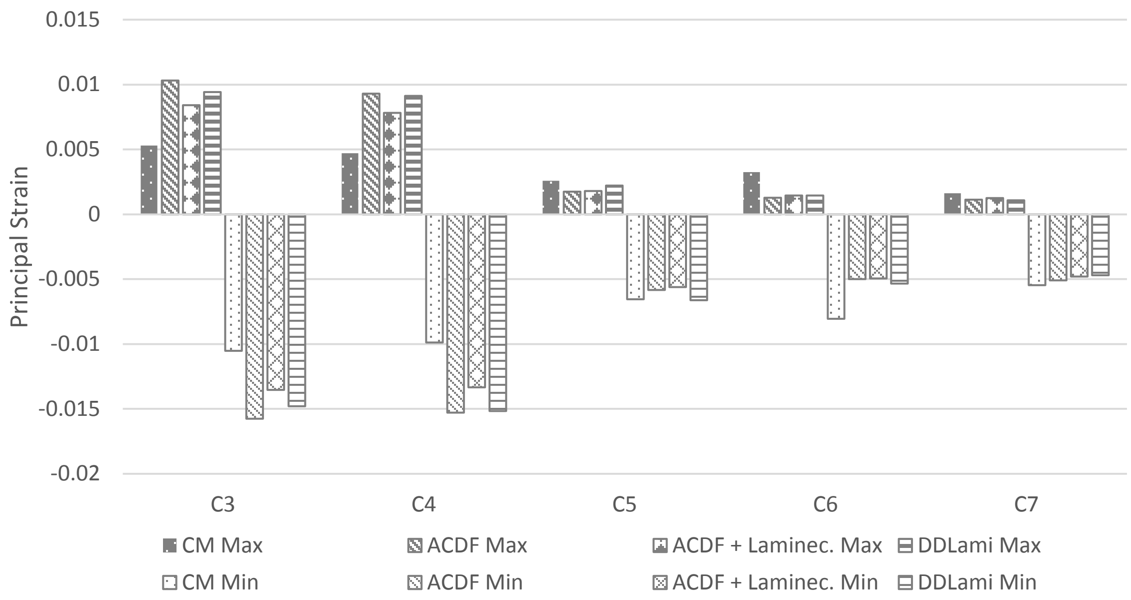

Figure 54: Comparison of principal strains in the spinal cord between CM and surgical intervention FE models in extension. Data is reported at maximum range of motion obtained in each corresponding subject cohort. CM Pre-Op: 12.86º, CM Post-Op: 16.74º.

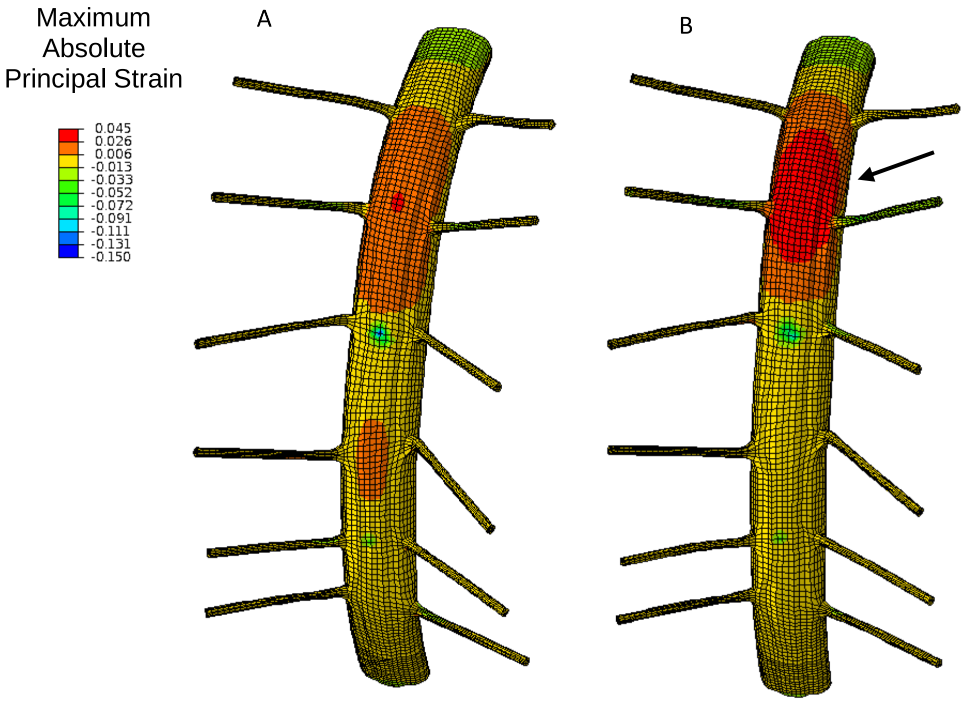

Figure 55: FE model of CM (A) and FE model of CM with ACDF intervention (B). An increase in strain at the C3-C4 level (arrow) and decrease at the C5-C6 level can be seen due to ACDF intervention.

Table 9: Principal strains obtained from CM FE model and pre-operative CM subjects in flexion and extension. Range of motion is 17.87º flexion and 12.86º for both FE model and MR imaging.

Flexion

Level	**CM FE Model Principal Strain**		**CM Pre-Op MR Imaging Principal Strain**	
	Min	*Max*	*Min*	*Max*
C3	-0.0014	0.0024	-0.18 ± 0.12	0.11 ± 0.04
C4	-0.0035	0.0048	-0.18 ± 0.15	0.13 ± 0.08
C5	-0.0038	0.0053	-0.15 ± 0.11	0.17 ± 0.07
C6	-0.0028	0.0041	-0.14 ± 0.07	0.13 ± 0.03
C7	-0.0016	0.0028	-0.15 ± 0.09	0.12 ± 0.05

Extension

Level	**CM FE Model Principal Strain**		**CM Pre-Op MR Imaging Principal Strain**	
	Min	*Max*	*Min*	*Max*
C3	-0.0105	0.0053	-0.23 ± 0.18	0.12 ± 0.05
C4	-0.0099	0.0047	-0.14 ± 0.09	0.15 ± 0.08
C5	-0.0065	0.0026	-0.13 ± 0.11	0.17 ± 0.06
C6	-0.0081	0.0033	-0.17 ± 0.14	0.14 ± 0.05
C7	-0.0055	0.0016	-0.16 ± 0.14	0.13 ± 0.05

Table 10: Principal strains obtained from surgical FE models and post-operative CM subjects in flexion and extension. Range of motion is 7.91° flexion and 16.74° for both FE model and MR imaging.

Flexion

Level	ACDF FE Model Principal Strain		ACDF + Laminec. FE Model Principal Strain		DDLami FE Model Principal Strain		CM Post-Op MR Imaging Principal Strain	
	Min	*Max*	*Min*	*Max*	*Min*	*Max*	*Min*	*Max*
C3	-0.0029	0.0051	-0.0025	0.0046	-0.0022	0.0044	-0.14 ± 0.05	0.18 ± 0.08
C4	-0.0021	0.0042	-0.0021	0.0041	-0.0020	0.0042	-0.13 ± 0.08	0.18 ± 0.06
C5	-0.001	0.0020	-0.0009	0.0025	-0.0010	0.0027	-0.18 ± 0.14	0.18 ± 0.07
C6	-0.0005	0.0016	-0.0007	0.0021	-0.0006	0.0021	0.20 ± 0.16	0.17 ± 0.09
C7	-0.0004	0.0014	-0.0006	0.0018	-0.0005	0.0017	-0.32 ± 0.32	0.16 ± 0.14

Extension

Level	ACDF FE Model Principal Strain		ACDF + Laminec. FE Model Principal Strain		DDLami FE Model Principal Strain		CM Post-Op MR Imaging Principal Strain	
	Min	*Max*	*Min*	*Max*	*Min*	*Max*	*Min*	*Max*
C3	-0.0158	0.0103	-0.0135	0.0103	-0.0148	0.0094	-0.18 ± 0.12	0.13 ± 0.05
C4	-0.0153	0.0093	-0.0133	0.0093	-0.0152	0.0091	-0.22 ± 0.06	0.12 ± 0.09
C5	-0.0058	0.0017	-0.0056	0.0017	-0.0066	0.0022	0.20 ± 0.10	0.19 ± 0.07
C6	-0.0050	0.0013	-0.0050	0.0013	-0.0053	0.0015	-0.09 ± 0.08	0.19 ± 0.03
C7	-0.0051	0.0011	-0.0048	0.0011	-0.0047	0.0011	-0.14 ± 0.08	0.14 ± 0.05

5.3.4 Spinal Cord Stress

The cervical myelopathy FE model showed an increase in von Mises stress compared to the healthy model at the C3 and C4 levels in flexion and C3 level in extension. All surgical techniques decreased von Mises stress at the C4 to C7 levels in flexion and extension. The ACDF + laminectomy and double door laminoplasty interventions also decreased stress at the C3 and C4 levels in flexion and extension. Conversely, the ACDF intervention increased stresses at the C3 and C4 levels in flexion and the C3 level in extension (Figures 56 and 57).

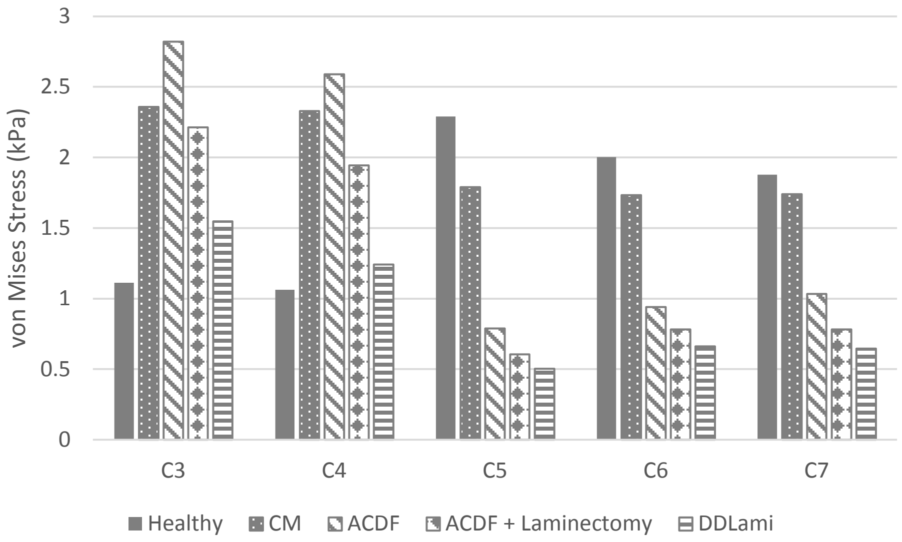

Figure 56: von Mises stress in spinal cord during FE model flexion. Data is reported at maximum range of motion obtained in each corresponding subject cohort. Healthy: 19.88º, CM Pre-Op: 17.87º, CM Post-Op: 7.91º.

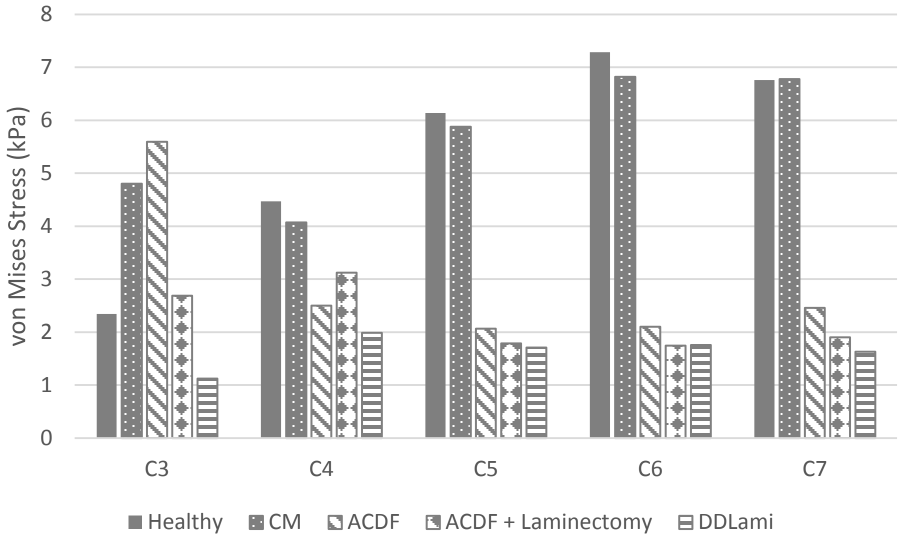

Figure 57: von Mises stress in spinal cord during FE model extension. Data is reported at maximum range of motion obtained in each corresponding subject cohort. Healthy: 19.82º, CM Pre-Op: 12.86º, CM Post-Op: 16.74º.

5.4 Discussion

In this study we developed an FE model of the C2 to T1 myelopathic cervical spine and incorporated common surgical treatments for cervical myelopathy to determine how both affect spinal cord mechanics. To our knowledge, we are the first group to develop an anatomically accurate C2 to T1 FE model of myelopathy that not only models surgical intervention, but models it during physiologic loading.

The spinal cord displacements obtained from the FE models of both cervical myelopathy and cervical myelopathy surgical intervention matched data previously obtained pre- and post-operatively from cervical myelopathy subjects. It is worth noting that while our model was within acceptable limits of data obtained from the imaging analysis, our model of cervical myelopathy did not decrease spinal cord displacement as much as expected. One main reason for this is the amount of compression present in the cervical myelopathy model. The 2 mm disc herniation and osteophyte generation did compress the spinal cord, but not to the same percentage as seen in patient imaging. Additionally some patients also exhibited posterior compression which this model did not include. Higher percentages of spinal cord compression would most likely decrease spinal cord displacement.

Comparing our FE strain results to the strain data obtained from MR imaging of CM subjects pre- and post-operation we see that our strain is much lower. This is not unexpected for two reasons. First, we are aware that the healthy FE model, from which the CM FE model was developed, underestimates strain compared to the MR data but matches other published FE models. This discrepancy is most likely due to the lack of literature data which fully characterizes the mechanics of the spinal cord. Secondly, as previously stated, an increase in osteophyte and disc herniation size would increase spinal cord compression and therefore strain. There are several groups who have developed impact and simplified cervical myelopathy FE models. While they utilize similar spinal cord material properties as we do, the spinal cord compression exhibited on the spinal cord can be as large as a 60% compression ratio. This results in strains ranging from 20 to 60 percent which is closer to that of the MR data. Kim et al and Khuyagbaatar et al also reported von Mises stresses of 0 - 400 kPa at similar compression ratios.[83,106] This is higher than the stresses we reported, but again, at a much higher amount of compression.

The increased motion of the spine at the C3 and C4 levels after surgical intervention agrees with both cadaveric testing and computational models of cervical fusion.[109,112,113] The altered loading of the spine after surgical intervention is believed to be responsible for the prevalence of adjacent segment degeneration.[114] As shown through our FE modeling, this phenomenon also transfers to the neural anatomy. The operated levels of the spine did exhibit a decrease in strain, most likely to a decrease in motion and therefore compression, but an increase in stress and strain was present at the adjacent spinal cord levels. This is most likely due to the increased rotational motion at those levels. This increased strain is greater than that seen in our healthy FE model during physiologic motion and essentially increases the base level of strain experienced by the spinal cord. If osteophytes begin to form at this level or a traumatic force is applied, the spinal cord may be predisposed to injury and failure.

Of all the surgical techniques, ACDF intervention increased adjacent level strain and stress the most. This may be due to the fact that the spinal canal has not been widened as in an ACDF with laminectomy or double door laminoplasty. This increase in canal width allows for more spinal cord displacement especially in extension (Figures 50 and 48), which may decrease the likelihood of the spinal cord impingement elsewhere along the canal. Additionally, the double door laminoplasty technique allows for more normal motion of the spine as it does not fuse the vertebral bodies.

As with all research, our study is not without limitations. Firstly, this FE model was based on a single subject’s anatomy. This means that this FE model is unable to capture all anatomic variants present in the population. Additionally, we only investigated anterior spinal cord impingement. Cervical myelopathy can also be caused by posterior impingement or a combination of the two. Anterior compression was chosen for clinical relevancy as our neurosurgeon collaborators most often see anterior compression in their clinic. Finally, we only investigated multilevel myelopathy and surgical intervention. This was also chosen to adequately evaluate anterior and posterior surgical techniques. According to neurosurgical practice at the UIHC, three affected levels may be addressed with either anterior or posterior intervention. More than three affected levels disqualifies patients from an ACDF and if fewer than three levels are affected, ACDF is favored to preserve spinal motion.

As this is the first reporting of altered segmental loading affecting the spinal cord, especially following ACDF, it is worth further investigation in both the biomechanics of the spinal cord and long term clinical and patient evaluation post-surgical intervention for cervical myelopathy.

CHAPTER 6: CONCLUSIONS

Cervical myelopathy occurs when the cervical spinal cord is chronically compressed due to bony or soft tissue impingement. It commonly affects adults over the age of 50 years and causes upper extremity numbness, loss of hand dexterity, gait disturbances, and decreased proprioception. Recent studies including flexion and extension MRI images of cervical spine have shown this injury is highly dependent on the dynamic motion of the spine.[115] However, there is little data on spinal cord stresses and strains which occur during cervical spinal motion either in healthy or cervical myelopathy subjects. To address this, the current study utilized MR imaging and FE modeling to investigate spinal cord mechanics. As far as we are aware, we are the first group to obtain *in vivo* 3D spinal cord strain data from human subjects and the first to develop a C2 to T1 FE model of the healthy and cervical myelopathic spine and spinal cord.

Utilizing high resolution MR imaging in neutral, flexion, and extension positions we were able to obtain spinal cord displacement fields from both healthy subjects and cervical myelopathy subjects before and after surgical intervention. In healthy subjects the spinal cord moves superiorly in flexion and inferiorly in extension. Localizations of high principal strain in extension can be seen in healthy subjects at areas of bony impingement and dural buckling. Cervical myelopathy subjects exhibited very little spinal cord displacement due to spinal cord compression. Principal strains during flexion and extension were greater in cervical myelopathy patients than in healthy patients, specifically at the C4-6 vertebral levels. Surgical treatments for cervical myelopathy did restore spinal cord motion, however not in the same pattern or direction as healthy subjects. Additionally, principal strains of the spinal cord were not reduced after surgical intervention. This indicates that surgical interventions are not adequately addressing the altered mechanics of spinal cord during cervical myelopathy.

To determine how common surgical techniques for cervical myelopathy affect spinal cord mechanics, a FE model of the cervical spine and spinal cord was developed. First neural anatomy was introduced in to a previously validated model of the C2-T1 spine.[89] The spinal cord mechanics was then validated against MR imaging data of healthy subjects. Once validated the modeled was used to develop a FE model of cervical myelopathy and surgical interventions.

The native FE model predicted spinal cord motion well and replicated bony spinal cord impingement and dural buckling seen in healthy subjects. The FE model of cervical myelopathy also replicated spinal cord motion well as compared to MR imaging data of cervical myelopathy. Three, C4 to C7, surgical interventions were introduced into the model, anterior discectomy and fusion, anterior discectomy and fusion with laminectomy, and double door laminoplasty.

Principal strains obtained from the healthy and cervical myelopathy FE models were similar in flexion, however in extension, principal strains were higher at the C3, C6 and C7 levels. This is different than the patterns exhibited in the MR imaging and is most likely due to the percent of spinal cord compression induced in the FE model. In flexion, all surgical treatments almost doubled spinal cord principal strains at the C3 level and minimal reduction in tensile strain was seen at C4. The majority of strain reduction occurred at C5-7. In extension all surgical techniques increased principal strains at the C3 and C4 levels. Little or no reduction in principal strains was seen at the C5 and C7 levels.

All surgical techniques reduced principal strains at the C6 level. Of the surgical techniques, ACDF tended to reduce spinal cord principal strains the least in both flexion and extension and tended to induce the highest von Mises stresses.

Combining the data obtained from MR imaging and FE modeling, we can see that cervical myelopathy alters spinal cord mechanics by limiting spinal cord motion and increasing spinal cord strain. Additionally, current surgical techniques are not addressing the change in spinal cord mechanics effectively. This indicates the need for both further research in spinal cord mechanics and improved treatments for cervical myelopathy.

6.1. Future Work

While this study answered many questions regarding spinal cord mechanics there is still much to be done in this field. First, as obtaining *in vivo* spinal cord data can be technically and ethically challenging, further development of FE modeling should be done to investigate spinal cord injury mechanics. Specifically, improving the FE material property definition of the spinal cord is necessary and calls for more thorough tissue level mechanical testing to fully characterize the spinal cord. Additionally, expanding the amount and location of spinal cord compression would be useful and provide more insight into cervical myelopathy. Running the model in axial rotation and lateral bending would give a more complete picture of physiologic spinal cord mechanics. Finally, this model could be modified to investigate other spinal cord injury mechanisms, electrophysiology, and fluid dynamics of the CSF.

REFERENCES

1. Nouri, A., Tetreault, L., Singh, A., Karadimas, S. K. & Fehlings, M. G. Degenerative Cervical Myelopathy: Epidemiology, Genetics and Pathogenesis. *Spine* 1 (2015). doi:10.1097/BRS.0000000000000913

2. Northover, J. R., Wild, J. B., Braybrooke, J. & Blanco, J. The epidemiology of cervical spondylotic myelopathy. *Skeletal Radiol.* **41,** 1543–1546 (2012).

3. Fehlings, M. G. *et al.* Is surgery for cervical spondylotic myelopathy cost-effective? A cost-utility analysis based on data from the AOSpine North America prospective CSM study. *JNS Spine Spec. Suppl.* **17,** 89–93 (2012).

4. Bernhardt, M., Hynes, R. A., Blume, H. W. & White, A. A. Cervical spondylotic myelopathy. *J. Bone Jt. Surg.* **75,** 119–128 (1993).

5. Lao, L., Zhong, G., Li, X., Qian, L. & Liu, Z. Laminoplasty versus laminectomy for multi-level cervical spondylotic myelopathy: a systematic review of the literature. *J. Orthop. Surg.* **8,** 45 (2013).

6. Zhu, R. *et al.* Comparisons of three anterior cervical surgeries in treating cervical spondylotic myelopathy. *BMC Musculoskelet. Disord.* **15,** 233 (2014).

7. Breig, A. *Biomechanics of the Central Nervous System: Some basic normal and pathologic phenomena*. (The Year Book Publishers, INC, 1960).

8. Jin, X., Yang, K. H. & King, A. I. Mechanical properties of bovine pia–arachnoid complex in shear. *J. Biomech.* **44,** 467–474 (2011).

9. Ozawa, H., Matsumoto, T., Ohashi, T., Sato, M. & Kokubun, S. Mechanical properties and function of the spinal pia mater. *J. Neurosurg. Spine* **1,** 122–127 (2004).

10. Tunturi, A. R. Elasticity of the spinal cord, pia, and denticulate ligament in the dog. *J. Neurosurg.* **48,** 975–979 (1978).

11. Bhatnagar, T. *et al.* In Vivo Measurement of Cervical Spinal Cord Deformation During Traumatic Spinal Cord Injury in a Rodent Model. *Ann. Biomed. Eng.* 1–14 (2015). doi:10.1007/s10439-015-1412-6

12. Viljoen, S. *et al.* MR-based measurement of spinal cord motion during flexion of the spine: implications for intradural spinal cord stimulator systems. *J. Med. Eng. Technol.* 1–4 (2013). doi:10.3109/03091902.2013.844207

13. Muhle, C. *et al.* Biomechanical aspects of the subarachnoid space and cervical cord in healthy individuals examined with kinematic magnetic resonance imaging. *Spine* **23,** 556–567 (1998).

14. Endo, K. *et al.* Kinematic Analysis of the Cervical Cord and Cervical Canal by Dynamic Neck Motion. *Asian Spine J.* **8,** 747 (2014).

15. Yuan, Q., Dougherty, L. & Margulies, S. S. In vivo human cervical spinal cord deformation and displacement in flexion. *Spine* **23,** 1677–1683 (1998).

16. White, A. A. & Panjabi, M. M. *Clinical Biomechanics of the Spine*. (J. B. Wippincott Company, 1978).

17. Cervical Instability - Physiopedia, universal access to physiotherapy knowledge. Available at: http://www.physio-pedia.com/Cervical_Instability. (Accessed: 1st February 2017)

18. Atlas - Physiopedia, universal access to physiotherapy knowledge. Available at: http://www.physio-pedia.com/Atlas. (Accessed: 1st February 2017)

19. File:Axis.png - Physiopedia, universal access to physiotherapy knowledge. Available at: http://www.physio-pedia.com/File:Axis.png. (Accessed: 1st February 2017)

20. Smith, L. J., Nerurkar, N. L., Choi, K.-S., Harfe, B. D. & Elliott, D. M. Degeneration and regeneration of the intervertebral disc: lessons from development. *Dis. Model. Mech.* **4,** 31–41 (2011).

21. Raj, P. P. Intervertebral Disc: Anatomy-Physiology-Pathophysiology-Treatment. *Pain Pract.* **8,** 18–44 (2008).

22. Imboden JB, Hellmann DB & Stone JH. *CURRENT Diagnosis & Treatment: Rheumatology, 3e*. (2013).

23. Morton, DA, Foreman, K & Albertine, KH. *The Big Picture: Gross Anatomy*. (2011).

24. Bilston, L. E. & Thibault, L. E. The mechanical properties of the human cervical spinal cordIn Vitro. *Ann. Biomed. Eng.* **24,** 67–74 (1995).

25. Byrne, T. N., Benzel, E. C. & Waxman, S. G. *Diseases of the Spine and Spinal Cord*. (Oxford University Press, 2000).

26. Ovid: Clinically Oriented Anatomy | Universities Education of Ukraine. Available at: http://ueu.co/ovid-clinically-oriented-anatomy-45/. (Accessed: 2nd February 2017)

27. MILLEN, J. W. & WOOLLAM, D. H. On the nature of the pia mater. *Brain J. Neurol.* **84,** 514–520 (1961).

28. Tunturi, A. R. Elasticity of the spinal cord dura in the dog. *J. Neurosurg.* **47,** 391–396 (1977).

29. Walter F. Boron & Emile L. Boulpaep. *Medical Physiology: With STUDENT CONSULT Online Access, 2e*. (Saunders, 2008).

30. Spector, R., Robert Snodgrass, S. & Johanson, C. E. A balanced view of the cerebrospinal fluid composition and functions: Focus on adult humans. *Exp. Neurol.* **273,** 57–68 (2015).

31. Abel, A. S. *et al.* Effect of Patient Positioning on Cerebrospinal Fluid Opening Pressure: *J. Neuroophthalmol.* 1 (2013). doi:10.1097/WNO.0000000000000074

32. EPSTEIN, B. S. AN ANATOMIC, MYELOGRAPHIC AND CINEMYELOGRAPHIC STUDY OF THE DENTATE LIGAMENTS. *Am. J. Roentgenol.* **98,** 704–712 (1966).

33. Gürer, B. *et al.* Microsurgical anatomy of the denticulate ligaments and their relationship with the axilla of the spinal nerve roots: Microsurgical Anatomy of the Denticulate Ligaments. *Clin. Anat.* **27,** 733–737 (2014).

34. Shi, B. *et al.* The morphology and clinical significance of the dorsal meningovertebra ligaments in the cervical epidural space. *Spine J. Off. J. North Am. Spine Soc.* **14,** 2733–2739 (2014).

35. STOOKEY B. Compression of the spinal cord due to ventral extradural cervical chondromas: Diagnosis and surgical treatment. *Arch. Neurol. Psychiatry* **20,** 275–291 (1928).

36. Rhee, J. M., Heflin, J. A., Hamasaki, T. & Freedman, B. Prevalence of Physical Signs in Cervical Myelopathy: A Prospective, Controlled Study. *Spine* **34,** 890–895 (2009).

37. Hashizume, Y., Iijima, S., Kishimoto, H. & Yanagi, T. Pathology of spinal cord lesions caused by ossification of the posterior longitudinal ligament. *Acta Neuropathol. (Berl.)* **63,** 123–130 (1984).

38. Beattie, M. S. & Manley, G. T. Tight squeeze, slow burn: inflammation and the aetiology of cervical myelopathy. *Brain* **134,** 1259–1261 (2011).

39. Hayashi, H. M. D., Okada, K. M. D., Hamada, M. M. D., Tada, K. M. D. & Ueno, R. M. D. Etiologic Factors of Myelopathy A Radiographic Evaluation of the Aging Changes in the Cervical Spine. *Clin. Orthop.* **214,** 200–209 (1987).

40. Ichihara, K., Taguchi, T., Sakuramoto, I., Kawano, S. & Kawai, S. Mechanism of the spinal cord injury and the cervical spondylotic myelopathy: new approach based on the mechanical features of the spinal cord white and gray matter. *J. Neurosurg. Spine* **99,** 278–285 (2003).

41. Yoshii, T. *et al.* Dynamic Changes in Spinal Cord Compression by Cervical Ossification of the Posterior Longitudinal Ligament Evaluated by Kinematic Computed Tomography Myelography. *Spine* (2013). doi:10.1097/BRS.0000000000000086

42. Baptiste, D. C. & Fehlings, M. G. Pathophysiology of cervical myelopathy. *Spine J.* **6,** S190–S197 (2006).

43. Shi, R. & Pryor, J. D. Pathological changes of isolated spinal cord axons in response to mechanical stretch. *Neuroscience* **110,** 765–777 (2002).

44. Kalsi-Ryan, S., Karadimas, S. K. & Fehlings, M. G. Cervical Spondylotic Myelopathy The Clinical Phenomenon and the Current Pathobiology of an Increasingly Prevalent and Devastating Disorder. *The Neuroscientist* **19,** 409–421 (2013).

45. Nurjck, S. The Pathogenesis of the Spinal Cord Disorder Associated with Cervical Spondylosis. *Brain* **95,** 87–100 (1972).

46. Breig, A., Turnbull, I. & Hassler, O. Effects of mechanical stresses on the spinal cord in cervical spondylosis. A study on fresh cadaver material. *J. Neurosurg.* **25,** 45–56 (1966).

47. Inufusa, A. *et al.* Anatomic Changes of the Spinal Canal and Intervertebral Foramen Associated With Flexion-Extension Movement. [Miscellaneous Article]. *Spine Novemb. 1 1996* **21,** 2412–2420 (1996).

48. Bartlett, R. J. V. *et al.* Extension MRI is clinically useful in cervical myelopathy. *Neuroradiology* **55,** 1081–1088 (2013).

49. Morimoto, T., Ohtsuka, H., Sakaki, T. & Kawaguchi, M. Postlaminectomy cervical spinal cord compression demonstrated by dynamic magnetic resonance imaging. *J. Neurosurg.* **88,** 155–157 (1998).

50. Buckwalter, J. A. Aging and degeneration of the human intervertebral disc. *Spine* **20,** 1307–1314 (1995).

51. Shiban, E. & Meyer, B. Treatment considerations of cervical spondylotic myelopathy. *Neurol. Clin. Pract.* **4,** 296–303 (2014).

52. Shammassian, B. & Hart, D. J. ‘Complications In Surgical Treatment Of Cervical Spondylotic Myelopathy – What We Think We Know’. *World Neurosurg.* doi:10.1016/j.wneu.2015.04.016

53. Luo, J. *et al.* Comparison of anterior approach versus posterior approach for the treatment of multilevel cervical spondylotic myelopathy. *Eur. Spine J.* 1–10 (2015). doi:10.1007/s00586-015-3911-4

54. Edwards, C. C., Heller, J. G., Murakami, H. & others. Corpectomy versus laminoplasty for multilevel cervical myelopathy: an independent matched-cohort analysis. *Spine* **27,** 1168–1175 (2002).

55. Heller, J. G. *et al.* Comparison of BRYAN Cervical Disc Arthroplasty With Anterior Cervical Decompression and Fusion: Clinical and Radiographic Results of a Randomized, Controlled, Clinical Trial. *Spine* **34,** 101–107 (2009).

56. ACDF Surgery | Anterior Cervical Discectomy and Fusion. Available at: http://www.mayfieldclinic.com/PE-ACDF.htm. (Accessed: 2nd February 2017)

57. Cervical Laminectomy Article - Patients | DePuy Synthes Companies. Available at: https://www.depuysynthes.com/patients/aabp/resources/articles_learn/id_58. (Accessed: 2nd February 2017)

58. Laminoplasty. Available at: http://www.neurosurgery-blog.com/archives/tag/laminoplasty. (Accessed: 2nd February 2017)

59. Breig, A. Overstretching of and circumscribed pathological tension in the spinal cord — A basic cause of symptoms in cord disorders. *J. Biomech.* **3,** 7–9 (1970).

60. Smith, C. G. Changes in Length and Position of the Segments of the Spinal Cord with Changes in Posture in the Monkey. *Radiology* **66,** 259–266 (1956).

61. Kroeker, S. G. & Ching, R. P. Coupling between the spinal cord and cervical vertebral column under tensile loading. *J. Biomech.* **46,** 773–779 (2013).

62. Oakland, R. J., Hall, R. M., Wilcox, R. K. & Barton, D. C. The Biomechanical Response of Spinal Cord Tissue to Uniaxial Loading. *Proc. Inst. Mech. Eng. [H]* **220,** 489–492 (2006).

63. Vavasour, I. M. *et al.* Increased spinal cord movements in cervical spondylotic myelopathy. *Spine J. Off. J. North Am. Spine Soc.* (2014). doi:10.1016/j.spinee.2014.01.036

64. Bhatnagar, T., Liu, J. & Oxland, T. Characterization of a Novel, Magnetic Resonance Imaging-Compatible Rodent Model Spinal Cord Injury Device. *J. Biomech. Eng.* **136,** 095001–095001 (2014).

65. Bhatnagar, T. QUANTIFICATION OF MORPHOLOGICAL CHANGES OF THE CERVICAL SPINAL CORD DURING TRAUMATIC SPINAL CORD INJURY IN A RODENT MODEL. (The University of British Columbia, 2015).

66. Holzapfel, G. A. *Nonlinear Solid Mechanics: A continuum Approach for Engineering*. (John Wiley & Sons, 2000).

67. Bartlett, R. J. V., Hill, C. A. R., Rigby, A. S., Chandrasekaran, S. & Narayanamurthy, H. MRI of the cervical spine with neck extension: is it useful? *Br. J. Radiol.* **85,** 1044–1051 (2012).

68. Revanappa, K. K. & Rajshekhar, V. Comparison of Nurick grading system and modified Japanese Orthopaedic Association scoring system in evaluation of patients with cervical spondylotic myelopathy. *Eur. Spine J.* **20,** 1545 (2011).

69. Reid, J. D. Effects of flexion-extension movements of the head and spine upon the spinal cord and nerve roots. *J. Neurol. Neurosurg. Psychiatry* **23,** 214–221 (1960).

70. Bilston, L. E. The biomechanics of the spinal cord during traumatic spinal cord injury. (University of Pennsylvania, 1994).

71. Beer, F. P., Johnston, E. R. & DeWolf, J. T. *Mechanics of Materials*. (McGraw-Hill, 2006).

72. Fujita, Y. & Yamamoto, H. An experimental study on spinal cord traction effect. *Spine* **14,** 698–705 (1989).

73. Morishita, Y., Maeda, T., Ueta, T., Naito, M. & Shiba, K. Dynamic somatosensory evoked potentials to determine electrophysiological effects on the spinal cord during cervical spine extension: clinical article. *J. Neurosurg. Spine* **19,** 288–292 (2013).

74. Goto, T. & Hoshino, Y. Electrophysiological, histological, and behavioral studies in a cat with acute compression of the spinal cord. *J. Orthop. Sci.* **6,** 59–67 (2001).

75. Karadimas, S. K. *et al.* A novel experimental model of cervical spondylotic myelopathy (CSM) to facilitate translational research. *Neurobiol. Dis.* **54,** 43–58 (2013).

76. Lee, J., Satkunendrarajah, K. & Fehlings, M. G. Development and Characterization of a Novel Rat Model of Cervical Spondylotic Myelopathy: The Impact of Chronic Cord Compression on Clinical, Neuroanatomical, and Neurophysiological Outcomes. *J. Neurotrauma* **29,** 1012–1027 (2011).

77. Klironomos, G. *et al.* New experimental rabbit animal model for cervical spondylotic myelopathy. *Spinal Cord* **49,** 1097–1102 (2011).

78. Russell, C. M., Choo, A. M., Tetzlaff, W., Chung, T.-E. & Oxland, T. R. Maximum Principal Strain Correlates with Spinal Cord Tissue Damage in Contusion and Dislocation Injuries in the Rat Cervical Spine. *J. Neurotrauma* **29,** 1574–1585 (2012).

79. Nishida, N. *et al.* Biomechanical analysis of cervical myelopathy due to ossification of the posterior longitudinal ligament: Effects of posterior decompression and kyphosis following decompression. *Exp. Ther. Med.* (2014). doi:10.3892/etm.2014.1557

80. Persson, C., Summers, J. & Hall, R. M. The Importance of Fluid-Structure Interaction in Spinal Trauma Models. *J. Neurotrauma* **28,** 113–125 (2011).

81. Greaves, C. Y., Gadala, M. S. & Oxland, T. R. A Three-Dimensional Finite Element Model of the Cervical Spine with Spinal Cord: An Investigation of Three Injury Mechanisms. *Ann. Biomed. Eng.* **36,** 396–405 (2008).

82. Kato, Y. *et al.* Biomechanical study of cervical flexion myelopathy using a three-dimensional finite element method. (2008).

83. Kim, Y. H., Khuyagbaatar, B. & Kim, K. Biomechanical effects of spinal cord compression due to ossification of posterior longitudinal ligament and ligamentum flavum: A finite element analysis. *Med. Eng. Phys.* **35,** 1266–1271 (2013).

84. Heidari Pahlavian, S. *et al.* The Impact of Spinal Cord Nerve Roots and Denticulate Ligaments on Cerebrospinal Fluid Dynamics in the Cervical Spine. *PLoS ONE* **9,** e91888 (2014).

85. Sparrey, C. J., Manley, G. T. & Keaveny, T. M. Effects of white, grey, and pia mater properties on tissue level stresses and strains in the compressed spinal cord. *J. Neurotrauma* **26,** 585–595 (2009).

86. Bahramshahi, N., Ghaemi, H. & Behdinan, K. Finite Element Study of Spinal Cord Mechanics During Biomechanical Response of Middle Cervical Spine. 443–448 (2010). doi:10.1115/IMECE2010-40573

87. Scifert, J., Totoribe, K., Goel, V. & Huntzinger, J. Spinal cord mechanics during flexion and extension of the cervical spine: a finite element study. *Pain Physician* **5,** 394–400 (2002).

88. Henao, J., Aubin, C.-É., Labelle, H. & Arnoux, P.-J. Patient-specific finite element model of the spine and spinal cord to assess the neurological impact of scoliosis correction: preliminary application on two cases with and without intraoperative neurological complications. *Comput. Methods Biomech. Biomed. Engin.* **19,** 901–910 (2016).

89. Kallemeyn, N. *et al.* Validation of a C2–C7 cervical spine finite element model using specimen-specific flexibility data. *Med. Eng. Phys.* **32,** 482–489 (2010).

90. Kode, S., Kallemeyn, N. A., Smucker, J. D., Fredericks, D. C. & Grosland, N. M. Biomechanical Effects of Laminoplasty and Laminectomy on the Stability of Cervical Spine. 843–844 (2011). doi:10.1115/SBC2011-53252

91. Nolte, J. *The Human Brain in Photographs and Diagrams: With STUDENT CONSULT Online Access, 4e*. (Saunders, 2013).

92. Kallemeyn, N. A., Tadepalli, S. C., Shivanna, K. H. & Grosland, N. M. An interactive multiblock approach to meshing the spine. *Comput. Methods Programs Biomed.* **95,** 227–235 (2009).

93. Kallemeyn, N. A., Natarajan, A., Magnotta, V. A. & Grosland, N. M. Hexahedral meshing of subject-specific anatomic structures using mapped building blocks. *Comput. Methods Biomech. Biomed. Engin.* **16,** 602–611 (2013).

94. Abaqus 6.14 Reference Documentation. (2014).

95. Ozawa, H., Matsumoto, T., Ohashi, T., Sato, M. & Kokubun, S. Comparison of spinal cord gray matter and white matter softness: measurement by pipette aspiration method. *J. Neurosurg. Spine* **95,** 221–224 (2001).

96. Schmidt, H. *et al.* Application of a new calibration method for a three-dimensional finite element model of a human lumbar annulus fibrosus. *Clin. Biomech.* **21,** 337–344 (2006).

97. Ichihara, K. *et al.* Gray matter of the bovine cervical spinal cord is mechanically more rigid and fragile than the white matter. *J. Neurotrauma* **18,** 361–367 (2001).

98. Yan, Y.-B. *et al.* Finite Element Study of the Mechanical Response in Spinal Cord during the Thoracolumbar Burst Fracture. *PLoS ONE* **7,** (2012).

99. Persson, C., Evans, S., Marsh, R., Summers, J. L. & Hall, R. M. Poisson's Ratio and Strain Rate Dependency of the Constitutive Behavior of Spinal Dura Mater. *Ann. Biomed. Eng.* **38,** 975–983 (2010).

100. Kumaresan, S. & Radhakrishnan, S. Importance of partitioning membranes of the brain and the influence of the neck in head injury modelling. *Med. Biol. Eng. Comput.* **34,** 27–32 (1996).

101. Frank, C., Amiel, D., Woo, S. L. & Akeson, W. Normal ligament properties and ligament healing. *Clin. Orthop.* 15–25 (1985).

102. Shetye, S. S. *et al.* Nonlinear viscoelastic characterization of the porcine spinal cord. *Acta Biomater.* **10,** 792–797 (2014).

103. Carlson, G. D. *et al.* Viscoelastic relaxation and regional blood flow response to spinal cord compression and decompression. *Spine* **22,** 1285–1291 (1997).

104. Li, X.-F. & Dai, L.-Y. Three-Dimensional Finite Element Model of the Cervical Spinal Cord: Preliminary Results of Injury Mechanism Analysis. [Miscellaneous Article]. *Spine May 15 2009* **34,** 1140–1147 (2009).

105. Khuyagbaatar, B., Kim, K. & Hyuk Kim, Y. Effect of bone fragment impact velocity on biomechanical parameters related to spinal cord injury: A finite element study. *J. Biomech.* **47,** 2820–2825 (2014).

106. Khuyagbaatar, B., Kim, K., Park, W. M. & Kim, Y. H. Effect of posterior decompression extent on biomechanical parameters of the spinal cord in cervical ossification of the posterior longitudinal ligament. *Proc. Inst. Mech. Eng. [H]* **230,** 545–552 (2016).

107. Maikos, J. T., Qian, Z., Metaxas, D. & Shreiber, D. I. Finite Element Analysis of Spinal Cord Injury in the Rat. *J. Neurotrauma* **25,** 795–816 (2008).

108. Kato, Y. *et al.* Biomechanical study of the effect of degree of static compression of the spinal cord in ossification of the posterior longitudinal ligament. *J. Neurosurg. Spine* **12,** 301–305 (2010).

109. Kode, S., Kallemeyn, N. A., Smucker, J. D., Fredericks, D. C. & Grosland, N. M. The Effect of Multi-Level Laminoplasty and Laminectomy on the Biomechanics of the Cervical Spine: a Finite Element Study. *Iowa Orthop. J.* **34,** 150–157 (2014).

110. Gong, J. K., Arnold, J. S. & Cohn, S. H. Composition of trabecular and cortical bone. *Anat. Rec.* **149,** 325–331 (1964).

111. Liu, D.-M. Preparation and characterisation of porous hydroxyapatite bioceramic via a slip-casting route. *Ceram. Int.* **24,** 441–446 (1998).

112. Wang, C.-S., Chang, J.-H., Chang, T.-S., Chen, H.-Y. & Cheng, C.-W. Loading effects of anterior cervical spine fusion on adjacent segments. *Kaohsiung J. Med. Sci.* **28,** 586–594 (2012).

113. Prasarn, M. L., Baria, D., Milne, E., Latta, L. & Sukovich, W. Adjacent-level biomechanics after single versus multilevel cervical spine fusion. *J. Neurosurg. Spine* **16,** 172–177 (2011).

114. Kong, L., Cao, J., Wang, L. & Shen, Y. Prevalence of adjacent segment disease following cervical spine surgery. *Medicine (Baltimore)* **95,** (2016).

115. Kim, C. H. *et al.* Cervical extension magnetic resonance imaging in evaluating cervical spondylotic myelopathy. *Acta Neurochir. (Wien)* **156,** 259–266 (2014).